Design and Resistance Analysis of a Co-Electrolysis Cell through Impedance Spectroscopy

by Florentin Treis

A thesis for the degree of
Master of Science

In the
Master Program in Engineering Sciences - Mechanical Engineering

At the
Faculty of Mechanical Engineering and Management, TU Wien

Supervised by
Univ.Prof Dipl.-Ing. Dr.tech. Markus Haider

and
Dipl.-Ing Martin Schulz

Dipl.-Ing Felix Ettlinger

Author
Florentin Treis
Matr. Nr.: 12225988
e12225988@student.tuwien.ac.at

Supervisor
Univ.Prof Dipl.-Ing. Dr.tech. Markus Haider
TU Wien
Institute for Energy Systems and Thermodynamics
Getreidemarkt 9, A-1060 Wien

Supervisor
Dipl.-Ing Martin Schulz
TU Wien
Institute for Energy Systems and Thermodynamics
Getreidemarkt 9, A-1060 Wien

Supervisor
Dipl.-Ing Felix Ettlinger
TU Wien
Institute for Energy Systems and Thermodynamics
Getreidemarkt 9, A-1060 Wien

Affidavit

I declare in lieu of oath, that I wrote this thesis and performed the associated research myself, using only literature cited in this volume. If text passages from sources are used literally, they are marked as such. I confirm that this work is original and has not been submitted elsewhere for any examination, nor is it currently under consideration for a thesis elsewhere.

Vienna, December 18, 2024

Florentin Treis

Abstract

CO_2 capture is a key component of the ecological transition towards achieving carbon neutrality. The directCCE project (direct Carbon Capture and Electrolysis) aims to develop a system capable of chemically absorbing CO_2 emitted by a waste treatment plant in Vienna and converting this absorbed CO_2 into syngas, specifically reducing it to H_2 and CO. This reduction process takes place in an electrochemical cell, known as a Co-Electrolyzer, where a voltage is applied to drive the reaction.

However, the energy supplied to the electrolyzer can not be used to full extent, as several components of the cell contribute to energy losses by imposing resistance to charge transport. This thesis focuses on impedance measurements under varying design parameters to evaluate the different sources of energy losses in each case. Additionally, it explores the feasibility of detecting CO_2 reduction through impedance spectroscopy.

The three main topics of this thesis include:

1. Stabilizing the impedance spectroscopy signal by minimizing noise to ensure consistent measurements. A solution was also implemented to amplify the voltage delivered to the electrolyzer using the PSM3750 spectrometer in combination with the Solartron device.

2. Conducting spectroscopic measurements on a 100 cm^2 active area Co-Electrolyzer under varying experimental conditions using four different absorption fluids for CO_2 capture.

3. Designing a new electrolyzer with a smaller 16 cm^2 active area optimized for impedance spectroscopy measurements.

The impedance spectroscopy results from the 100 cm^2 cell revealed that the cell's response varies depending on the CO_2-absorption fluid. For some catholytes (electrolyte on the cathode side), such as KOH, the charge transfer resistance associated with CO_2 reduction could be identified, while in other cases, this identification proved more challenging. The design of a smaller electrolyzer will enable localized impedance spectroscopy measurements at the electrode level, facilitated by the inclusion of a reference electrode. This approach allowed the separation of resistances from the two reactions in the Nyquist diagrams obtained through impedance spectroscopy. Understanding and evaluating the various sources of potential losses in the cell provides a clearer insight into its behavior and helps identify areas for improvement.

Kurzfassung

Die CO_2-Abscheidung ist ein wesentlicher Bestandteil der ökologischen Transition hin zur Erreichung der Klimaneutralität. Das Projekt directCCE zielt darauf ab, ein System zu entwickeln, das in der Lage ist, chemisch CO_2 aus den Emissionen einer Müllverbrennungsanlage in Wien aufzunehmen und dieses absorbierte CO_2 in Synthesegas umzuwandeln, indem es speziell zu H2 und CO reduziert wird. Dieser Reduktionsprozess findet in einer elektrochemischen Zelle statt, die als Co-Elektrolyseur bezeichnet wird und an der eine Spannung als elektrochemische Triebkraft für die Reaktion angelegt wird.

Die Energie, die dem Elektrolyseur zugeführt wird, wird jedoch nicht vollständig für die chemische Umwandlung genutzt. Mehrere Komponenten der Zelle verursachen Energieverluste, indem sie Widerstände im Ladungstransport erzeugen. Diese Arbeit konzentriert sich auf die Impedanzmessungen unter variierenden Designparametern, um die verschiedenen Energieverlustquellen in jedem Fall zu bewerten. Darüber hinaus wird untersucht, ob die CO_2-Reduktion durch Impedanzspektroskopie nachgewiesen werden kann.

Die Arbeit gliedert sich in drei Hauptteile:

1. Stabilisierung des Signals der Impedanzspektroskopie durch Minimierung von Störungen, um konsistente Messungen zu gewährleisten. Zusätzlich wurde eine Lösung implementiert, um die an den Elektrolyseur gelieferte Spannung mit Hilfe des PSM3750-Spektrometers in Kombination mit dem Solartron-Gerät zu verstärken.

2. Durchführung spektroskopischer Messungen an einem Co-Elektrolyseur mit einer aktiven Fläche von 100 cm^2 unter variierenden experimentellen Bedingungen mit vier verschiedenen Absorberflüssigkeiten zur CO_2-Abscheidung.

3. Entwicklung eines neuen Elektrolyseurs mit einer kleineren aktiven Fläche von 16 cm^2, der für Impedanzspektroskopiemessungen optimiert ist.

Die Ergebnisse der Impedanzspektroskopie mit der 100 cm^2 Zelle zeigten, dass die Zellreaktion je nach CO_2 Absorptionsmittel Flüssigkeit variiert. Für einige Katholyte wie KOH konnte der Ladungsübertragungswiderstand, der mit der CO_2-Reduktion verbunden ist, identifiziert werden, während dies in anderen Fällen schwieriger war. Das Design eines kleineren Elektrolyseurs wird ermöglichen lokalisierte Impedanzspektroskopiemessungen auf Elektrodenebene, erleichtern durch die Integration einer Referenzelektrode. Dieser Ansatz erlaubte die Trennung der Widerstände der beiden Reaktionen in den durch die Impedanzspektroskopie erhaltenen Nyquist-Diagrammen.

Acknowledgments

I would like to express my heartfelt gratitude to my thesis supervisor, Professor Markus Haider, for providing me with the opportunity to work on a hands-on project that aligns closely with my interests and aspirations. His support throughout this journey have been indispensable.

I would also like to extend my heartfelt thanks to Professor Guenter Fafilek for the time he dedicated to answering my questions on electrochemistry and for helping me stabilize my impedance spectroscopy measurements. I was particularly touched by the time he spent working with me directly in the workshop to jointly inspect and fine-tune my measuring equipment. His support and expertise were invaluable to the success of this work.

I am deeply thankful to the two doctoral researchers, Martin Schulz and Felix Ettlinger, who supervised my thesis. Their guidance, insightful suggestions, and solution-oriented approach were crucial in overcoming challenges and achieving meaningful progress in my research.

I would also like to extend my sincere thanks to all the employees of the Arsenal workshop for their assistance in designing and fabricating the necessary components for my experiments. Their expertise and collaboration were instrumental in the successful execution of this work.

Inhaltsverzeichnis

Nomenclature

Acronyms

A	Chemical Species
AEM	Anion Exchange Membrane
DC	Direct current
EIS	Elecrochemical Impedance Spectroscopy
O	Oxidant
PEM	Proton Exchange Membrane
ppm	Part Per Million
R	Reductant
OER	Oxygen evolution reaction
SHE	Standard hydrogen electrode
AC	Alternating current

Chemical Species

A_g	Silver
A_gCl	Silver Chlorid
AMP	2-Amino-2-methylpropanol
C	Carbon
Cl^-	Chloride ion
CO	Carbon monoxide
CO_2	Carbon dioxide
CO_3^{2-}	Carbonate ion
H^+	Proton
H_2	Dihydrogen
H_2O	Water
HCO_3^-	Bicarbonate ion
IrO_2	Iridium dioxide
K_2CO_3	Potassium carbonate
KOH	Potassium Hydroxide
MEA	Monoethanolamine
O_2	Oxygen
OH^-	Hydroxide ion

Greek symbols

α	Transfer Coefficient	-
η	Overpotential	V
η_s	Surface Overpotential	V
η_{conc}	Diffusion Overpotential	V
η_{ohm}	Ohmic Overpotential	V

Roman symbols

ΔG	Gibb's Energy	J
ΔG_f	Gibb's Formation Energy	J
A	Surface area	m^2
C	Capacity	F
c	Concentration	gL^-1
d	Thickness	m
E_a	Activation energy	$J\,mol^{-1}$
I	Current	A
i	Current Density	mA/cm^{-2}
i	Exchange Current Density	$mAcm^{-2}$
j	Imaginary unit (complex number)	-
L	Inductance	H
M	Molar mass	$g\,mol^{-1}$
n		
p	Pressure	Pa
R	Resistance	Ω
s	Stochiometric Coefficient	Ω
T	Temperature	
U	Equilibrium Potential	V
U^θ	Standard Equilibrium Potential	F
W	Work	J
Z	Impedance	Ω

1. Introduction

1.1. Motivation

The European objectives regarding climate change are clear. In the latest report from the European Parliament in July 2024 [13], the new European Climate Law once again raised the target for reducing net greenhouse gas emissions to 55% (compared to 1990 levels) by 2030, up from the previous target of 40%. Europe reaffirms its ambition to become the first global entity to achieve the Paris Agreement's goal and carbon neutrality by 2050.

While fuel combustion is responsible for more than three-quarters of greenhouse gas emissions in the EU [13], Europe is embarking on a strategy for carbon capture, storage, and utilization. By 2030, Europe aims to store 50 million tons of CO_2 per year, and up to 450 million tons annually by 2050, representing 13% of European emissions [24]. The British government, for its part, announced in October 2024 a £22 billion subsidy plan to accelerate the carbon capture and storage (CCS) process. Three key projects are targeted as part of this plan: carbon capture at a gas-fired power plant by BP and Equinor, a hydrogen production facility by Essar, and a waste-to-energy plant by Encyclis and Biffa. [20]

While the economic cost of such operations is often emphasized, the equally significant energy cost tends to receive less attention :

- The industrial operator chooses to maintain the same level of production while adding a carbon capture system to the facility. This requires an additional energy expenditure of 17% to 42%.
- The industrial operator agrees to allocate 15% to 30% of their available energy to the carbon capture system instead of their primary activity.

Downstream storage of captured CO_2, such as storing it underground as is commonly done today, represents a clear ecological benefit but a net loss for the industrial operator. An interesting solution would be to successfully convert the captured carbon into a new usable product without consuming excessive resources in the process.

As part of the Direct Carbon Capture and Electrolysis (directCCE) project, one solution involves capturing CO_2 from the gas emissions of a waste treatment plant in Vienna and converting it into syngas (H_2 + CO) instead of storing it. The development of such

a project offers a more advantageous and innovative solution for a company aiming to reduce its greenhouse gas emissions.

1.2. Scope of Work

The goal of this thesis is to analyze various parameters of the CO-Electrolyzer and measure their impact on the cell's resistance using impedance spectroscopy. A specific design for conducting impedance spectroscopy analysis is then proposed to enhance the conclusions and experiments.

This work focuses on several key aspects :

- The research and implementation of a setup to achieve stable and consistent measurements when applied to CO-electrolyzer cells.
- Measuring the influence of certain cell parameters (membrane, electrode, CO_2 absorbent fluid) on its impedance and determining the advantages and disadvantages of each of them.
- Proposing a smaller cell design better suited for impedance spectroscopy analysis to obtain more precise results and facilitate the overall development of the CO-electrolyzer cell within the framework of the directCCE project.
- Attempting to detect the reduction reaction of CO_2 to CO at the cathode during the spectroscopic analysis.

The first part of the thesis provides the theoretical foundations of CO_2 electrolysis into syngas, as well as the basics of impedance spectroscopy analysis. The second part will detail the components used in the spectroscopic analysis setup, as well as the steps involved in designing a smaller cell adapted for this purpose. Finally, the last part will present the results of the influence of various parameters on the cell performing the co-electrolysis.

2. Impedance Spectroscopy : Theoretical Background

2.1. Basics of electrochemical cells

2.1.1. Principle of the half-cell

A half-cell is a simple arrangement consisting of an electron conductor, called electrode, and an ion conductor brought into contact [10]. The contact between the two systems induces heterogeneous electron-transfer reactions that can be generally written as :

$$\mathrm{O} + \mathrm{ne}^- \longleftrightarrow \mathrm{R} \tag{2.1}$$

where R and O are two chemical species, belonging rather to the electrode or the ionic conductor. In electrochemistry, O is generally called the oxidized species and R the reduced species. Thus, the direction of equation 2.1 is known as reduction, while the reverse direction as oxidation. The half-cell reaction has the particularity to have electrons e^- at either a reactant or a product. It is heterogeneous, which means that the reactants are present in different states (solid, liquid or gas) [28].

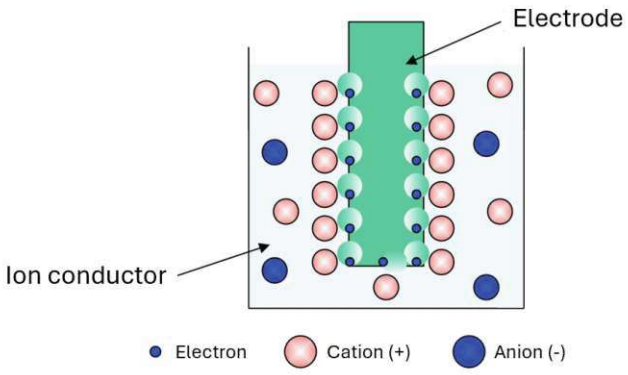

Figure 2.1.: *Scheme of a simple half-cell [10]*

The electrode is the only part of the system where the movement of electrons occurs. The ionic conductor doesn't conduct or either contains free electrons. It is constituted of a mixture of negatively charged ions, anions, and positively charged ions, cations [28]. Thus, to allow the proper execution of the charge transfer reaction 2.1, contact between

the ionic conductor and electron conductor is necessary.

At steady state, the charge transfer reaction in the system will be in equilibrium. This equilibrium corresponds to a certain equilibrium electrical potential U, characteristic for each reaction. If this equilibrium gets disturbed, for example by shifting the electrode electric potential through an externally applied voltage, change of equilibrium induces movement of charges, and electric currents flow in the circuit. [10]

If the electrode is made of a material with chemical symbole C, the haf-cell where reaction 2.1 occurs is conventionally written as C|O|R.

2.1.2. Electrochemical Cell

A typical electrochemical cell is composed of two electrodes : an anode where the oxidation occurs, and a cathode where the reduction takes place. Two charge transport regions are distinguished based on the nature of the charge carriers. Electrons travel through an external circuit using an electronic conductor that links the anode to the cathode. Ionic charges move within an ionic conductor that connects the cathode and the anode. The ionic conductor of the cell is called the electrolyte. [28]

At the surface of each electrode a half-cell reaction takes place between the electrode and the electrolyte as depicted in section 2.1.1. In a closed circuit, electrons are produced at the anode and consumed at the cathode. This process induces a movement of charges that creates an electric current within the full-cell. The two independent half-cell reactions are combined to form a single overall reaction, the full-cell reaction, generally written [28]:

$$\alpha_c \mathrm{O}_c + \beta_a \mathrm{R}_a \longrightarrow \alpha_a \mathrm{O}_a + \beta_c \mathrm{R}_c \tag{2.2}$$

with O_c, R_c chemical species at the cathode, O_a, R_a chemical species at the anode, α_c, α_a, β_c and β_a stoichiometric coefficients. The net charge balance of the full-cell is then unchanged.

Generally, the study of an electrochemical cell focuses only on a single half-cell reaction of interest. The electrode where it occurs is known as *working electrode*. The other electrode is then named *counter electrode*.

Some half-cells made up of phases having essentially constant composition (certain electrode in a certain electrolyte with fixed regulated conditions) are standardized. They are called *reference electrodes*. [29]

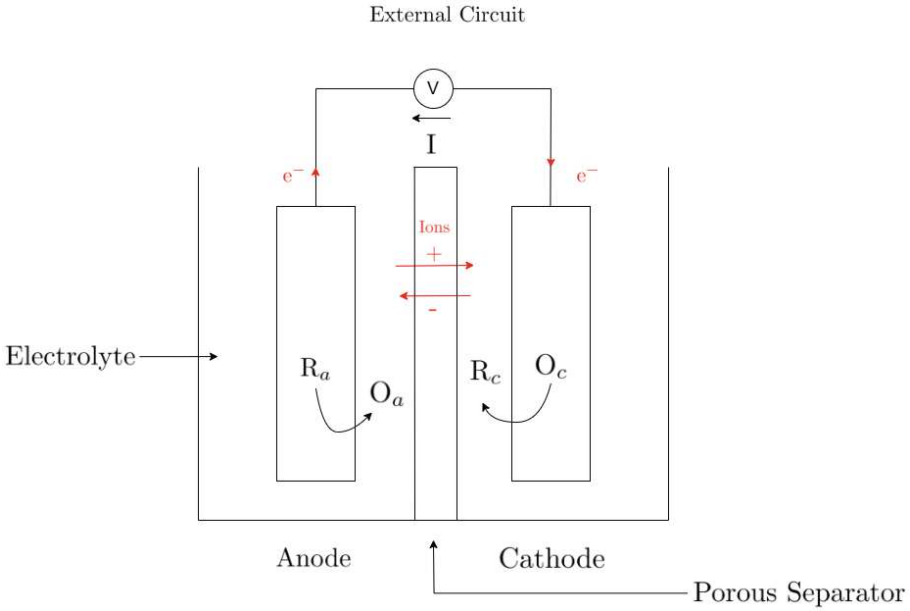

Figure 2.2.: *Scheme of a Full-Cell (According to Reaction 2.2)*

2.1.3. Electrochemical Reaction in directCCE project

The scrubbing solution absorbing carbon dioxide CO_2 is an active species diluted in water. CO_2 and H_2O are converted by an electrochemical cell into syngas through reduction at the cathode, producing hydrogen gas (H_2) and carbon monoxide (CO). This half-reaction is balanced at the anode by the oxidation of water, producing oxygen O_2. The general equation of this conversion is written :

$$CO_2 + H_2O \longrightarrow H_2 + CO + O_2 \tag{2.3}$$

Under standard conditions, this overall full-cell reaction is the balance equation of the two half-cell reactions :

Cathode

$$2\,H^+ + 2\,e^- \longrightarrow H_2 \tag{2.4}$$

$$CO_2 + 2\,e^- + 2\,H^+ \longrightarrow CO + H_2O \tag{2.5}$$

Anode

$$2\,H_2O \longrightarrow O_2 + 4\,H^+ + 4\,e^- \tag{2.6}$$

Equations 2.4 and 2.6 are actually reactions commonly encountered in electrochemistry and often occur at one of the electrodes of an electrochemical cell. The reduction

of protons H^+ into dihydrogen is called *Hydrogen Evolution Reaction* (HER) and the oxydation of water into oxygen *Oxygen Evolution Reaction* (OER).

However, the Co-Electrolyzer used in the directCCE project operates in an alkaline environment. While the overall reaction remains the same, the half-reactions involve the exchange of OH^- ions [12] :

Cathode

$$2\,H_2O + 2\,e^- \longrightarrow H_2 + 2\,OH^- \tag{2.7}$$
$$CO_2 + H_2O + 2\,e^- \longrightarrow CO + 2\,OH^- \tag{2.8}$$

Anode

$$4\,OH^- \longrightarrow 2\,H_2O + O_2 + 4\,e^- \tag{2.9}$$

2.1.4. Thermodynamics fundamentals for Electrochemical cells

According to the first law of Thermodynamics 2.10, there exists a form of energy, known as internal energy U^*, which is an intrinsic property of a system [19]. In a closed system, the change in internal energy is determined by the heat transferred and the work performed on the system. :

$$dU^* = dQ + dW \tag{2.10}$$

From the introduction of internal energy, two types of energy arise that are useful for the description of the thermodynamic aspects of electrochemical systems : enthalpy H and Gibbs free energy G.

$$H = U^* + pV$$
$$G = H - TS$$

with p, T, V representing the pressure, temperature and volume of the system. S is the entropy function of the system. Enthalpy takes into account internal energy, but also the energy associated with the work done by the system against the ambient pressure when the volume changes. It is therefore mainly used in processes at constant pressure. The Gibbs free energy G is the maximum technical work that a system can perform when it transitions from one equilibrium state to another at constant temperature constant and constant pressure, in particular through electrochemical process. This free energy is particularly useful in electrochemistry. [19]

In a general multi-component system with N components, the Gibbs fundamental equation is defined as :

$$dG = -SdT + Vdp + \sum_{i=1}^{N} \mu_i dx_i \tag{2.11}$$

μ_i is called the chemical potential of species i. It indicates how much the Gibbs energy of a system increases during a quasi static state change solely due to material transport when one mole of substance i is added to the system. [19]

At constant temperature and pressure, the Gibbs energy of a system at equilibrium remains unchanged, meaning its derivative is zero, therefore :

$$\sum_i s_i \mu_i = 0 \tag{2.12}$$

with s_i stoichiometric coefficient of the chemical species i.

2.1.5. Cell potential

When each electrode's half-cell reaction is at equilibrium at steady-state, no net anodic or cathodic reactions occur. Therefore, charge transfer ceases at the electrode surfaces and no current flows in the cell. Since electrons are involved in both half-cell reactions, their energy in each conductor is governed by the reaction equilibrium at the respective electrode, resulting in different electrical potentials for each electrode. This electrical potential difference between both electrodes at equilibrium is called the thermodynamic equilibrium cell potential U. [28]

For a closed reversible system at equilibrium, under fixed temperature and pressure conditions, the electrical work given by the full-cell to the surroundings W_{el} is given by the first law of Thermodynamics 2.10 considering the variation in Gibbs energy G :

$$\Delta G = -W_{el} \tag{2.13}$$

The variation of Gibbs energy for the full-cell chemical reaction 2.2 is given by the difference between the Gibbs free energy of formation, noted ΔG_f, of the products and reactants, which can be found in standard experimental tables.

A charge balance indicates that the total amount of transferred charges in the full reaction is nF, with n the number of moles of electrons in the balanced full-cell equation. F is the Faraday's constant which is the number of Coulombs per mole of electrons [28]. Since the electric potential energy of a charged system is given by the product of its charge and its own electric potential, equation 2.13 for the cell at equilibrium becomes :

$$\Delta G = -nFU \tag{2.14}$$

Equation 2.14 links then actual chemical cell equilibrium to the equilibrium cell potential U.

By convention, the equilibrium cell potential U is defined positively. Thus, the equilibrium cell potential can also be expressed as the difference between the equilibrium potential of the electrode with the highest potential U^+ and that of the electrode with the lowest potential U^-.

$$U = U^+ - U^- \tag{2.15}$$

The equilibrium cell potential U is defined when no current flows in the system. The cell behaves as if the external circuit were open, U is also known under the name *open-circuit potential*.

2.1.6. Faradaic Process

When electrons are transferred across the metal-solution interface, oxidation or reduction takes place as described by the general half-cell equation 2.1. Consequently, materials are generated and consumed at the surface of each electrode.

Equation 2.1 can be generalized in a more global half-cell reaction :

$$\sum_i s_i A_i = ne^- \tag{2.16}$$

with s_i stoichiometric coefficient of the chemical species A_i, rather positive or negative. n is the number of electrons transferred in the half-cell reaction.

From a charge balance the global number of charges can be determined from the progress of reaction :

$$Q = F \times \text{number of mol of electrons} = Fn\frac{n_i}{|s_i|} \tag{2.17}$$

This leads to the number of mole of species A_i that are consumed or produced. This equation is known as the Faraday's law :

$$n_i = \frac{Q}{F\frac{n}{|s_i|}} \tag{2.18}$$

Faraday's Law states that the extent of a chemical reaction caused by an electric current is directly proportional to the amount of charge transferred.[29]

Faraday's Law defines the faradaic efficiency as the ratio of the actual mass of the product obtained to the theoretical mass calculated based on the current [28]. By differentiating equation 2.18 with respect to time :

$$\eta_f = \frac{\dot{m}_i}{IM_i/nF} \tag{2.19}$$

It is worth noting that under certain conditions, an electrode-solution interface may exhibit a potential range where no charge-transfer reactions take place due to thermodynamic or kinetic constraints. However, processes like adsorption and desorption can still occur, and the structure of the electrode-solution interface may change with variations in potential or composition. This processes are called nonfaradaic processes. [29]

2.1.7. Reference electrode and Standard Potential

It has been discussed in section 2.1.5 that the equilibrium cell potential U is defined as the potential difference between each electrodes with respective half-cell reaction at equilibrium. Some half-cells are standardized and known as reference electrode.

Since only potential differences between two electrodes can be measured, the hydrogen electrode under standard conditions 2.1 is selected as the absolute reference potential. The standard hydrogen electrode (SHE) is assigned a value of $U^\theta = 0\text{V}$, and all other electrode potentials are measured relative to it. [10]

$2\,\text{H}^+\,(\text{aq}) + 2\,\text{e}^- \longleftrightarrow \text{H}_2\,(\text{g})$
Activities of species equal to 1 (p=1atm, pH=0)
Standard temperature of $25°C$
Flat platinium electrode

Table 2.1.: *Standard condition for the definition of SHE [29]*

The potential difference between the two electrodes, where the half-cell reaction of interest and the hydrogen electrode are in equilibrium under standard conditions, is referred to as the standard potential of the half-cell reaction. The standard potentials of the various half-reactions are listed in experimental tables. The standard potential of the overall cell reaction can then be calculated from the standard potentials of the two half-cell reactions (relative to the SHE) as follows:[28] :

$$U^\theta_{cell} = U^\theta_{+/SHE} - U^\theta_{-/SHE} \tag{2.20}$$

The cell standard potential is by convention defined positive as explained in section 2.1.2. In a closed circuit, the electrons will naturally migrate towards the electrode with the highest electric potential (negative charge attracted by the highest positive potential). Therefore, electrons are generally consumed at the electrode with the highest equilibrium potential relative to SHE, resulting in reduction. Conversely, the electrode

with the lowest equilibrium potential will produce electrons, leading to oxidation.

Although the standard hydrogen electrode offers a stable potential, maintaining a consistent solution composition under such conditions is difficult and requires safety precautions. **??**. As a result, secondary reference electrodes are commonly used for comparison, offering ease of handling and less stringent conditions compared to the SHE.. These electrodes consist of a metal electrode in contact with a sparingly soluble salt, which regulates the activity of the metal ion. [10] Some reference electrodes that are often used to carry out measurements and have stable potential are listed in table 2.2.

Half-cell	Reference Solution	Reaction at electrode	Pot. vs SHE (V)
$Ag\|AgCl\|Cl^-$	$a_{Cl^-} = 1$	$AgCl + e^-$	+0.224
Silver/Silver chloride	saturated KCl	$\longleftrightarrow Ag + Cl^-$	+0.1976
	KCl (c=1mol/L)		+0.2368
	KCl (c=0.1mol/L)		+0.2894
$Hg\|Hg_2Cl_2\|Cl^-$	$a_{Cl^-} = 1$	$Hg_2Cl_2 + 2\,e^-$	+0.2682
Calomel electrode	saturated KCl	$\longleftrightarrow 2\,Hg + 2\,Cl^-$	+0.2415

Table 2.2.: *Equilibrium potentials for secondary reference electrodes*

For measuring cell properties during tests and designing a 16 cm^2 cell suitable for spectrometric analysis, an Ag/AgCl electrode is used due to the availability of its components and its simple design.

The half-reactions occurring within the co-electrolysis cell that converts chemically absorbed CO2 into syngas are summarized in the table 2.3 .The standard potential relative to the SHE of the electrode where the reaction of oxygen into water occurs is more positive than those of the reaction of CO_2 into CO and water into H_2 at the other electrode. When the circuit is closed under standard conditions, O_2 is naturally reduced to water, while H_2 and CO are oxidized into protons and CO_2.

Reactions	**Standard potential U^θ (V)**
$2\,H^+ + 2\,e^- \longrightarrow H_2$ (pH=0)	0
$CO_2 + 2\,e^- + 2\,H^+ \longrightarrow CO + H_2O$ (pH=0)	-0.11 [33]
$2\,H_2O \longrightarrow O_2 + 4\,H^+ + 4\,e^-$ (pH=0)	1.229

Table 2.3.: *Standard potentials of reactions in a co-electrolysis cell*

2.1.8. Types of electrochemical cells

Electrochemical cells are flowing are divided into two categories: galvanic cells or electrolytic cells. The differences are explained in table 2.4.

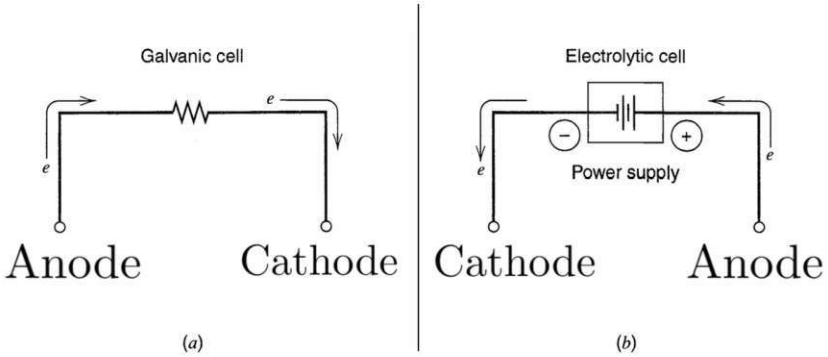

Figure 2.3.: *Schemes of current circulation in (a) Galvanic cell (b) Electrolytic cell [29]*

Galvanic Cell	**Electrolytic Cell**
- The reactions occur spontaneously at the electrodes when they are connected externally by an electron conductor	- The reactions are affected by the imposition of an external voltage greater than the open-circuit potential of the cell U
- Measured cell voltage $V_{cell} < U$	- Measured cell voltage $V_{cell} > U$
- Often employed in converting chemical energy into electrical energy	- Generally employed to carry out desired chemical reactions by using electrical energy
- General application in non-rechargeable cells, rechargeable cells, fuel cells	- General application in electrolytic syntheses, electro-refining, electro-plating

Table 2.4.: *Comparison between Galvanic and Electrolytic Cells [29]*

As described in section 2.1.7, a combined H^+/H_2 and CO_2/CO electrode in contact with an H2O/O2 electrode will naturally tend to oxidize CO into CO_2 and reduce O_2 into H_2O. To reverse the direction of the reaction and reduce CO_2 into CO, the application of an external voltage higher than the cell's equilibrium potential is required.

Applying a voltage to a cell to alter the direction of the reaction essentially involves modifying the potential at each electrode, moving it away from the equilibrium poten-

tial associated with the half-reaction. Increasing the potential at an electrode relative to its equilibrium potential increases its electron-attracting capability. If equilibrium is disrupted, the system will favor oxidation at the electrode to counteract the change and restore balance (Le Chatelier's principle). Conversely, decreasing the electrode potential relative to its equilibrium potential reduces its electron-attracting capability, and the reduction reaction is favored.

In this context, the electrolysis of CO_2 into CO occurs when the electrode potential is decreased relative to its equilibrium potential. To achieve this, the electrode involved in the reduction of the absorbed CO2 solution must be connected to the negative pole (-) of an external voltage supply. This electrode therefore serves as the cathode of the Co-electrolysis cell. On the other side, the electrode responsible for the oxidation of water must be connected to the positive pole (+) of the external voltage supply. This electrode thus serves as the anode of the Co-electrolysis cell.

The difference between the actual potential of an electrode and its equilibrium potential U (both measured relative to the same reference electrode) is defined as surface overpotential, noted η_s :

$$\eta_s = V - U \tag{2.21}$$

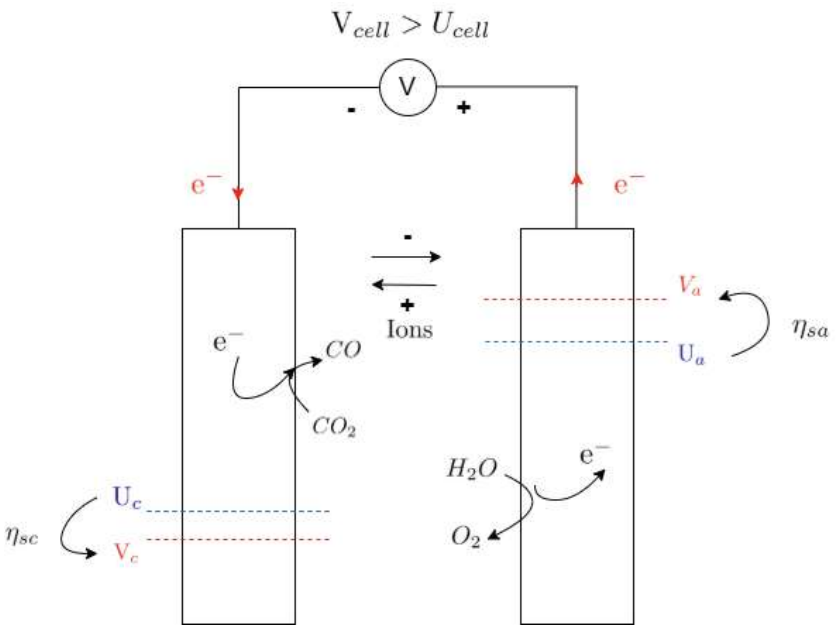

Figure 2.4.: *Charge circulation in a Co-Electrolysis cell*

A key element for electrochemical systems analysis is to find the relationship between the current and the potential. In other words, it means finding the corelation between

the reaction rate (I) of the electrochemical system and the driving force (V). For better comparability between electrochemical cells, the current passing through the cell is often normalized by its active surface area. Consequently, there is a tendency to establish the relationship between potential V and current density i. The function between the current density and the potential is often represented in a current-voltage curve.

Two different approaches in order to find the relationship between the current and the potential are distinguished for electrochemical system's analysis [29] :

- Potentiostatic mode, where the potential difference between both electrodes is maintained constant and the variation of current flowing in the cell is measured.
- Galvanostatic mode, where the current flowing in the cell is maintained constant and the variation in the potential difference between both electrodes is measured.

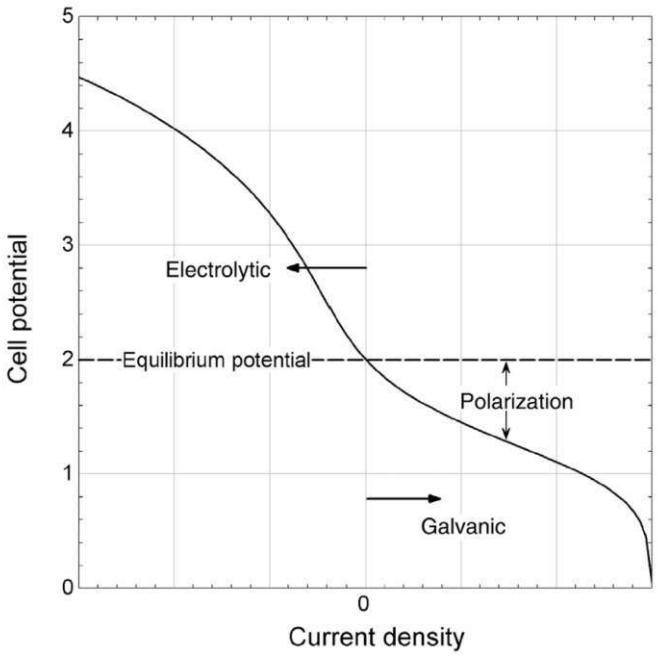

Figure 2.5.: *Representative relationship between current and potential at steady-state. The dividing line between galvanic and electrolytic is at current density of zero. [28]*

2.2. Relationship between Voltage and Current

There are different source of losses in an electrolytic type cell [28] :

$$V_{cell} = U_{cell} + |\eta_{s,anode}| + |\eta_{s,cathode}| + |\eta_{conc,anode}| + |\eta_{conc,cathode}| + |\eta_{ohmic}| \quad (2.22)$$

U_{cell} is the equilibrium potential of the cell and is determined thermodynamically. $\eta_{s,anode}$ and $\eta_{s,cathode}$ are the surface over-potentials of each half-cell reactions at the anode and cathode. They are depending on the kinetics of reactions at each electrodes. $\eta_{conc,anode}$ and $\eta_{conc,cathode}$ are the concentrations over-potentials and account for concentration gradient effects at the electrode.

2.2.1. Impact of Thermodynamics on the Cell Potential

Temperature Influence on the Cell Potential

The Gibbs energy G has been introduced in section 2.1.4. According to Gibbs' fundamental law, at constant pressure and a fixed number of moles, the derivative of the Gibbs free energy with respect to temperature is equal to the negative value of the system's entropy:

$$\frac{\partial G}{\partial T}\Big|_p = -S \quad (2.23)$$

Considering equation 2.14 at standard conditions, the derivative of the standard potential U^θ with respect to temperature is determined:

$$\frac{\partial U^\theta}{\partial T}\Big|_p = \frac{\Delta S^0}{nF} \quad (2.24)$$

Assuming that ΔS does not change significantly over the temperature range of interest, it follows that [28] :

$$U^0_{cell}(T) = U^\theta_{cell} + (T - 25°C) \times \frac{\Delta S^0}{nF} \quad (2.25)$$

Influence of Educts Pressure and Concentration on the Cell Potential

The Gibbs energy change ΔG for the reaction is determined through the Gibbs energy change for the reaction at standard conditions ΔG^0 :

$$\Delta G = \Delta G^0 + RTln \prod a_i^{s_i} \quad (2.26)$$

with a_i the activity of species i and s_i the associated stoichiometric coefficient. Combining equation 2.26 with equation 2.14 yields :

$$U_{cell} = U^\theta_{cell} - \frac{RT}{nF} ln \prod a_i^{s_i} \quad (2.27)$$

This equation which express the equilibrium potential U_{cell} with the standard potential U^θ_{cell}.

$$U_{cell} = U^{\theta}_{cell} - \frac{RT}{nF} ln \prod_i \left(\frac{c_i}{c_i^0}\right)^{s_i} \left(\frac{p_i}{p_i^0}\right)^{s_i} \tag{2.28}$$

2.2.2. Impact of Surface Overpotential on Reactions Kinetics

This section will define the origin of potential losses relative to the half-reaction occurring on the electrode surface when a current flows through the cell.

Double layer

A metal electrode in an electrolyte solution typically carries a charge, even at equilibrium. Excess charge accumulates on the outer surface of the electrode, near the electrode-electrolyte interface. Consequently, charged species in the electrolyte solution align at the interface to counterbalance the electrode's excess charge. This interaction leads to the formation of a double layer. [28].

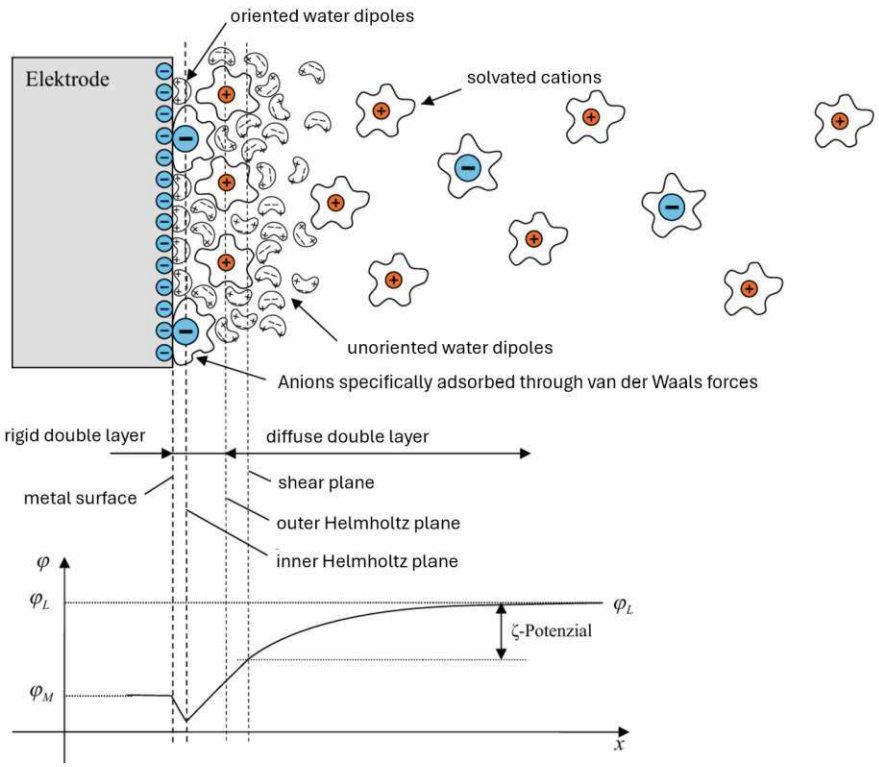

Figure 2.6.: *Description of electrical double layer [10]*

The double layer is a complex structure composed of distinct regions, with solvent molecules playing a crucial role in their formation. In most cases, water serves as the

solvent. Polarized water molecules surround the ions in solution, forming a hydration layer or sheath. [28]

1. The first structure is known as the *inner Helmholtz plane* (IHP). It is defined as the position of the centers of ions or molecules that directly adsorb onto the electrode surface. This region also contains water molecules due to their dipole nature. For an ion to adsorb directly onto the surface, it must at least partially shed its hydration shell. Negatively charged ions (anions) generally hydrate less strongly than positively charged ions (cations) and are therefore more commonly found in the inner Helmholtz plane.[28]

2. The next structure is known as the *outer Helmholtz plane* (OHP). It represents the closest approach of solvated ions to the electrode surface, where the solvent sheath prevents direct adsorption. Its position is determined by the radius of the largest solvated ions, including their hydration shell, which is approximately $0.2nm$.

3. The final structure is called the diffuse double layer. It contains both positive and negative charges, with the excess charge gradually diminishing as the distance from the OHP increases, eventually reaching electrical neutrality on the solution side. The thickness of the diffuse double layer is dependent of the species concentration in the solution, given by the Debye length function :

$$DL = \sqrt{\frac{\epsilon RT}{F^2 \sum z_i^2 c_{i,bulk}}} \tag{2.29}$$

with ϵ the permittivity of the solution.

The depicted separation of the charges accross the double-layer is associated with a capacitance. High concentration of ions in the solution leads to a constant double layer capacity using the parallel plate capacitor model [10] :

$$C_{dl} = \frac{\epsilon_0 \epsilon_r A}{d} \tag{2.30}$$

with A area surface of the electrode, d the plate distance which is the OHP. ϵ_0 and ϵ_r are respectively the permittivity of free space and relative permittivity of water.

The composition of this double layer is particularly important in electrochemistry as it influences charge transfer at the surface and reaction kinetics.

Reaction rate and current density

Returning to the half-cell equation 2.1, both the forward (reduction) and reverse (oxidation) reactions involve overcoming an activation energy barrier to reach a transition state (i.e., an activated complex). This transition state represents the peak of the energy

curve. The rate of the reduction reaction can be expressed as a function of the reactant concentration and a rate constant k_f, which depends on the Gibbs energy difference under standard conditions, ΔG^I, between the initial reactants and the transition state [28]. This rate k_f provides the proportion of ions that can reach the transition state following a Boltzmann distribution :

$$r = k_f c_O = k_f^0 c_O \exp \frac{-\Delta G^I}{RT} \tag{2.31}$$

where c_O is the concentration of oxidant in the solution.

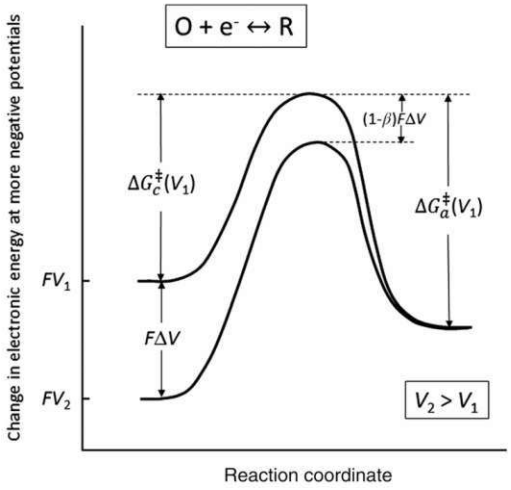

Figure 2.7.: *Change in energy associated with reaction at an electrode surface [28]*

The energy required for oxidation is denoted as ΔG_a^I, while the energy required for reduction is ΔG_c^I. An increase in potential from V_1 to V_2 shifts the energy of an electron in the oxidized state relative to the reduced state by $-F(V_2-V_1)$, as described in equation 2.14. This change also affects the activation energy for both reaction pathways, reducing it by $(1-\alpha)\Delta V$. Reaction rate for reduction is then :

$$\frac{i_c(V_2)}{F} = -r_c(V_2) = k_c^0 c_O \exp - \frac{\Delta G_c^I(V_1) + \alpha F(V_2 - V_1)}{RT} \tag{2.32}$$

The same logic can be applied for oxidation :

$$\frac{i_a(V_2)}{F} = r_a(V_2) = k_a^0 c_R \exp - \frac{\Delta G_a^I(V_1) - (1-\alpha) F(V_2 - V_1)}{RT} \tag{2.33}$$

The exchange-current density value at equilibrium, i_0, is defined considering $k_c = k_c^0 \exp -(\Delta G_c(0)/RT)$, which is the value reached by $-i_c(U) = i_a(U)$:

$$\frac{i_0}{F} = -k_c c_0 \exp - \frac{\alpha F V}{RT} = k_a c_R \exp \frac{(1-\alpha) F U}{RT} \tag{2.34}$$

The expression known as the *Butler-Volmer equation* (BV) for current density depending on the surface overpotential η_s is then obtained by combining 2.32, 2.33 and 2.34 :

$$i = i_c + i_a = i_0 \left[\exp\left(\frac{\alpha F \eta_s}{RT}\right) - \exp\left(-\frac{(n-\alpha)F\eta_s}{RT}\right)\right] \tag{2.35}$$

α is called the transfer coefficient, it is a measure of the symetry barrier [29]. In most systems, α typically ranges between 0.3n and 0.7n, where n represents the number of electrons transferred in the half-reaction. Both α and i_0 are empirical parameters.

For large values of η_s, the BV equation 2.35 can be inverted to find the expression of the potential as a function of the current density (for surface over-potential η_s values greater than $0.1V$). This relationship is known as the Tafel approximation :

$$\eta_s = \frac{RT}{\alpha F} \ln i - \frac{RT}{\alpha F} \ln i_0 \tag{2.36}$$

The Tafel approximation 2.36 quantifies the losses depending of the kinetics at each electrodes. In practice, the Tafel equation is typically expressed using the base-10 logarithm..

$$\eta_s = \frac{2.303RT}{\alpha F} \log i - \frac{2.303RT}{\alpha F} \log i_0 \tag{2.37}$$

The Tafel approximation 2.37 is particularly useful for determining the exchange current density i_0 for each half-cell reaction. This is achieved by plotting the surface overpotential η_s as a function of the logarithm of the current density $\log i$. The curve exhibits two linear regions: one for low values of i and another for high values of i. When plotting this curve, the tangent to the linear region corresponding to high i values intersects the x-axis at the value of $\log i_0$.

Exchange-current density

The exchange current density i_0 represents the rate per unit area of the forward and reverse reactions for a specific half-cell equation at equilibrium, where the net current is zero. Reactions with higher exchange current densities proceed more readily and results in higher current densities for a given overpotential. Therefore, when two reactions occur simultaneously, such as in Co-Electrolysis where CO_2 and water reduction take place at the cathode, the reaction with the higher exchange current density is more likely to dominate at the electrode. The value of i_0 for a given reaction can vary significantly depending on various parameters. [28] :

1. Electrode's surface state and material
2. Temperature, parameter for which i_0 follows an Arrhenius law with a certain energy activation E_a and fixed coefficient A

$$i_0(T) = A \exp -\frac{E_a}{RT} \tag{2.38}$$

The higher the system temperature, the more i_0 increases, thus favoring the reaction

3. Species surface concentration, that can be estimated from a measured reference exchange-current density with in know steady state

$$i_0 = i_{0,ref} \left(\frac{c_O}{c_{O,ref}} \right)^{\gamma_O} \left(\frac{c_R}{c_{R,ref}} \right)^{\gamma_R} \tag{2.39}$$

The concentration exponents γ_O and γ_R can be determined either through a mechanistic analysis of the reaction or by measuring i_0 at varying concentrations. [28]

2.2.3. Impact of mass-transfer on ohmic and concentration over-potential

The overpotential losses associated with the ohmic drop and the concentration variations of the active species at the electrode surface are now analyzed.

The current density is related to the charged species' flux in the electrolyte N_i through Faraday's law [28]:

$$i = \sum_i z_i N_i \tag{2.40}$$

with z_i the charge of species (positive or negative). N_i is given by the Nernst-Planck equation for electrochemical flux

$$N_i = \underbrace{-z_i u_i F c_i \nabla \phi_i}_{\text{Migration}} \underbrace{- D_i \nabla c_i}_{\text{Diffusion}} + \underbrace{c_i v}_{\text{Convection}} \tag{2.41}$$

The electrochemical flux is a combination of three terms, each accounting for a physical mass transport phenomenon [28].

- Migration refers to the transport of ions driven by a gradient in electrical potential. This motion is caused by an external electric field, specifically the field created by the potential difference across the electrolyte. The ion mobility, u_i, represents the velocity of an ion in the solution when subjected to a uniform electric field.
- Diffusion refers to the transport of chemical species driven by a concentration gradient, causing them to move from regions of higher concentration to regions of lower concentration. The diffusion coefficient, D_i, characterizes the rate at which a species diffuses through the solution.
- Convection refers to transport driven by the overall movement of the electrolyte, where v represents the velocity of the electrolyte.

Ohmic loss

In the case of electrochemical flux driven solely by migration, the transport can be described using the Nernst-Planck equation 2.41 with Faraday's law 2.40 :

$$i = -F^2 \nabla\phi \sum_i z_i^2 u_i c_i \tag{2.42}$$

Defining $\kappa = F^2 \sum z_i^2 u_i c_i$ the electrical conductivity of the electrolyte, the ohmic drop is induced from equation 2.42 :

$$\eta_{ohmic} = \frac{l}{\kappa} i \tag{2.43}$$

with l typical length of the electrolyte. The typical characteristic of Ohm's law is observed, which dictates that the relationship between current and voltage is linear.

Concentration Overpotentials

The concentration-dependent version of the Butler-Volmer equation 2.35 provides an estimate for the concentration over-potential drop formula [10]:

$$\eta_{conc} = \frac{RT}{nF} \ln \prod_i \frac{c_{i,bulk}^{s_i}}{c_{i,surf}^{s_i}} \tag{2.44}$$

with $c_{i,surf}$ and $c_{i,bulk}$ concentrations of the species at the surface and in the bulk solution, s_i stoichiometric coefficient.

To determine the concentration overpotential as a function of current, we start by considering the Nernst-Planck equation 2.41, focusing exclusively on the diffusion term. This is then combined with Faraday's law 2.40 to establish the relationship :

$$i = -nFD \frac{c_{i,bulk} - c_{i,surf}}{\delta} \tag{2.45}$$

with δ the diffusion layer thickness. The limiting current density i_{lim} occurs in the extreme case where the concentration of the reactive species at the electrode surface drops to zero. This results in an insufficient supply of the species to sustain the reaction.

$$i_{lim} = -nFD \frac{c_{i,buk}}{\delta} \tag{2.46}$$

Thus, combining equation 2.45 and 2.46 in the concentration difference over-potential formula 2.44 [10] :

$$\eta_{conc} = \frac{RT}{nF} \ln \left(1 - \frac{i}{i_{lim}}\right) \tag{2.47}$$

2.2.4. Summary

It might be observed that several factors influence the different electrical over-potentials. These factors account for various loss mechanisms. When a voltage is applied, various factors resist the flow of current within the cell. This resistance is directly related to the opposition these factors create against current generation. A method to distinguish and evaluate the various sources of resistance is necessary to conduct a cell optimization analysis. One possible method is impedance spectrometric analysis, the basic concepts of which are presented in the next paragraph.

Losses type	Surface reaction	Ohmic	Concentration Difference
$\eta(i)$	$\frac{2.303RT}{\alpha F}\log i - \frac{2.303RT}{\alpha F}\log i_0$	$\frac{l}{\kappa}i$	$\frac{RT}{nF}\ln\left(1-\frac{i}{i_{lim}}\right)$

Table 2.5.: *Summary of the different sources of losses and its values*

2.3. Notion of Impedance

In the field of electrical engineering, the concept of resistance is the ability of a circuit element to resist the flow of electrical current. [2] The resistance is defined after Ohm's law as the ratio of voltage V and current I applied to the circuit element:

$$R = \frac{V}{I} \tag{2.48}$$

This relationship is in fact limited to only one circuit element, which is the ideal resistor. An ideal resistor is defined mainly trough 3 simplified properties [2]:

(a) An ideal resistor follows Ohm's law at all current and voltage values.
(b) The resistance value of the ideal resistor is independent of frequency.
(c) AC (Alternating Current) current and voltage signals are in phase with each other.

In reality there are circuit elements that exhibit much more complex behavior. Instead of the concept of resistance the notion of impedance is used for a more general circuit parameter. Like the resistance, impedance is a measure of the ability of a circuit to resist the flow of electrical current, but unlike the resistance, it is not limited by the 3 simplifying properties [2].

Analogous to Ohm's Law, using time-dependant expressions for E and I the impedance of a system can be defined as [4] :

$$Z = \frac{V(t)}{I(t)} \tag{2.49}$$

2.4. Linear System

Generally two types of signal are distinguished in electronics. The first type is the DC (Direct Current) signal where the voltage or current propagates in one way with a constant value over time. The second one is the AC (Alternating Current) signal which direction of propagation changes periodically.

A simple AC signal is expressed as a function of time with a sinusoidal shape [2] :

$$X(t) = X_0 \sin(\omega t) \tag{2.50}$$

AC signals are thus characterised by their amplitude X_0 and and linear frequency f expressed in Hz. The radial frequency ω from equation 2.50 and the linear frequency are linked by the relation $\omega = 2\pi f$.

A linear system in electronics is defined as an entity that, when an excited potential $E(t)$ with a sinusoidal form is applied, returns a current response signal $I(t)$ which also has a sinusoidal form [2]. This response signal has however a different amplitude, and is shifted in phase :

$$V(t) = V_0 \sin(\omega t) \Rightarrow I(t) = I_0 \sin(\omega t + \phi) \tag{2.51}$$

with E_0 the potential's amplitude, I_0 current's amplitude and ϕ the shifted phase. The radial frequency ω remains the same for both signals.

Plotting the E-I response curve for a linear system gives the Lissajous plot [3].

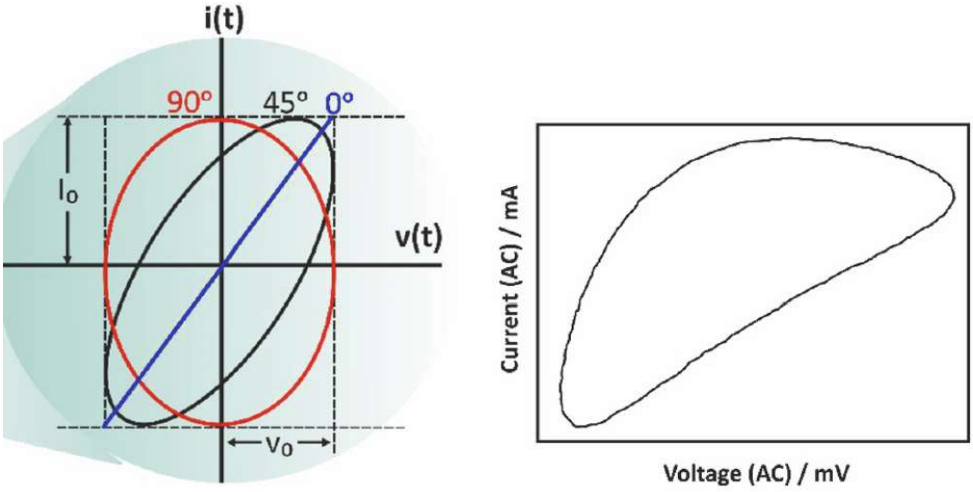

Figure 2.8.: *Comparison between Lissajous plots : linear (left) and non linear (right) [3]*

Depending on the magnitude of the signals and the phase difference between them, an oval plot is obtained. It turns out that when the phase difference is 0° or 90°, the plot appears as a diagonal or circle. For a non linear system, the shape of the plot is distorted. [3]

The Impedance's Equation 2.49 can be applied particularly to a linear system keeping the same parameters as before :

$$Z = \frac{V_0 \sin(\omega t)}{I_0 \sin(\omega t + \phi)} \tag{2.52}$$

A more practical computational approach is to use complex numbers through Euler's equation 2.53, which expresses cosine and sine functions as complex exponentials. Impedance analysis comes down to analyzing the real and imaginary parts :

$$\exp j\Phi = \cos(\Phi) + j \sin(\Phi) \tag{2.53}$$

The impedance for a linear system is thus defined through equations 2.52 and 2.53:

$$Z(\omega) = Z_0 e^{j\phi} = |Z|(\cos(\phi) + j \sin(\phi)) = Z' + jZ'' \tag{2.54}$$

with Z' and Z'' respectively real and imaginary part of $Z(\omega)$. $|Z|$ or Z_0 is called magnitude of $Z(\omega)$, and ϕ the phase (or argument) of $Z(\omega)$.

The complex impedance definition for $Z(\omega)$ in 2.56 allows a graphical representation for different values of ω where the real part Z' is plotted on the X-axis and the inverse of the imaginary part, $-Z''$, on the Y-axis. This representation is known as the Niquist Plot [2].

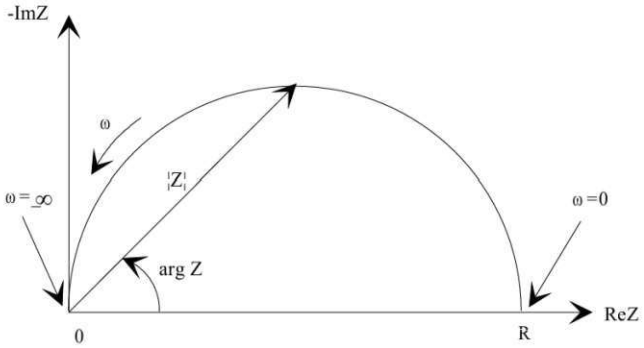

Figure 2.9.: *Example of a Niquist Plot [2]*

On the Nyquist Plot, the impedance can be represented as a vector of length $|Z(\omega)|$. The angle between this vector and the X-axis is the phase angle $arg(Z(\omega)) = \phi$ [2].

However, the Nyquist plot has the drawback of not providing the frequency of a specific point on the curve in a directly readable manner. A Nyquist Plot is often complemented by a Bode diagram, where the impedance is plotted with log frequency on the X-axis and both the magnitude $|Z|$ and the phase-shift ϕ on the Y-axis [2].

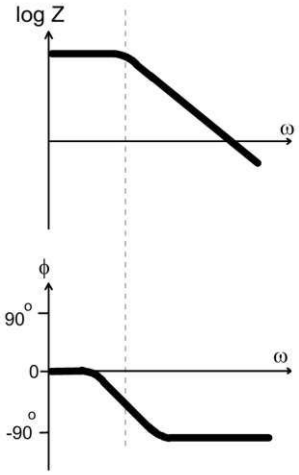

Figure 2.10.: *Example of a Bode Diagram [2]*

2.5. Properties of a linear system

2.5.1. Signal Superposition

If the Input is a weighted sum of several signals, then the output is the superposition, that is the weighted sum of the responses of the linear system to each of the signals [2]. With $y_1(t)$ the answer to the signal $x_1(t)$, and $y_2(t)$ the one to $x_2(t)$ [2]:

(a) $y_1 + y_2$ is the response to $x_1 + x_2$

(b) ay_1 is the response to ax_1

2.5.2. Impedance in series

Several linear systems connected in series form a linear system, and its equivalent impedance is the sum of the impedance of all subsystems.

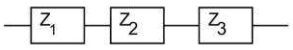

Figure 2.11.: *Impedance in serie [2]*

$$Z_{eq} = Z_1 + Z_2 + Z_3 \tag{2.55}$$

2.5.3. Impedance in parallel

Several linear systems connected in parallel form a linear system, and the inverse of its equivalent impedance is the sum of all subsystems impedance's inverse.

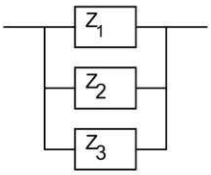

Figure 2.12.: *Impedance in parallel [2]*

$$\frac{1}{Z_{eq}} = \frac{1}{Z_1} + \frac{1}{Z_2} + \frac{1}{Z_3} \tag{2.56}$$

2.6. Common linear systems

A linear system is generally and composed by an arrangement of three simple passive elements.

Name	Electrical Symbol	Complex Impedance $Z(\omega)$
Resistor	R	R
Capacitor	C	$\frac{1}{jC\omega}$
Inductor	L	$jL\omega$

Table 2.6.: *Three simple passive elements composing linear systems*

All of those three elements have different influences on a system. The resistor R limits or control the current (flux of charges) in the circuit. For this purpose it dissipates the incoming energy in the form of heat. The capacitor C stores charges passing through. It stores the energy in the form of an electrical field. Finally the inductor L has the ability to resist to current variations. It stores the energy in the form of a magnetic field.

Each of those simple elements have associated characteristic Niquist plot and Bode diagrams.

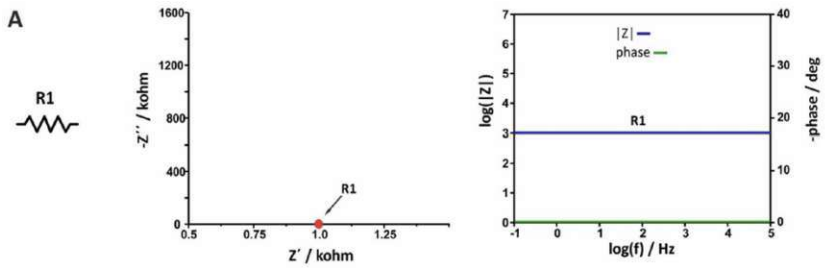

Figure 2.13.: *Niquist Plot and Bode Diagram for the Resistor R [3]*

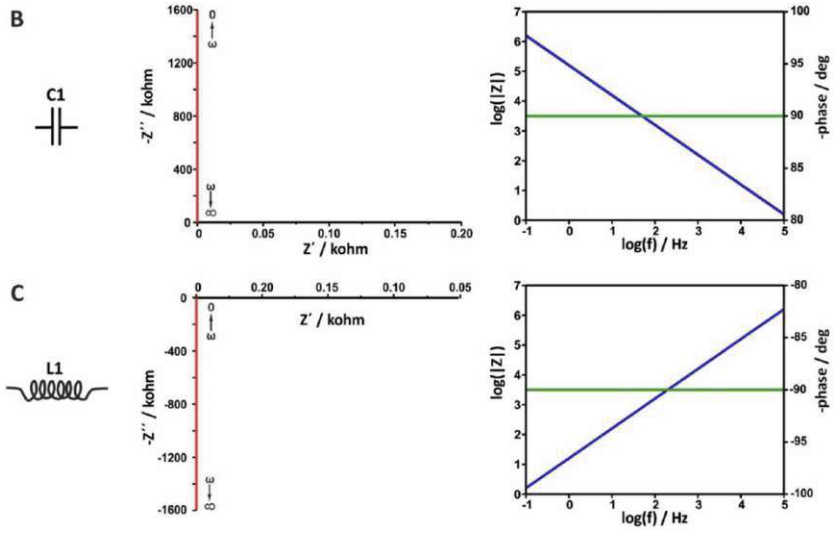

Figure 2.14.: *Niquist Plot and Bode Diagram for the Capacitor C and the Inductor L [3]*

The characteristic Niquist plot for a resistor is a point because its impedance is constant to R and doesn't vary with ω. Both impedances for Capacitor C and Inductor L are imaginary numbers depending on ω, thus the Niquist Plot is the positive part for the Y-axis for C and the negative part for L.

Different configurations of electrical elements can be used to model electrochemical systems.

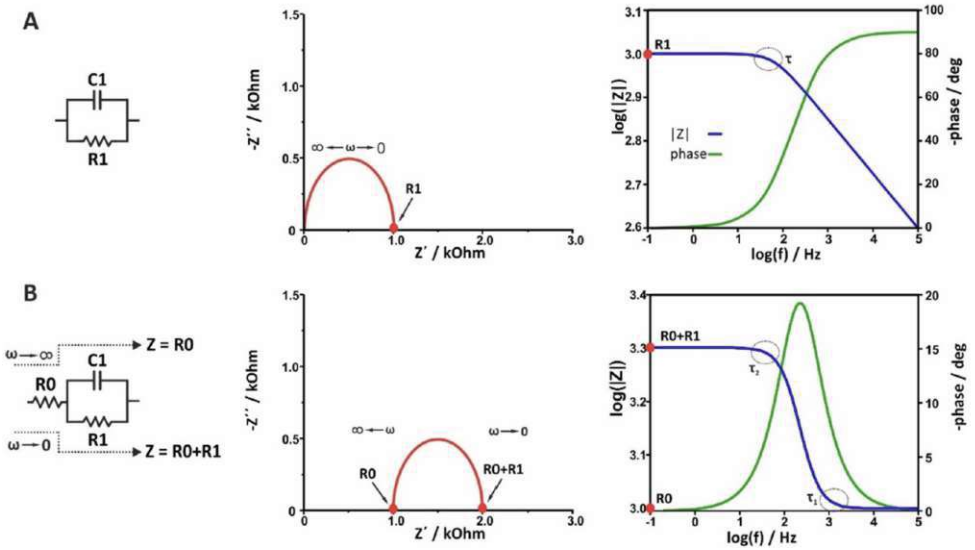

Figure 2.15.: *Niquist Plot and Bode Diagram for a Resistor R in parallel with a Capacitor C [3]*

The circuit with resistor R in parallel with capacitor C (noted $R//C$) is the most commonly found circuit in the analysis of electrochemical systems. The impedance Z of the $R//C$ circuit is derived from the properties described in part 2.5 :

$$Z(\omega) = \frac{1}{\frac{1}{R} + j\omega C} = \frac{R}{1 + (\omega RC)^2} - j\frac{\omega R^2 C}{1 + (\omega RC)^2} \tag{2.57}$$

The Nyquist plot of the system describes a semi-circle which radius is the value of the resistor R. The high frequency intercepts the value of the frequency-independent contribution, noted R_0 in Figure 2.15. The low-frequency intercept gives $R_0 + R_1$. A very useful property is that the maximum of the imaginary part, i.e, the peak of the semicircle, is reached at a characteristic radial frequency $\omega_c = \frac{1}{RC}$. [4]

2.7. Application to Electrolysis Cell

As described in section 2.2, several factors hinder the creation of current in an electrolytic cell. In fact, each source of loss can be assimilated to an electrical circuit. This analogy between electrochemical impedance and electrical impedance enables the analysis of electrochemical systems through spectrometric analysis. This section will present the different resistance values and their representation in the Niquist diagram.

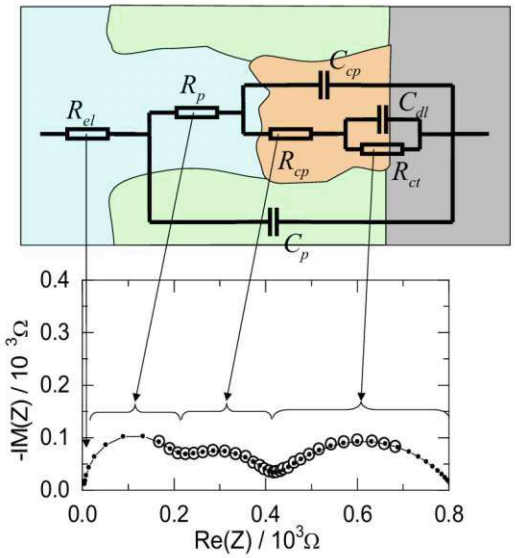

Figure 2.16.: *Example of electrochemical system's equivalent circuit [10]*

2.7.1. Application Conditions

It has been introduced in section 2.4 that impedance analysis can only be conducted on linear systems. An electrochemical system, however, does not constitute a linear

system due to its complexity. An electrochemical system is considered pseudo-linear, meaning that locally, at a fixed point on the voltage-current curve, the system behaves linearly. Impedance analysis can therefore be conducted around specific voltage and current points by applying a small-amplitude analysis voltage, ensuring the signal remains within the valid range.

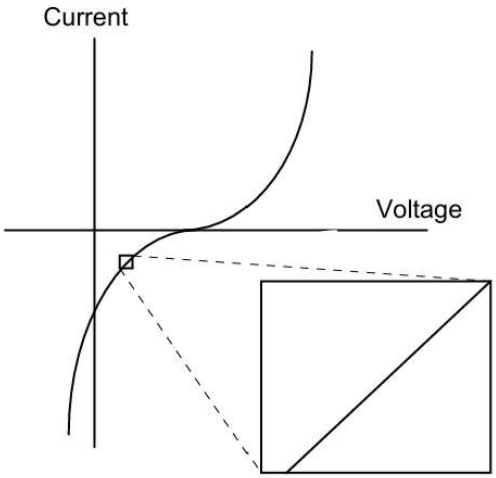

Figure 2.17.: *Pseudo-linearity of an electrochemical system [2]*

In pratice, a small AC voltage is applied to the system (1 to 10mV) [2].

2.7.2. Surface half-reaction kinetics resistance

As depicted in part 2.2.2, The surface half-reaction over-potential primarily depends on the reaction kinetics and the structure of the double layer at the electrode surface. This double layer is characterized by an equivalent capacity. Hence, the charge transfer impedance at the electrode surface is represented by a charge transfer resistance R_{ct} in parallel with the characteristic double layer capacity C_{dl}.

The value of the charge transfer resistance R_{ct} depends on η_s and is defined as its derivative with respect to the current density i [10]:

$$R_{ct} = \frac{d\eta_s}{di} = \frac{RT}{\alpha|i_{avg}|} \tag{2.58}$$

In impedance spectroscopy analysis, it is rare to measure perfect semicircles for the equivalent impedance of the surface half-reaction, as these represent the case of a perfect electrochemical process. In the vast majority of cases, a flattened semicircle (half-oval) is observed, indicating a non-ideal process. For the analytical impedance expression, a

modified version of the electrical capacitance is used, which is called the Constant Phase Element (CPE) [17]:

$$Z_{CPE}(\omega) = \frac{1}{(j\omega)^a Q} \tag{2.59}$$

with a the exponent of the CPE which is a constant number varring between 0 and 1, Q the equivalent capacity value of the double layer. When $a = 1$, it corresponds to the case of the perfect semicircle. As a becomes smaller, the equivalent semicircle becomes more flattened.

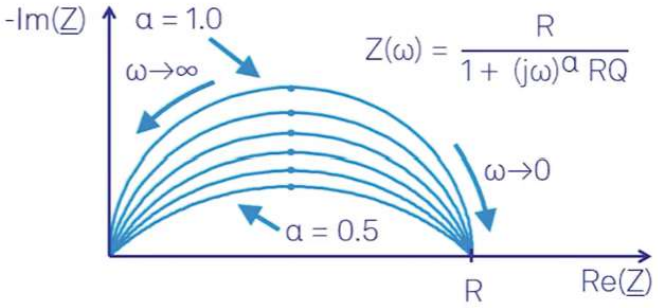

Figure 2.18.: *Nyquist Plot of a resistor R parallel to a Constant Phase Element (CPE)[17]*

Finally, a semicircle corresponding to a surface half-reaction, the spectrometric study of a complete cell thus presents several semicircles in the Nyquist diagram due to the linearity property of a linear system discussed in Section 2.5. These semicircles may be distinct or overlap. The position of the semicircle depends on the characteristic time of its appearance, $\tau = R_{ct}C_{dl}$, and is therefore strongly dependent on the capacitance of the double layer at the electrode.

2.7.3. Ohmic resistance

The Ohmic resistance accounts for charge transport through the application of a potential difference. Thus, the internal resistance of the connection cables as well as the resistance of the electrolyte between the two electrodes are considered in the ohmic resistance, denoted as R_{ohm}.

The influence of the ohmic resistance in the equivalent circuit is represented by a simple resistor. As depicted in figure 2.15, a resistor in series with an certain circuit shifts the curve of the Nyquist diagram to the right by a value of R_{ohm}.

The value of R_{ohm} is given by the derivative of the ohmic over-potential η_{ohm} from equation 2.43 with respect to the current density :

$$R_{ohm} = \frac{l}{\kappa} \tag{2.60}$$

2.7.4. Concentration Difference Resistance

The impedimetric response in semi-infinite linear diffusion can be effectively modeled using an infinite-length transmission line. This is represented by a network of resistors and capacitors, where the resistors denote the diffusion resistance per unit length and the capacitors represent the chemical capacitance for diffusion per unit length [3].

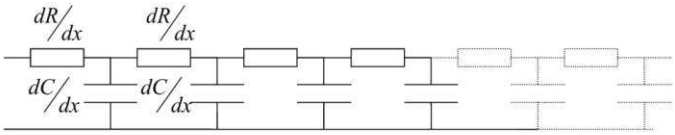

Figure 2.19.: *Transmission Line for Warbung impedance Model[10]*

The equivalent impedance of this transmission line is given by Warbung and is characterized in a Nyquist diagram by a 45° straight line.

$$Z_W(\omega) = \frac{RT}{(zF)^2} \frac{2}{c_0\sqrt{2D\omega}}(1+j) \tag{2.61}$$

The Warbung impedance is actually consistent with the linearized solution of the diffusion equation combined with the linearization of the Nernst equation.

2.7.5. Geometric artifact

In a medium temperature range, a small semicircle occasionally appears in the spectra, unrelated to any electrochemical phenomena or measurement device artifacts. These semicircles can be interpreted as geometric artifacts of the cell [11].

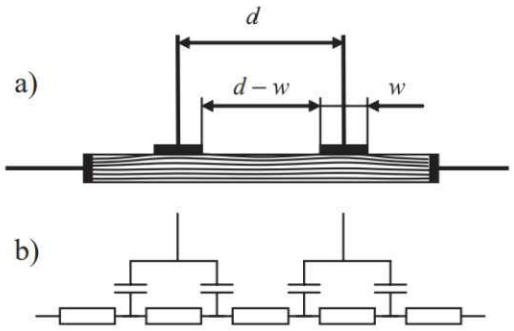

Figure 2.20.: *Geometric artifact model on a voltage strip electrode [11]*

Using the simplified model of a strip electrode, the semicircle depression can be attributed to a transmission line effect along the width of the electrode strip. At low

frequencies, the measured voltage is derived from the centerlines of the strips (d in Figure 2.20), whereas at high frequencies, it is measured between the inner edges of the electrodes ($d - w$). Hence, the positions of the potential points considered for the voltage drop vary with frequency.

A similar electrical circuit model can be adapted to explain the observation of geometric artifact semicircles for porous electrodes.

3. Methodology

This chapter will present the different methods applied with which EIS measurement were conducted.

- Firstly, the overall setup for experiments is discussed. Specific emphasis is placed on the connection between the spectrometer and the electrochemical cell.
- Secondly, the design of a second cell generation is discussed which is focused on improved results with EIS.

Firstly, the overall setup used for experiment conduction. In particular the linkage with the cell will be detailed. Finally, the different steps of a new cell design conception will be introduced.

3.1. Cell Test Rig

In the laboratories of TU Wien, a test rig has been set up to conduct measurements on electrolysis cells. The test rig consists of two reactant supply circuits: one for the anode side and the other for the cathode side. An external potentiostat is available to apply a test voltage, and the test rig is also equipped with a spectrometer dedicated to EIS analysis. A detailed diagram of the test rig is shown in Figure 3.1.

3.1.1. Hardware Tools

The tests are conducted with solutions of high pH levels. Thus, all components of the test rig need to be chemically resistant to the solutions used.

Electrolyte Storage Tank (x2)

Two laboratory bottles (DURAN) were used as storage tanks for the catholyte and the anolyte. The bottles are transparent to visually monitor the color of the electrolyte. All components are suitable for use up to $140°C$ [6].

Pumps (x2)

Two peristaltic pumps (Ecoline VC-280, ISMATEC) were used for each electrolyte circuit flowing. The pump presents a speed range between 3.5 and 350 rpm. The rotational speed can be precisely set to any value between 1% and 100% of the maximum speed

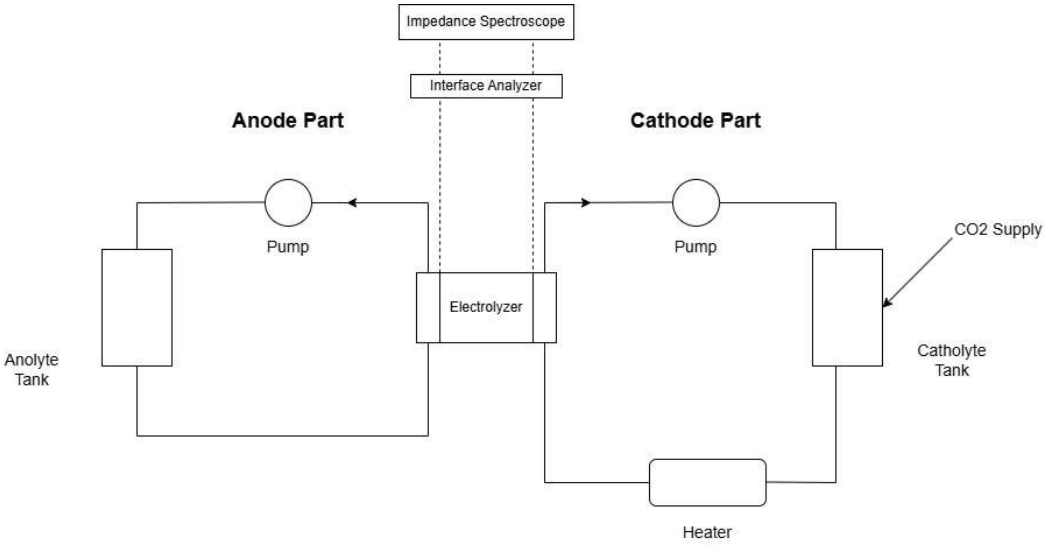

Figure 3.1.: *Scheme of Test Rig*

Figure 3.2.: *Photo of the ventilation hood (left) and the test rig (right)*

using a manual 2-digit slider. It features a 2 rollers rotor. Using an inner diameter 8mm tube for the chemical species supply for the cell, this corresponds to an effective flow range between 35 and 3500 mL/min. Each pump has a power cosumption of 100W.

Further information is available in the Ecoline VC-280 datasheet [15].

Tubing

Tubes with an inner diameter of 8mm are used for electrolyte supply circuit.

Heating element

The inlet temperature of the electrolyzer is controlled by an electric heater that warms the cathode-side supply circuit. The process values were measured using a PT100 temperature sensor, with the signal transmitted to a PID controller. Different temperatures were applied to the cell system, up to 60°C.

This feedback-controlled heating system ensures precise thermal regulation of the catholyte, crucial for experiments where temperature-dependent behaviors, such as reaction kinetics and impedance variations, are being investigated.

CO Detector

A CO dector (RS Pro) has been used to verify the production of CO by the cell when a voltage is applied, and estimate roughly its quantity. The CO detector detects the quantity of carbon monoxid in ppm. The CO detector is also used for safety reasons, as low concentrations of CO cause headaches and nausea, while higher concentrations can be fatal.[21]

BNC cables

BNC cables (Bayonet Neill-Concelman) is a type of coaxial cable used primarily for carrying high-frequency signals. Those cables are particularly important to deliver the high-frequency signal of the impedance spectrometer to the cell, and detect the repsonse. There are three primary components on any BNC: the center conductor, the ferrule finger/bayonet assembly, and the outer crimp sleeve [5]. The central conductor propagates the relevant measuremet signal. The outer crimp sleeve's potential is usually set constant to the ground of the measuring device, which connection is facilitated by the finger assembly. The application of BNC cables for signal stabilization will be explored in section 3.2.2.

Carbon dioxide CO_2 gas bottle

CO_2 gas bottle (Linde) was used to introduce the reagent into the catholyte. The bottle is connected to the gas introduction circuit through a capped regulator, enabling precise control of the reagent introduction rate.

Nitrogen gas N_2 bottle

Nitrogen gas bottle (Linde) was used to introduce N_2 into the cathode reaction fluid and purge the CO_2 that was physically absorbed during its previous preloading. This allows conducting tests with only the CO_2 that is chemically absorbed by the cathode reaction fluid.

Ag/AgCl Reference Electrode

To carry out overpotential measurements on the anode side and potentially perform spectrometric analysis independently at each electrode, an Ag/AgCl reference electrode was constructed. Simultaneous measurement of the overpotential and the current density passing through the cell allows, in particular, the estimation of the exchange current density, as detailed in section 2.2.2 .

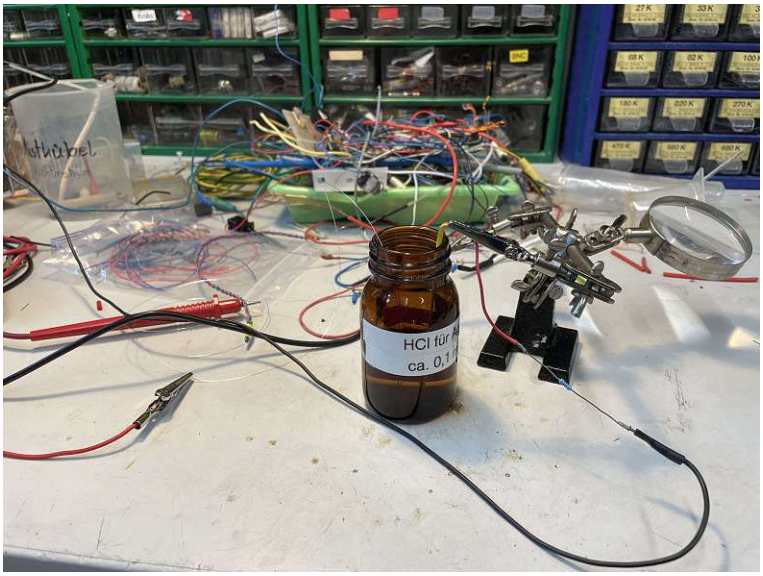

Figure 3.3.: *Photo of the preparation of the reference electrode*

To coat the silver wire with a layer of silver chloride, the silver wire was immersed in a 0.1 M HCl solution and subjected to a 10 V potential for 5 minutes.

The silver wire was then placed in a suitable tube filled with a 1 M KCl solution. A frit was used to create a bridge between the KCl solution of the reference electrode and the electrolyte in which the reference electrode is immersed.

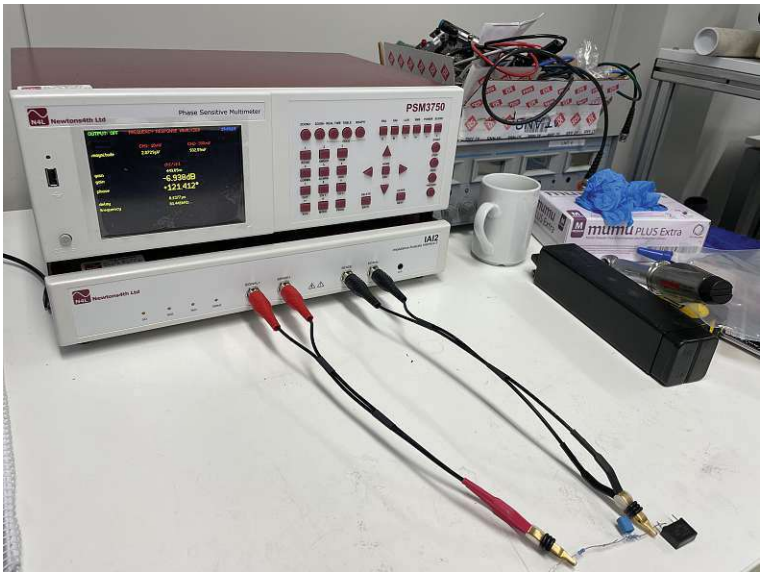

Figure 3.4.: *Impedance spectrometer PSM3750 and Impedance Analysis Interface IAI2*

3.1.2. Devices

Impedance spectroscope : PSM3750 + Impedance Analysis Interface : IAI2

The device PSM3750 (Newton4th) has been used for impedance spectroscopy cell analysis. The device has in total 5 operational modes : FRA (Frequency Response Analyzer), PAV (Vector Voltmeter), LCR (Impedance Analysis), RMS (RMS Voltmeter), Power (Power meter), Scope (Oscilloscope). It is able to measure a voltage amplitude of $\pm 10V$ peak in a frenquency range from 20mHz to 1MHz.

The device is able to deliver a DC signal with a superimposed AC signal of the desired amplitude. The acquisition speed is adjustable between 1/80s and 10s for a measuring point; a slower measurement speed corresponds to a longer integration time for each measurement point. This allows more samples to be captured and reduces the impact of random variations such as noise [23].

The device features :

- One output port OUTPUT
- Three input ports CH1, CH2 and CH3

In LCR mode, the internal generator of the PSM3750 delivers an AC signal to the Device Under Test (DUT) via the OUPUT chanel. Input chanel port CH1 is then used to measure the voltage accross the component under test, whereas input chanel port CH2 measures the current through it. Chanel CH2 practically measures the voltage across

a resistor connected in series, whose resistance is known and is referred to as a shunt resistor. The current value is deduced using Ohm's law from the voltage measured by CH2 and the input value of the shunt resistance [23].

For this purpose, the PSM3750 was initially connected to the Impedance Analysis Interface (IAI2) to perform cell impedance measurements. The IAI2 offers a selection of four selectable shunts to sense the current through the DUT [23] : LOW (5Ω), NORMAL (50Ω), HIGH ($5k\Omega$), VERY HIGH ($500k\Omega$). The electrical impedance measurement diagram of the PSM3750 is presented in Figure 3.5.

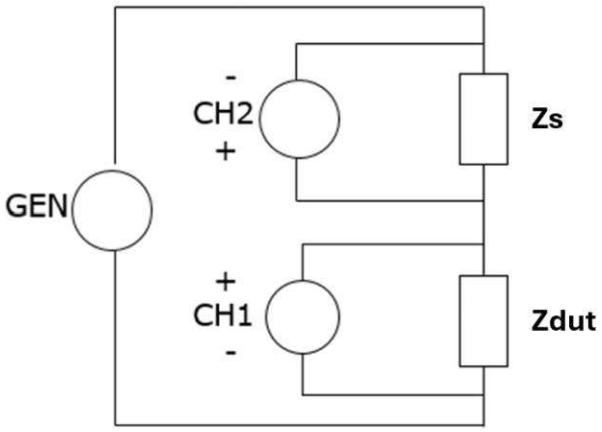

Figure 3.5.: *Electrical impedance measurement diagram of the [23]* PSM3750

The different shunts built into the IAI2 allow the test conditions to be modified to optimise the measurement accuracy. In general, a higher shunt resistance increases the magnitude of the current signal and decreases the magnitude of the voltage signal across the component; conversely a lower shunt resistance decreases the magnitude of the current signal and increases the magnitude of the voltage signal. Optimum accuracy is when the voltage and current signals have approximately same value (the impedance of the shunt is approximately the same as the impedance of the DUT), but good results can be obtained with impedances within a factor of 100 of the shunt value. [23]

The IAI2 features four input ports for impedance measurement : SIGNAL+, SENSE+, SENSE-, SIGNAL-. Generally the lead measuring the response voltage is called SENSE, and the one measuring the current through the cell SIGNAL.

Solartron SI 1286

The Solartron SI1286 Advanced Electrochemical Interface is a versatile instrument that enhances the precision and stability of measurements obtained by the connected impedance

spectroscope, ensuring accurate DC polarization. The Solartron can function as either a potentiostat or a galvanostat, depending on the application.

The Solartron was utilized to supply the necessary voltage to the cell for facilitating CO_2 reduction and CO detection. Detailed information on its application is provided in section 3.2.4.

Figure 3.6.: *Solartron linked to the PSM3750 and Computer for analysis*

The SI1286 features four input ports for impedance measurement : CE, RE1, RE2, WE.

Computer

The DELL®WindowsXP Serial COM RS232 Port - 2GB 60GB 14 computer was used for processing the data generated by the PSM3750. The computer and the PSM3750 are connected via a VGA-to-VGA cable.

3.1.3. Software tools

Signal input parameter and curve display

Software *javalab17112014* from Electrochemistry Institute of TU Wien has been used for signal input parametrization. The software is running on the Dell PC during the measurement acquisition.

The software features 7 different menus : FILE for data saving, INSTRUMENT for device selection, MEASUREMENT for input signal parametrization, CYCLES for the definition of a measurement set, DATA and GRAPHICS for data display, and INFO.

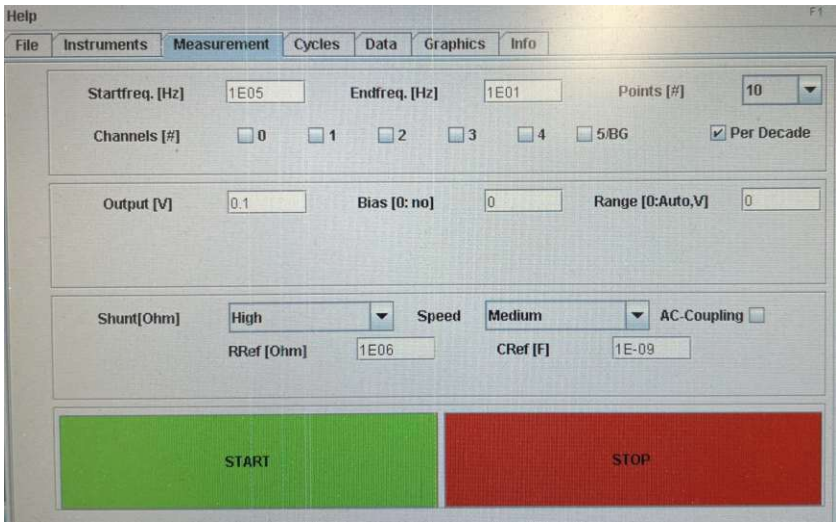

Figure 3.7.: *MEASUREMENT menu on javalab17112024 software interface*

The MEASUREMENT menu is particularly important for generating data by parameterizing the input AC signal :

1. *Startfreq* and *Endfreq* set the limits of the frequency range scanned during the SWEEP
2. *Points* sets the number of points acquired during the measurement. If the *Per Decade* option is checked, the number of points will be entered for each decade of the imposed frequency range
3. *Output* defines the amplitude of the low-amplitude AC signal for impedance measurement in the linear range
4. *Bias* allows the application of a DC shift to the AC signal, enabling the study of the cell's behavior at a specific voltage
5. *Shunt* It is the known value of the shunt resistance used to measure the current intensity

6. *Speed* sets the acquisition speed of the measurement as specified in the section 3.1.2
7. AC-Coupling sets the superposition of the AC signal and the imposed bias
8. *Start* and *Stop* initiate and halt the measurement

The software is then used to transmit the measurement data for further analysis.

ZView

The *ZView* software from the Electrochemistry Institute of TU Wien has been used for Nyquist diagrams analysis formed from the data points measured by the PSM3750. Figure 3.8 presents the graphical interface of the software. The software specifically allows displaying the Nyquist diagram (shown on the left side of the interface), approximating the curve by selecting an equivalent electrical circuit, and then converging the values of the different components of the electrical circuit to the measured data using a fit function. The right side of the interface presents the Bode diagrams.

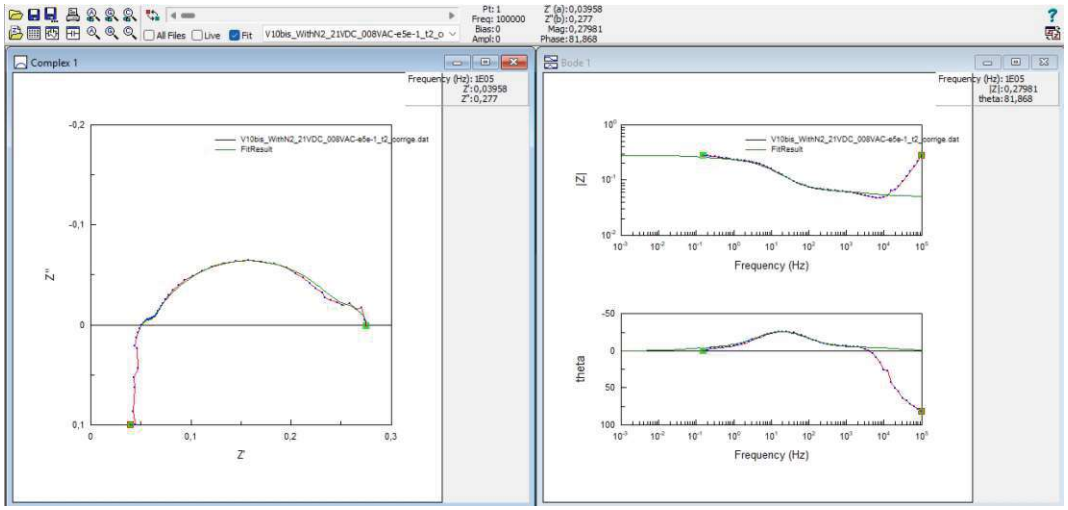

Figure 3.8.: *ZView analysis Interface*

Figure 3.8 illustrates an example of a Nyquist curve approximation obtained through measurement. The equivalent circuit used for the approximation, along with corresponding values, is shown in Figure 3.9.

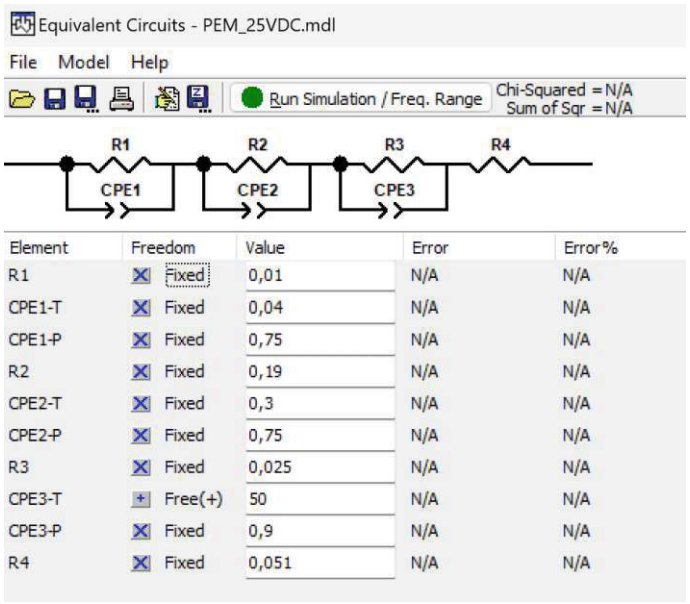

Element	Freedom	Value	Error	Error %
R1	Fixed	0,01	N/A	N/A
CPE1-T	Fixed	0,04	N/A	N/A
CPE1-P	Fixed	0,75	N/A	N/A
R2	Fixed	0,19	N/A	N/A
CPE2-T	Fixed	0,3	N/A	N/A
CPE2-P	Fixed	0,75	N/A	N/A
R3	Fixed	0,025	N/A	N/A
CPE3-T	Free(+)	50	N/A	N/A
CPE3-P	Fixed	0,9	N/A	N/A
R4	Fixed	0,051	N/A	N/A

Figure 3.9.: *Equivalent electric circuit input on ZView*

3.1.4. Cells Under Test

PEM Cell

A first test set with impedance spectrometer has been carried out with a PEM (Proton Exchange Membrane) Eletrolyzer (H-TEC EDUCATION).

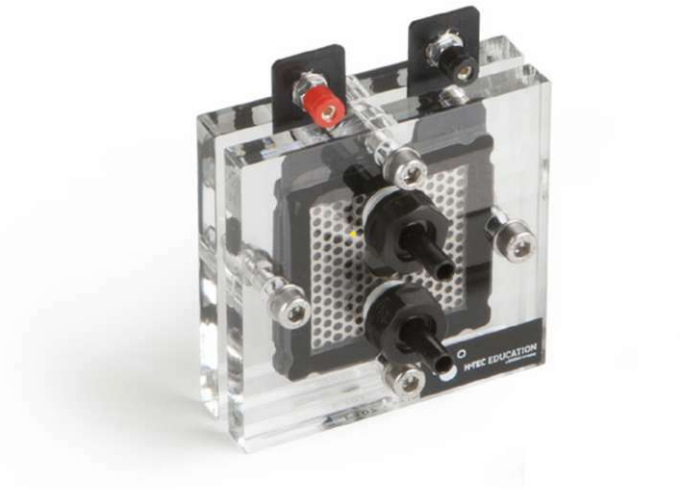

Figure 3.10.: *PEM from H-TEC EDUCATION [14]*

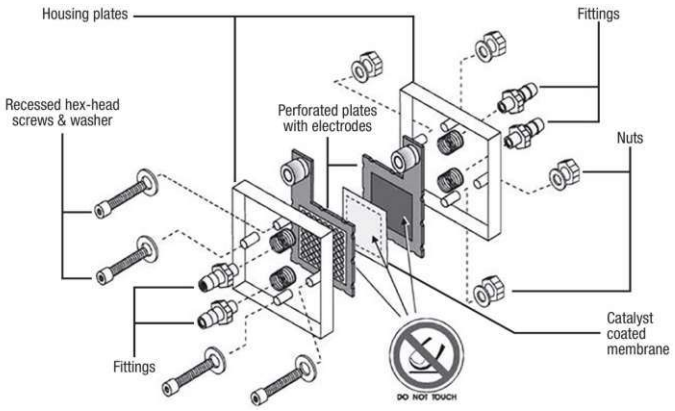

Figure 3.11.: *Exploded view from H-TEC EDUCATION's PEM [14]*

From a certain applied voltage, the H-TEC's PEM cell reduces protons H^+ to H_2 at the cathode, and oxidizes water H_2O into oxygen O_2 at the anode, following the chemical half-reactions 2.4 and 2.6 described in section 2.1.2. Protons H^+ are the charge carriers which are transferred via ionic conduction through the catalyst coated membrane. Table 3.1 summarized the different materials constituting the PEM cell.

Perforated Plate + Cathode	Catholyte + Anolyte	CCM	Perforated Plate + Anode
Carbon Based GDL	dist. Water	Nafion $0.5mg/cm^2$ of 60% PtC (cathode) $2mg/cm^2$ of IrRuOx (anode)	Metallic Mesh

Table 3.1.: *Composition of the PEM H-TEC electrolysis cell [14]*

The electrode area is $16cm^2$. The input voltage range applicable to the cell is 0-2V, whereas the one for current is 0-5A. Maximal temperature of the electrolyte is $60°C$. Further information is to be found in the operating instruction manual of H-TEC [14].

AEM Design 3.0

Figure 3.12.: *AEM Design 3.0 Cell*

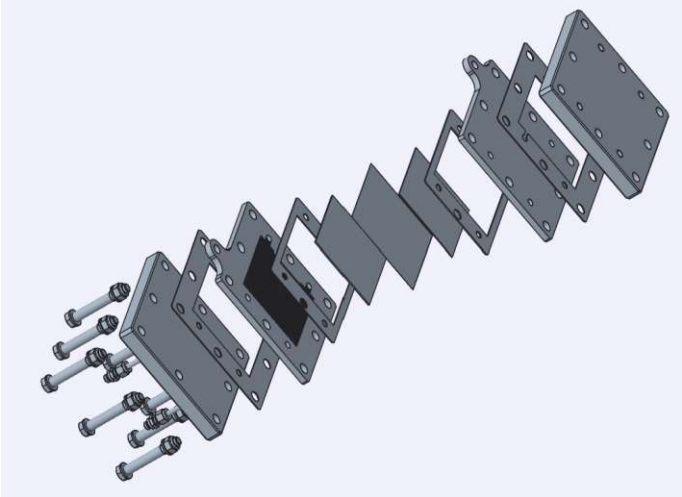

Figure 3.13.: *Exploded view from 3.0 Design AEM cell*

A second set test with impedance spectrometer has been carried out with the AEM Design 3.0 Cell. The Design 3.0 of the AEM Co-Electrolysis Cell was designed by Martin

Schulz and Felix Ettlinger, more details on the layout of the cell can be found in [25] and [7]. The electrode area of the cell is 100cm^2. The cell operates in an alkaline environment and is capable of reducing CO_2 to CO at its cathode, while water is oxidized into O_2 at the anode. Different cell configurations are tested to determine their influence on the cell impedance.

(1) Flowfield plates

The flowfield grid used features 20 channels arranged in a serpentine pattern with 4 passes. Each channel has a width of 0.8 mm and a depth of 0.3 mm. The width of a rib separating two channels is 0.45 mm. The flowfield plate is made of titanium.

(2) Membranes

Two types of anion exchange membranes (AEMs) were evaluated. Prior to testing, the membranes require activation for a minimum of 24 hours. Delivered in a form containing various counterions, the membranes are soaked in KOH to facilitate the exchange of negative counterions with OH^- ions.

· Sustainion®X37-50 Grade RT Membrane (Dioxide Materials).

Property	Value
OH^- Conductivity	$> 130\ mS.cm^{-1}$ $(70°C)$
Water uptake	$> 80\ wt\%$
Thickness	$50\ \mu m$

Table 3.2.: *Sustainion properties [12]*

· Fumasep FAA-3-130 (Fumatech).

Property	Value
OH^- Conductivity	$30.8\ mS.cm^{-1}$
Water uptake	10-25 $wt\%$
Thickness	$130\ \mu m$

Table 3.3.: *Fumasep FAA-3-130 properties [12]*

(3) Cathode Electrocatalyst

For CO_2 reduction at the cathode, silver is used as a catalyst. Two cathode electrocatalyts are available for testing :

· A carbon gas diffusion layer Sigracet 35 BC GDL coated with silver nanoparticules (Dioxide Materials).

Property	Value
Thickness	325 μm
Porosity	80%
Electrical Resistance	$< 15\ m\Omega cm^2$

Table 3.4.: *Sigracet 35 BC coated carbon gas diffusion layer properties [8]*

Property	Value
Thickness	1.6 mm
Pore size	580 μm

Table 3.5.: *Ag-Foam properties*

· A silver foam (Ag-Foam) from the firm Alantum.

(4) Anode Electrocatalyst

The choice of electrocatalyst at the anode is also important in the context of impedance measurement since the oxygen oxidation reaction is responsible for the majority of the surface reaction resistance. The activation energy for O_2 oxidation is higher than that for CO_2 and water reduction at the cathode. Two choices of anode electrocatalysts were tested.

· Nickel Foam from the firm Fuelcell Store

Property	Value
Thickness	1.0 mm
Pore Per Inches	80-120 μm

Table 3.6.: *Nickel Foam properties [9]*

· A carbon gas diffusion layer coated with iridium oxide particules IrO_2. The gas diffusion layer is the same used than for the cathode elecrocatalyst from the firm Dioxide Materials Sigracet 35 BC GDL.

(5) Cathode Electrolyte

Different solutions used for CO_2 capture at the cathode were tested to determine their influence on CO_2 reduction, and thus CO synthesis, as well as their impact on the cell's impedance.

· 1M KOH solution

· 1M aminomethylpropanol AMP solution

- Monoethanolamine MEA solution in different concentrations : 30% wt, 20% wt, 10% wt, 5% wt
- Potassium carbonate K_2CO_3 in different concentrations : 0.5%wt and 0.25%wt

The effect of temperature on the cathode electrolytes was also measured during the tests. The temperature was varied from 23°C to 60°C.

(6) Anode Electrolyte

The electrolyte at the anode was not changed; a 1M KOH solution was always used.

3.2. Setup of spectroscopic analysis and signal stabilization

3.2.1. Superposition of the DC and AC signals

During the experiments, a 4-wire configuration was chosen to measure the voltage and current of the cell. This configuration enables the separate measurement current (SIGNAL+ and SIGNAL- inputs) and voltage (SENSE + and SENSE - inputs).

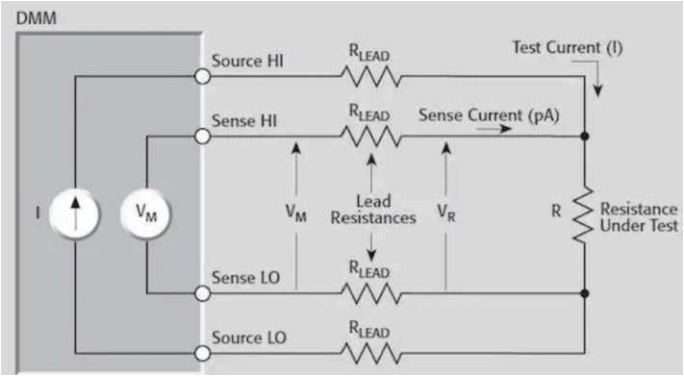

Figure 3.14.: *4-wire leads connection [16]*

In the case of a low resistance under test value, the voltage measurement is significantly affected by the internal resistance of the cables. To address this issue, the voltage is measured directly at the cell using an additional set of leads, with the application of a minimal current. [16]

The low-amplitude AC signal for spectroscopic impedance measurement must be superimposed with the desired offset DC voltage value. In cases where the sources for applying the DC signal and the AC signal are decoupled, it is possible for the measurement circuit to be short-circuited, causing the spectrometer to measure the impedance of the DC signal source instead of the resistance under test. A system where an external potentiostat applies a certain DC voltage to the cell, while the spectrometer applies an AC analysis signal, is often prone to inaccuracies. Such a setup actually requires special attention and precautions to prevent the occurrence of a short circuit.

The PSM3750, in combination with the IAI2 or the Solartron SI1286, enables the superposition of the AC analysis signal with the DC shift of the voltage point of interest for the measurement.

3.2.2. Limitation of Noise and Induction Effects at High Frequency

Induction effects are the main source of instability during spectroscopic impedance measurements. Passing an AC signal through the cable creates a magnetic field, which induces an electromotive force according to Faraday's law, thus generating an opposing current. One method to minimize this phenomenon is to use cables protected by a

grounded shield. This option provides a preferred low-impedance path for the induced magnetic currents, thereby reducing the inductive effect on the measurement [35]. The connection of the BNC cable shield (outer clamp sleeve) to the ground of the PSM3750 spectrometer is ensured by the ferrule finger assembly [5].

In particular at high frequency, inductive effects come particularly from the length of the cables and their positioning to each other and to external electromagnetic fields sources. One approach to minimize induction effects caused by cable positioning is to group and coil the current measurement cables together on one side, while separately grouping and coiling the voltage measurement cables on the opposite side. [3]

Finally, to avoid noise at lower frequencies, the measurement at a certain frequency point can be averaged over several periods instead of just one, thus increasing the integration time, as suggested by Warkentin et al. in [32]. During the experiments, an integration time of 10 cycles was used for each spectroscopic impedance measurement point. This action is directly configured in the acquisition menu of the PSM3750 spectrometer in the *cycles* tab.

3.2.3. Physical Limitation of Measurement by the PSM3750

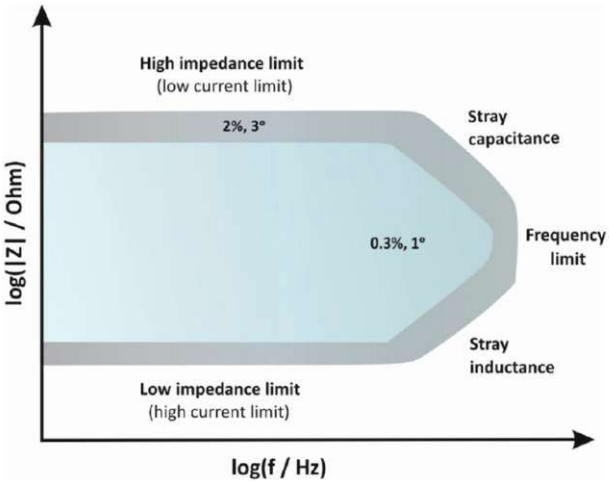

Figure 3.15.: *Example of an accuracy contour plot under specific experimental conditions [3]*

Figure 3.15 shows how impedance accuracy is limited by the value of the impedance under test and the frequency range of analysis.

The lower the impedance value, the more challenging it becomes to perform EIS. In the Bode diagram, see Figure 3.16 are plotted the influence of the resistance under test value on the bandwidth of the device. The characteristic frequency concerning the occurrence

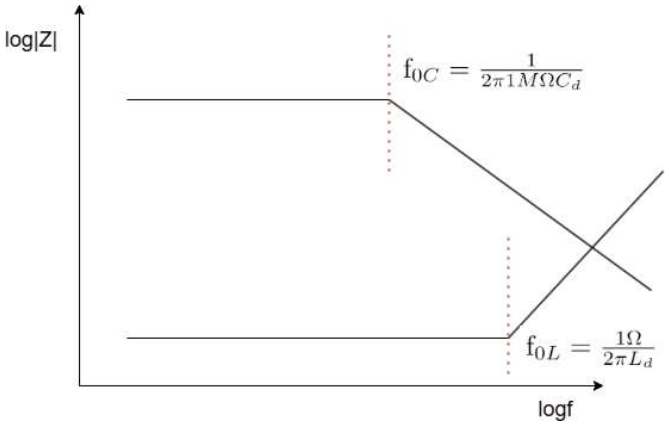

Figure 3.16.: *Illustration of the bandwidth of a spectrometer in a Bode diagram*

of internal inductance effects within the device L_d is $f_{0L} = R/2\pi L_d$. The one related to the occurrence of the device's capacitive effects C_d is $f_{0C} = 1/2\pi RC_d$. When the resistance value of the cell is small (in the example around 1Ω), the critical inductance frequency of the device is reached earlier in the frequency sweep range for analysis. The impedance test series conducted with the PSM3750 reveals the influence of induction, particularly around a frequency of 10 kHz. The analysis of the large cell is therefore only valid at frequencies lower than 10kHz. The vertical line diverging downward, characteristic of the inductance in the Nyquist diagram, is observed for frequency values above the critical value. Figure 3.15 also highlights the limitations associated with excessively high impedance values during testing. This constraint stems from the capacitive effects of the device, which become dominant as the limiting frequency is inversely proportional to the impedance value.

Another physical limit comes from the value of the shunt resistance described section 3.1.2. Taking into account the equivalent circuit in Figure 3.5, The voltage divider theorem provides the value of the voltage applied to the impedance Z_{DUT} as follows:

$$U_{DUT} = \frac{Z_{DUT}}{Z_{shunt} + Z_{DUT}} E \tag{3.1}$$

The minimum value for the shunt resistance provided by the analysis interface device IAI2 is 5Ω. Therefore, if the resistance of the cell under test is around 1Ω, only 1/6th of the voltage delivered by the PSM3750 is applied to the test cell. This constitutes a major limitation point for the application of voltage in the context of the directCCE project. The tested 3.0 Design cell has an internal resistance of around 1Ω. Therefore, problems occur as the resistance is not much larger than the shunt resistance.

3.2.4. Amplification of the Applied Voltage

Amplification with external DC support and protection

One initial option considered for amplifying the DC voltage applied to the test cell is the application of the DC signal using an external potentiostat. However, as explained in section 3.2.1, the application of a DC signal using an external potentiostat requires special precautions to avoid creating a short circuit while simultaneously measuring the impedance resulting from the DC supply. A measurement protection solution was developed inspired by one proposed by the spectrometer PSM3750's company Newton4th in [22].

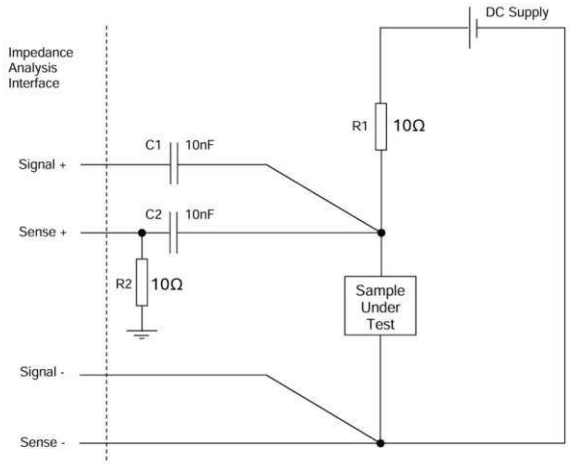

Figure 3.17.: *Diagram of the electrical circuit implemented for impedance analysis with an external DC supply*

Figure 3.17 shows the diagram of the electrical circuit that has been implemented for external DC supply. In this circuit, the inputs of the PSM3750 are connected to the cell under test subjected to an external DC signal. Two condensators C_1 and C_2 with both a capacity of 10nF are introduced on SIGNAL+ and SENSE+ leads. Their function is to block the DC signal of the external supply, allowing only the AC component of the signal to pass through. On the SENSE+ lead, a parallel resistor R_2 connected to ground allows the dissipation of charges accumulated on the capacitor C_2, thus preventing fluctuations or offsets in the measured voltage. Finally, the resistor R_1 is placed in series with the DC source to limit the current flowing through the circuit. It notably protects the various components from excessive current and helps reduce interference caused by the external DC source. [22]

Since the impedance value of the test cell is in the order of 1Ω, resistors R_1 and R_2 of 10Ω should be sufficient to ensure proper isolation of the external DC supply. However, care must be taken to ensure that the chosen resistor type can withstand the dissipated, which is the product of current flowing through the resistor and voltage :

$$P = VI = \frac{V^2}{R} \tag{3.2}$$

According to the voltage divider rule, the resistor R1 will be subjected to a significant portion of the voltage supplied by the external potentiostat. For an applied voltage of 10V, this represents a power of 10W.

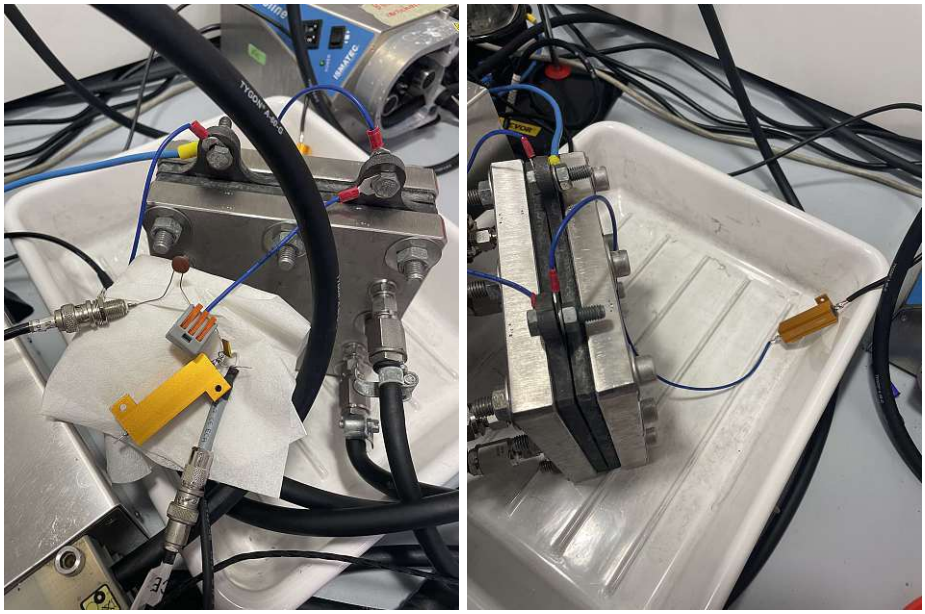

Figure 3.18.: *Implementation of the circuit shown in diagram 3.17*

As shown in Figure. A.4 50W capacity resistors were therefore used to prevent the risks of overheating and damage. The image on the left of Figure .A.4 shows the modified part of the circuit at the SIGNAL+ and SENSE+ leads connected to the test cell. On the right is illustrated the resistor at the DC source connected in series with the external potentiostat.

Unfortunately, the results of the spectroscopic impedance measurements with this setup exhibited parasitic noise. Due to the limited capacity of the components and the difficulty in identifying the source of the noise, alternative amplification methods were considered.

Amplification circuit proposal

A proposal to amplify the voltage and current delivered to the cell under test is the combined use of OPA operational amplifiers.

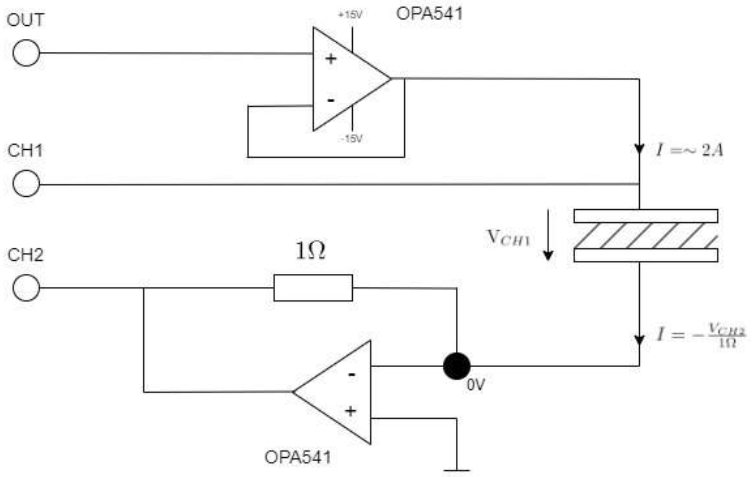

Figure 3.19.: *Proposal of Amplification circuit with use of OPA541 from Texas Instruments®*

The circuit uses two OPA541 operational amplifiers from Texas Instruments®. In the table 3.7 are summarized characteristics of the OPA541 for the design of the amplifier circuit. More informations are availabe in the OPA5441's datasheet. [30]

Max. Power Supplies	$\pm 40V$
Max. Output Current	$10A$ peak
Current limit	Programmable

Table 3.7.: *Useful OPA541 characteristics from datasheet [30]*

Such an electrical system connects directly to the OUT output and the CH1 and CH2 inputs of the PSM3750. The IAI2 analysis interface does not need to be connected to the spectrometer. The upper OPA is configured as a buffer (voltage follower) since its inverting input (-) is connected to its output. The signal generated by the PSM3750 is thus modulated by the upper OPA, which applies the voltage with an amplified current across the cell under test.

The lower operational amplifier (OPA) has its positive input (+) connected to ground, which sets its negative input (-) to a potential of $0V$. This configuration allows the measurement of the voltage applied to the cell under test via input CH1. Input CH2 measures the voltage across a 1Ω resistor, which acts as a shunt resistor. The PSM3750 then deduces the current value as it would if connected to the Impedance Analyzer IAI2.

The value of the impedance measured by the PSM3750 is then given by the equation :

$$Z = \frac{V_{CH1}}{-\frac{V_{CH2}}{1\Omega}} \tag{3.3}$$

This solution appears satisfactory; however, it is more costly. There is an alternative solution that makes impedance analysis and spectroscopy measurements more flexible.

Signal amplification by the Solartron SI1286

The device Solartron SI1286 has been introduced in section 3.1.2. This section will explain the operation of the Solartron, how it amplifies the signal from the PSM3750, and present the configuration used for measuring the Design 3.0 cell.

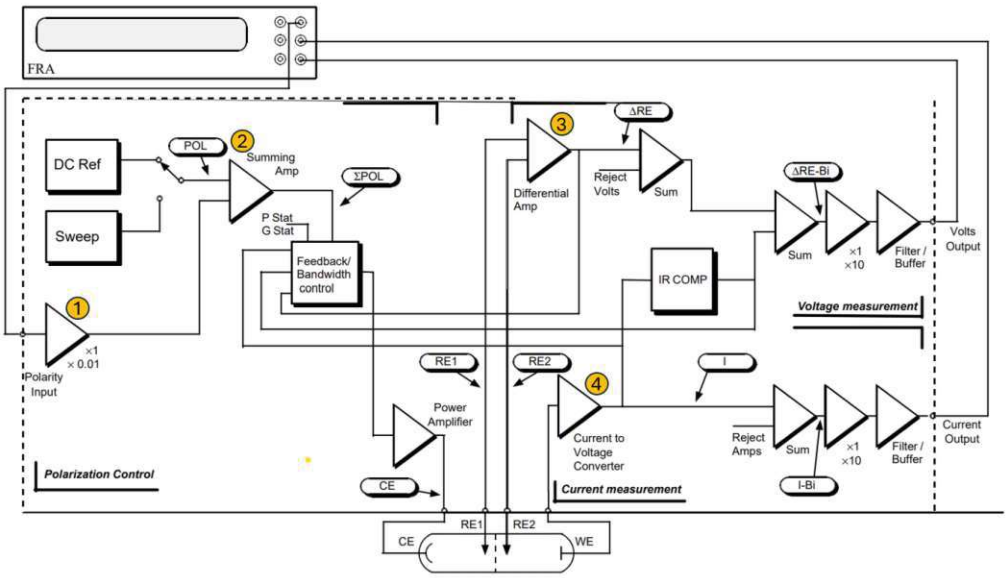

Figure 3.20.: *Solartron SI1286 block schematic [27]*

The OUT output of the PSM3750 is connected to the Polarity Input of the Solartron, while the CH1 and CH2 inputs of the PSM3750 are connected respectively to the Volts output and Current output of the Solartron.

The PSM3750 is pre-programmed to send the AC signal for spectroscopic impedance analysis. The signal was deliberately set to a higher amplitude (100 times greater than that actually used for the measurement), as the Solartron has the capability to reduce the AC signal amplitude by a factor of 0.01 **(1)**. This function allows for a more precise AC input signal for analysis.

This AC signal is then directly coupled by the Solartron with the accurate and stable DC signal produced by its generator. This coupling is achieved through an internal

summing amplifier **(2)**.

In potentiostat mode, the Solartron delivers the coupled signal into the cell under test. Like the Impedance Analyzer IAI2, the Solartron has four measurement input terminals: CE, WE, RE1, and RE2. The differential of voltage between RE1 and RE2 is measured by a differential amplifier **(3)**. This voltage measurement is used to verify and stabilize the signal sent to the cell under test. This is also the voltage value that is transmitted to the PSM3750 for impedance measurement.

The current is measured through the WE input of the Solartron, derived from the voltage measurement across a user-selectable shunt resistor **(4)**. This value is transmitted to the PSM3750 CH2 input and is used as current data for impedance calculations.

Shunt Resistor (Ω)	0.1	1	10	100	1k	10k	100k	1M
Maximum Current (A)	2	200m	20m	2m	200μ	20μ	2μ	200n

Table 3.8.: *Solartron shunt resistor value selection [27]*

Specifically, the application of a 0.1Ω shunt resistor is particularly interesting as it allows for a maximum current of 2A, thereby providing a sufficient associated voltage to achieve the desired voltage required for CO_2 reduction to CO within the framework of the DirectCCE project.

The advantage of using the Solartron for signal amplification lies in its ease of implementation and setup. Additionally, the configuration is very straightforward, and delivering a current of 2A is generally a very good value for spectroscopic impedance analysis. When the Solartron is connected to the PSM3750, the impedance value of the cell is inverted in the readings obtained by the PSM3750, resulting from the device's internal configuration. Furthermore, the input for the shunt resistance value in the *javalab17112014* software is predefined with a minimum of 5 Ohms. Therefore, a correction must be applied during data analysis.

3.3. Design of an electrochemical cell with a surface area of 16 cm^2

Considering the various challenges encountered during spectroscopic impedance measurements with the Design 3.0 cell, several factors justified the development of a new cell with a reduced active area:

- A current applied to a smaller active surface increases the cell resistance. Indeed, with a smaller active surface, the available active sites for electrochemical reactions on the electrode surface are reduced. The same amount of current must pass through a more limited reactive area, which requires an increased reaction rate to

compensate, inevitably leading to greater resistance [31]. A cell with higher resistance is subjected to a higher voltage difference across its electrodes, as deduced from the voltage divider theorem when connected to a shunt resistor.

· The design of a specific electrolytic cell for spectroscopic impedance and voltammetry measurements is particularly valuable for future tests, especially when considering a design that includes the introduction of a reference electrode in contact with the cell membrane. Measuring the potential with a reference electrode would notably allow for the measurement of overpotentials at each electrode and provide a better understanding of the resistive causes at each electrode. Additionally, within the framework of the DirectCCE project, the use of the reference electrode also enables the measurement of the surface reaction resistance associated with CO_2 reduction to CO as highlighted in [18].

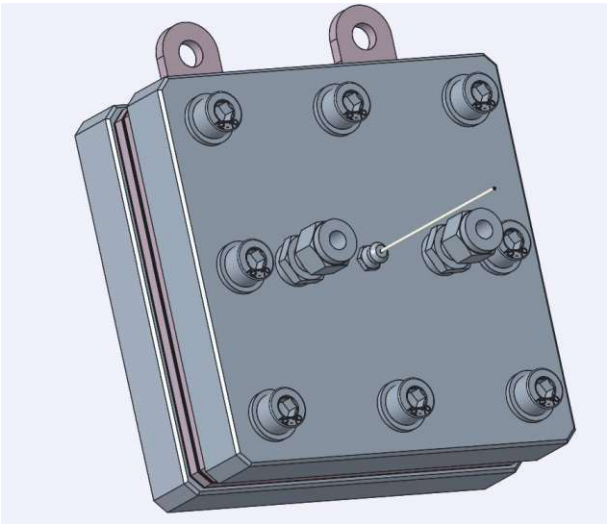

Figure 3.21.: *Assembly view of the 16cm^2 Cell Design*

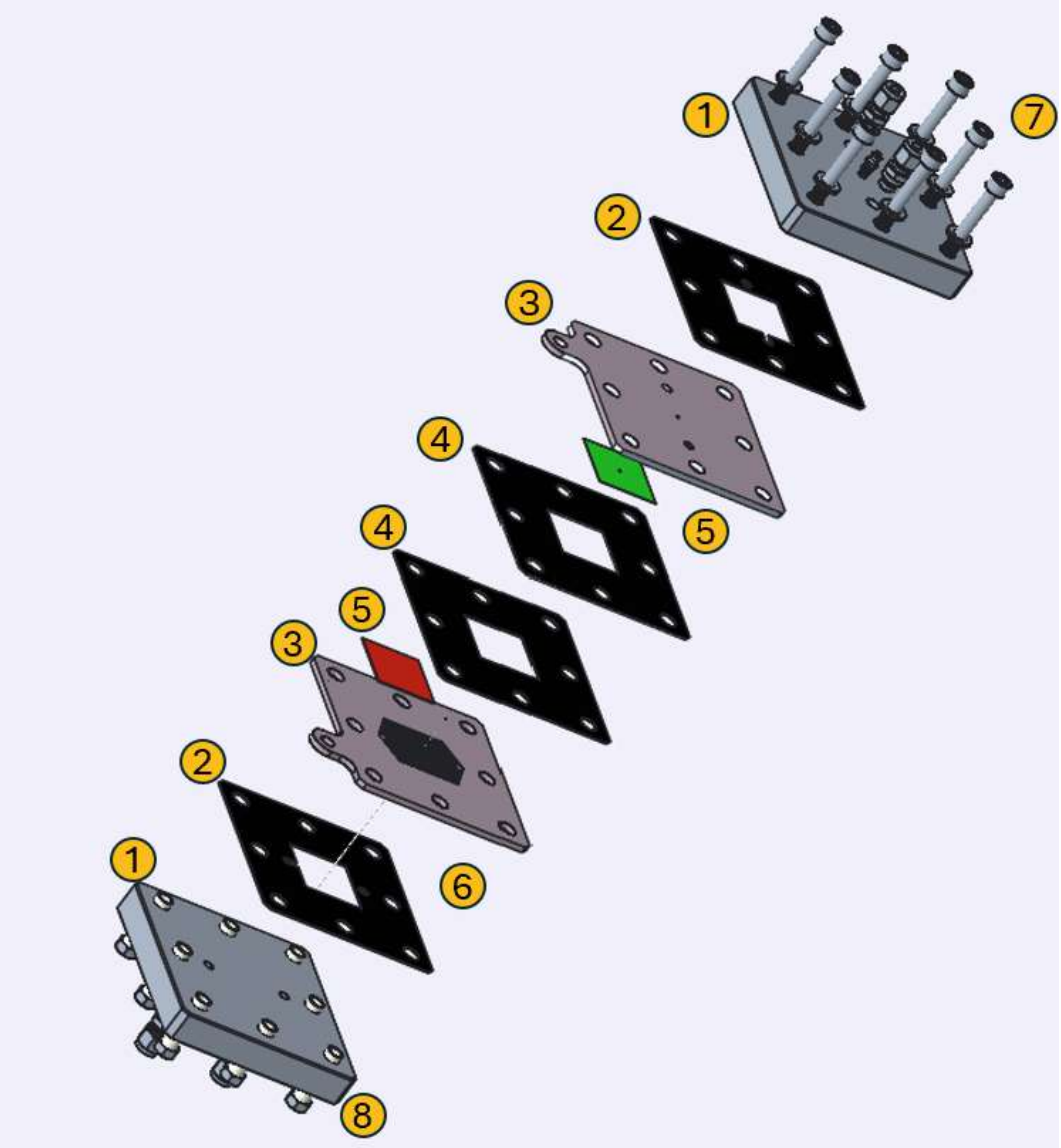

Figure 3.22.: *Exploded View of the 16cm^2 Cell Design*

(1) Endplates

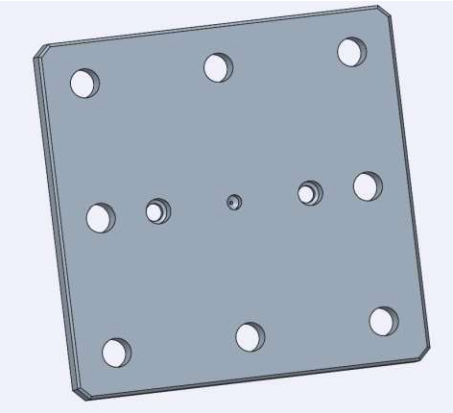

Figure 3.23.: *CAD drawing of the endplate*

The endplates are made of stainless steel. Their primary purpose is to evenly distribute the compression force across the entire contact surface where load transfers occur. The endplates also serve as the inlet and outlet for the reactant fluid within the cell.

The dimensions of the endplates are 12.4 cm x 12.4 cm, with a thickness of 20 mm. Two pipe connectors are used to ensure proper sealing of the supply through external pipes. Each endplate includes a fluid inlet and outlet to ensure the supply of catholyte or anolyte to the cell. The thread size of these pipe connectors is G1/8. For space-saving purposes, the reactant fluid enters through a G1/8 port and is transmitted to the flowfield via a 6 mm diameter conduit. Also for a better arrangement, 8 holes are drilled to accommodate M8 screws, allowing the assembly of the cell.

The endplate positioned on the cathode side additionally has a central hole to allow the passage of the reference electrode. The hole is designed to fit an M6 pipe connector, which ensures the sealing of the reference electrode assembly. The outlet hole on the flowfield side has a diameter of 1.1 mm to allow the reference electrode to pass through the flowfield to the membrane

(2) Gasket Endplate - Flowfield

The gasket positioned between the endplate and the flowfield ensures sealing between the two components. The gasket measures 12 cm x 12 cm and has a rectangular hole in its center to allow fluid circulation and equalize pressures at the front and back of the flowfield plate during the reactant fluid supply. The gasket is made of EPDM material, which is a polymer resistant to the alkaline environment in which the cell operates. The material has a shore hardness of 70A.

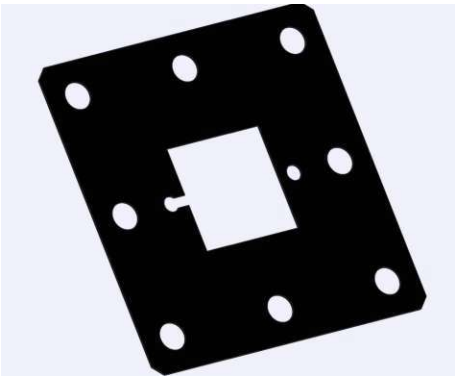

Figure 3.24.: *CAD Drawing of the gasket ensuring sealing between endplate and flowfield*

(3) Parallel Flowfield Plate

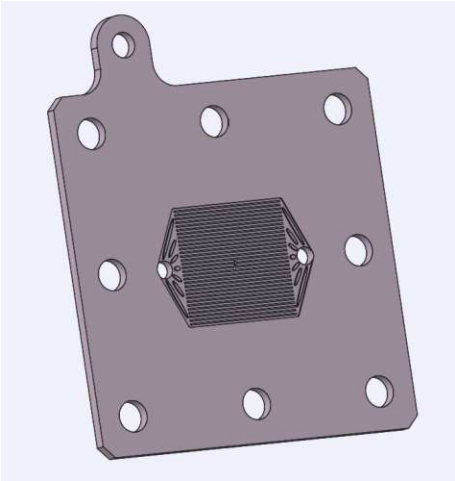

Figure 3.25.: *CAD Drawing of the parallel flowfield*

The primary purpose of the flowfield plate is to supply the gas diffusion electrode with reactants to enable the electrochemical reaction of the species. Inspired by the 3.0 cell design, the flowfield plate also functions as a current collector, as it includes an extension that allows direct connection of electrical cables to apply the test voltage. The material used for the flowfield plate is titanium. The plate dimensions are 12 cm x 12 cm, and its thickness is 4 mm.

A parallel design was adopted for the flowfield grid as depicted in Figure 3.26. This allows for a comparison with the serpentine design of the Design 3.0 cell. The active contact surface is actually 40 mm x 39.55 mm. The grid features 32 channels, each

0.8 mm wide and 0.5 mm deep. The width of the ribs is 0.45mm. The width of the channels and ribs remains the same as in Design 3.0. Only the channel depth was increased from 0.3 mm to 0.5 mm to measure and compare the effect of channel depth on reactant supply, and consequently, on the cell's impedance. In [37], Zhou et al. compare different rib/channel ratio configurations for parallel flowfield using a simulation on COMSOL and verify the results experimentally. They take into consideration the ohmic resistance, the surface reaction kinetics, and mass transport for a hydrogen/oxygen cell. The rib/channel ratio that optimizes the surface current density production and thus minimizes the cell's impedance is around 0.5. The ratio for the 16 cm^2 cell design is 0.56, which ensures a good distribution of channels across the active surface.

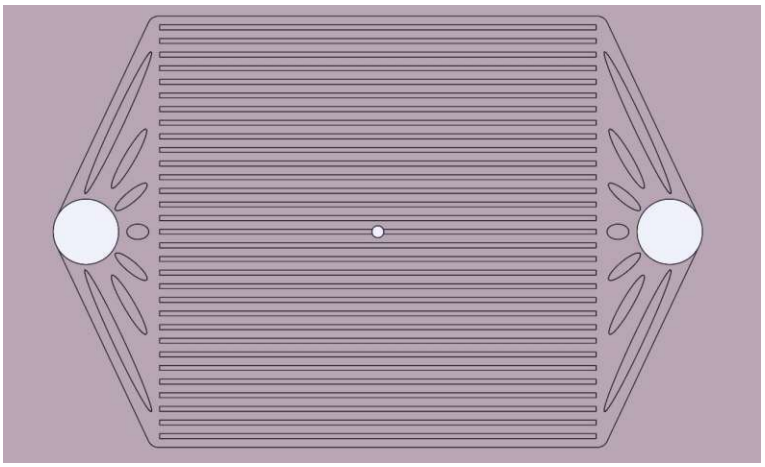

Figure 3.26.: *Detailed view of the parallel flow grid design*

Figure 3.26 specifically features the parallel grid of the flowfield. Oval fins with a thickness of 1 mm are arranged in star pattern at the inlet and outlet of the reactant fluid to better distribute the flow across the different channels.

The cathode-side flowfield plate has a central hole with a diameter of 1.1 mm to allow the reference electrode to pass through as can be observed in Figure 3.26.

(4) Gasket Flowfield - Membrane

This gasket provides insulation between the flowfield and the membrane. Dimensions of the gasket is 12 cm x 12 cm. It is made from the same material as the gasket (2). At its center, the gasket has a square hole measuring 4 cm x 4 cm to accommodate the gas diffusion electrode. The thickness of the gasket is adjusted based on the thickness of the diffusion electrode. When the cell is tightened, this arrangement ensures that the gas diffusion electrode is in contact with and compressed between the flowfield and the

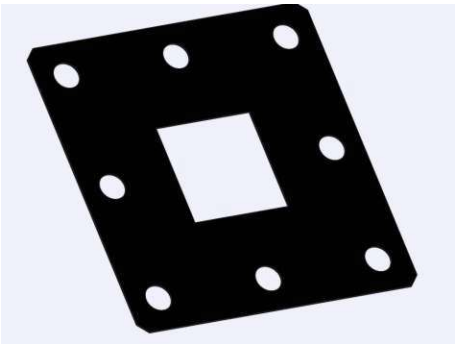

Figure 3.27.: *CAD Drawing of the gasket ensuring sealing between flowfield and membrane*

membrane.

This insulation specifically ensures complete separation of the cathodic and anodic reactant fluids, preventing unwanted chemical species exchange between the two half-cells. This isolation also marks the termination of the reactant fluid inlet and outlet channels.

(5) Gas Diffusion Electrode

The gas diffusion electrodes measure 4 cm x 4 cm. The thicknesses of anode and cathode differ. Similar to Design 3.0, the cathode can be composed of either silver or silver deposited on carbon with a thickness of 0.315 mm. The anode materials include nickel in the form of nickel foam with a thickness of 1 mm or iridium oxide coated on carbon paper with a thickness of 0.315 mm.

(6) Reference Electrode

The reference electrode consists of a PTFE tube filled with a KCl solution and a silver wire coated with silver chloride (AgCl). The PTFE tube has an outer diameter of 1 mm and an inner diameter of 0.5 mm. The silver wire is measured to have a diameter of 0.25 mm. The different reference potential values for the Ag/AgCl electrode depending on the solution's concentration are explained in section 2.1.7. Two thin pieces of membrane can also be inserted into the reference electrode tube to ensure better charge conduction and achieve a more stable reference signal. Particular attention must be paid to the absence of air bubbles in the tube, as they negatively affect conductivity. One method is to fill the PTFE tube with the KCl solution by suction rather than injection.

Figure 3.29 shows a cross-section of the reference electrode assembly. The thin reference electrode is brought into contact with the membrane by passing successively through the endplate (grey), the flowfield (pink), and the gas diffusion electrode (green). The

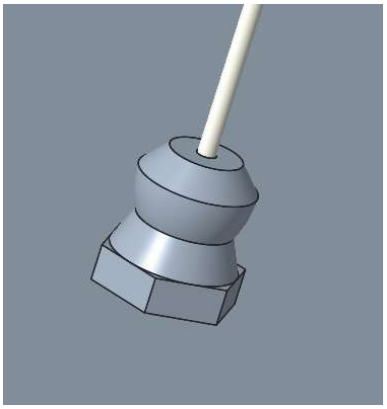

Figure 3.28.: *CAD Drawing of the reference electrode and the tube connector*

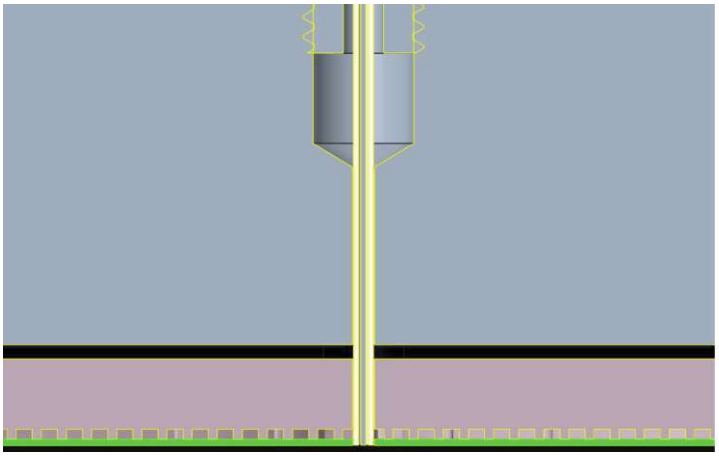

Figure 3.29.: *Cross-sectional diagram of the reference electrode assembly*

overpotential at the cathode can then be measured by the potential difference between the flowfield, acting as the current collector, and the silver wire of the reference electrode.

(7) Screws

Eight M8 screws are used to pressurize the 16 cm^2 cell. It is not easy to predict the exact compression required for the cell to establish the desired contact between the gas diffusion electrode and the flowfield. However, an initial estimate can be made. It is assumed that the gasket is harder to compress than the gas diffusion electrode. With the EPDM having a Shore hardness of 70A, this corresponds approximately to a Young's modulus of $E = 20$ MPa [26]. The gasket is assumed to be compressed from a thickness of $l_{ini} = 0.5$ mm to $l_{end} = 0.2$ mm. Assuming the material remains in the elastic domain, the normal stress σ is determined by :

$$\sigma = E\left(1 - \frac{l_{end}}{l_{ini}}\right) \tag{3.4}$$

The calculated normal stress is then $\sigma = 12$ MPa. Given that the nominal diameter of an M8 screw is $d_{screw} = 8$ mm, the stress pro screw is a function of the number of screw N_{screw}, the contact area $A_{contact}$ and the screw area A_{screw}:

$$\sigma_{/screw} = \frac{A_{contact}}{A_{screw}} \times \frac{\sigma}{N_{screw}} = 47.75 \text{ MPa} \tag{3.5}$$

The friction coefficient k is assumed to be high, as no lubrication is considered, with $k = 0.3$. The required torque for one screw is then [28] :

$$T = k \times \sigma_{/screw} A_{screw} \times d_{screw} = 5.76 \ Nm \tag{3.6}$$

A tightening torque of 6 Nm is therefore considered to apply sufficient pressure to the 16 cm^2 cell.

(8) Screw Insulations

Eight PTFE tubes are used as screw insulators to maintain the electrical insulation of the screws from the cell. Their inner diameter is 8.1 mm, and the outer diameter is 10 mm.

4. Results and Discussion

In this section, the results obtained from impedance measurements via spectroscopy are presented and discussed. First, the results concerning the PEM will be addressed. An exchange current density value for the anode part of the Design 3.0 cell will be estimated. Finally, different configurations will be tested with the Design 3.0 cell, and their influence on the spectroscopic impedance measurements will be demonstrated.

4.1. Calibration

As mentioned in the previous section, many external factors disrupt the spectroscopic impedance measurement using the PSM3750. In the course of this diploma thesis, the following had an influence:

- The position of the PSM3750 relative to the electrically connected elements (pumps, multi-socket outlet). Interference from electrical devices significantly disturbs the measured signal by introducing noise. The PSM3750 must therefore be isolated as much as possible within the available space in the exhaust hood.
- The BNC to U-shaped terminal connection located at the end of the BNC cables, which enables the connection between the PSM3750 transmission cables and the cell, must not come into contact with the cell. Any potential contact short-circuits the connection and introduces noise that disrupts the analysis signal.
- The contact surface between the U-shaped terminal and the cell's current collector must be checked. A poor connection, such as improper tightening or misalignment of the U-shaped terminal, results in signal transmission loss.

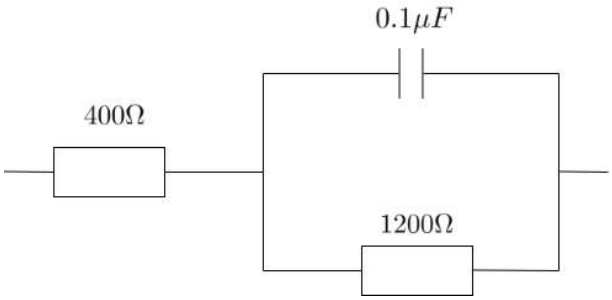

Figure 4.1.: *Electrical diagram of the signal stability test circuit*

To verify that the signal is not disturbed by external electrical elements, a preliminary test is performed with a simple system consisting of a resistor in series with a resistor in parallel to a capacitor. The details of the values of the different components are given in Figure 4.1. The spectrometric impedance measurement of this simple system produces a Nyquist curve showing a semicircle if it is not disturbed by external interferences.

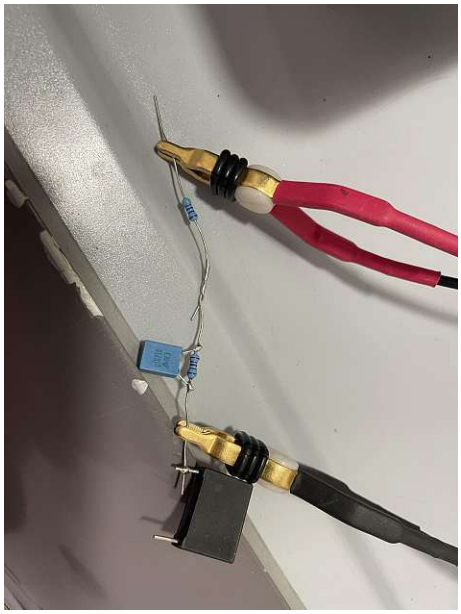

Figure 4.2.: *Photo of the signal stability test circuit*

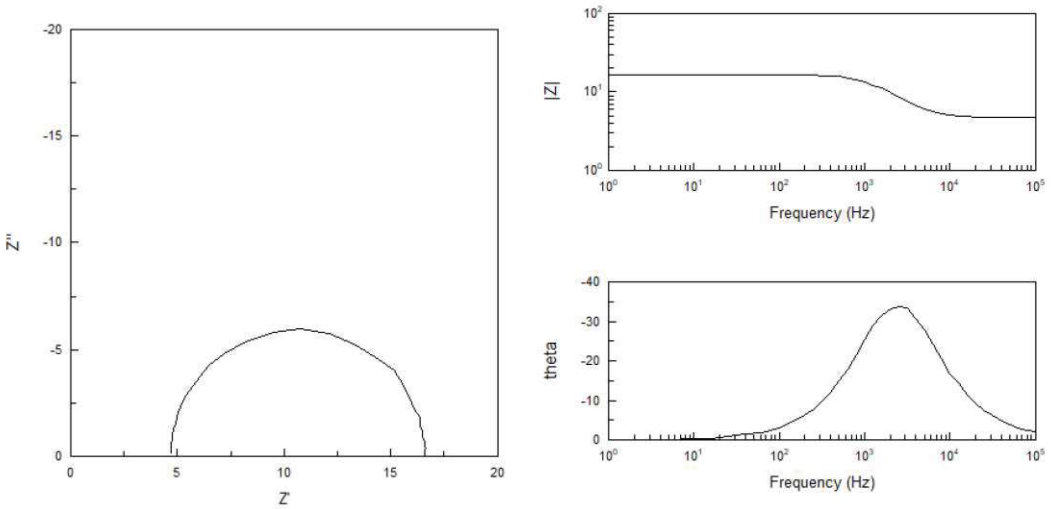

Figure 4.3.: *Nyquist diagram (left) and Bode diagram (right) of the stability test circuit*

The spectroscopic analysis of the test system is performed over a frequency range

from 100 kHz to 1 Hz with an AC signal amplitude of 10 mV. The number of acquisition points is set to 10 points per decade of frequency. The Nyquist and Bode diagrams of the system are presented in Figure 4.1. The typical curve of the system obtained when the PSM3750 is placed under proper conditions is a semicircle arc that starts at 400Ω and ends at 1600Ω, as suggested by the theory presented in section 2.6. The peak of the semicircle arc obtained on the sample is reached at a frequency of 1259 Hz. This value can be read from the Bode diagram. This is also consistent with the theory, which dictates that the peak occurs at $f_0 = 1/2\pi RC = 1326$Hz.

4.2. PEM Cell Impedance Spectroscopy analysis

Now, an analysis of a first electrochemical system is performed with the measurement of the PEM Electrolyzer from H-TEC EDUCATION presented in section 3.1.4. The active area of the cell is 16cm^2.

The measurements were carried out using the impedance analyzer IAI2 over a range of 10 different DC BIAS values varying from 1 to 5 with a step of 0.5. The effective voltage across the cell terminals was measured with a voltmeter, and the current was measured using an induction ammeter.

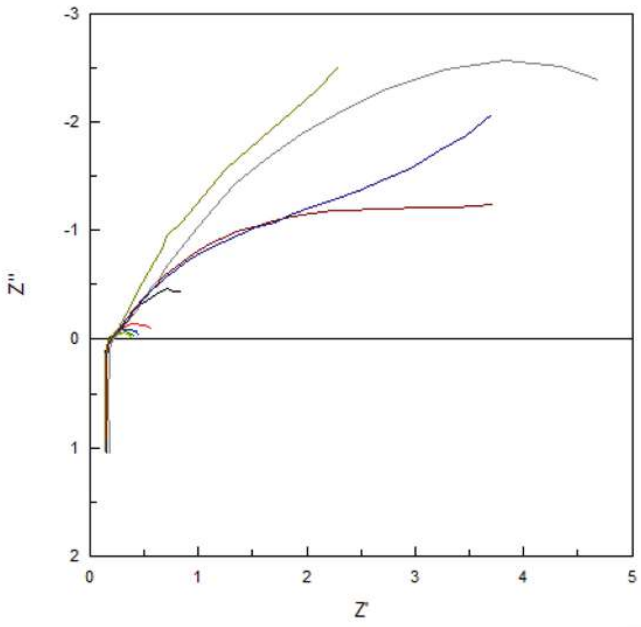

Figure 4.4.: *Nyquist diagram (left) and Bode diagram (right) of the stability test circuit*

The effective voltage range varies between 0.84 V and 1.6 V. Different effects are observed in Figure 4.4. Three phases can be distinguished globally: a galvanic phase

from 0.84 V to 0.97 V (the brown curve corresponds to an applied voltage of 0.84V, the grey one to 0.87V,the blue one to 0.97V), an equilibrium phase at 1.24 V (the gold curve), and finally an electrolysis phase between 1.43 V and 1.6 V. This last electrolysis phase is the focus of this test, and a more detailed impedance analysis is therefore performed starting from 1.24 V.

Ucell [V]	i [mA/cm^2]	Rohm [Ω]	R 1cc [Ω]	C 1cc [F]	P 1cc [1]	R 2cc [Ω]	C 2cc [F]	P 2cc [1]
1.43	4.06	0.24				1.2	0.9	0.76
1.52	5.94	0.174	0.045	0.19	0.68	0.41	1.1	0.76
1.55	8.13	0.176	0.04	0.26	0.62	0.265	1.1	0.78
1.58	11.25	0.183	0.03	0.18	0.68	0.205	1.1	0.76
1.6	13.75	0.19	0.03	0.15	0.68	0.17	1.0	0.74

Table 4.1.: *Hydrogen Electrolysis Cell PEM H-TEC Education*

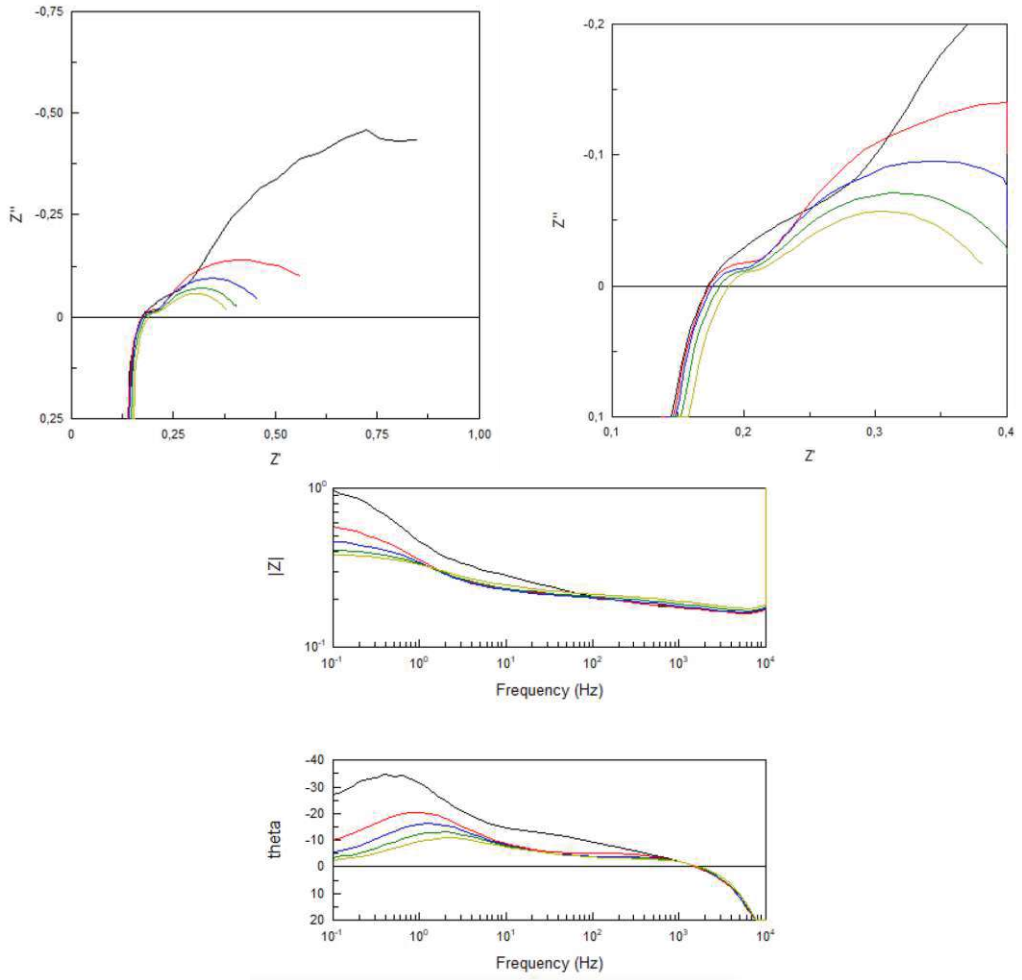

Figure 4.5.: *Nyquist diagram (top) and Bode diagram (botton) of the PEM*

The black curve is associated with a DC voltage of 1.43 V, the red curve with 1.52 V, the blue curve with 1.55 V, the green curve with 1.58 V, and the yellow curve with 1.6 V.

The samples are taken over a frequency range varying from 10^5 Hz to 10^{-1} Hz. The AC voltage signal applied in superposition to the DC voltage has an amplitude of 10 mV. Figure 4.5 provides a more detailed view of the Nyquist diagram of the PEM in the electrolysis phase, as well as the associated Bode diagram. An inductance at high frequency, as well as two different semicircles, can be distinguished. Therefore, an equivalent electrical circuit adapted for fitting the Nyquist diagram can be proposed, consisting of an ohmic resistance in series with two resistances $R1$ and $R2$, each in parallel with a Constant Phase Element $CPE1$ and $CPE2$. The circuit used for fitting the Nyquist curve is shown in Figure 4.6, and the different values associated with each source of impedance are listed in Table 4.1. It is important to note that a Constant Phase Element (CPE) is characterized by two key parameters: the equivalent capacitance C and the phase exponent α, as detailed in section 2.7.2.

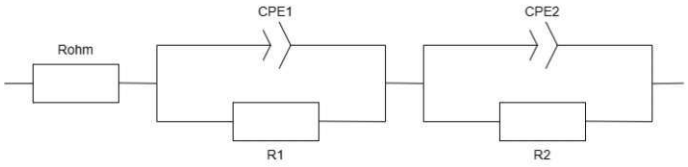

Figure 4.6.: *Equivalent electrical circuit used for fitting the Nyquist diagram in the spectroscopic impedance analysis of the PEM.*

The total resistance of the cell is below 1Ω during its operation, and the observed inductive part originates from the bandwidth limitation of the PSM3750, as detailed in section 3.2.3.

The first small semicircle varies little with the applied voltage; it likely originates from a geometric artifact described section 2.7.5.

The second semicircle likely originates from the charge transfer resistance during the surface electrochemical reaction. The radius of this semicircle strongly depends on the value of the applied voltage, and vary inversely proportional to the applied current. The oxygen oxidation reaction OER is responsible for the majority of the cell's charge resistance, as this reaction requires more energy to occur. Unfortunately, in the absence of a reference electrode, it is not possible to distinguish the semicircles associated with the two different reactions, as they occur at similar characteristic times. The spectroscopic impedance measurement by directly applying a signal between the working electrode and the counter electrode only provides access to the combined value of the charge resistance in this case.

For a voltage of 1.52 V, the measured current density is approximately 6 mA/cm². The Tafel approximation 2.58 under the high-potential assumption gives, assuming an alpha value of 0.6 for the OER reaction at the Iridium oxide electrode [36] :

$$R_{ct,OER} = \frac{8.314\text{Jmol}^{-1}\text{K}^{-1} \times 294.15\text{K}}{0.6 \times 6\text{mA/cm}^2} = 0.44\Omega \tag{4.1}$$

This value is close to the measured charge transfer resistance for the OER obtained from the spectrometer, which is 0.41 Ω. Assuming hat the Nafion membrane has a conductivity of 0.1 S/cm [1] and a thickness of 50 μm :

$$R_{ohm} = \frac{50\mu m}{0.1\text{Scm}^{-1} \times 16\text{cm}^2} = 0.031\Omega \tag{4.2}$$

This time, a discrepancy ten times higher than the theoretical ohmic resistance of the membrane is measured by the PSM3750. However, the value of 0.14 Ω could correspond to the resistance of the cables used during the measurement, which adds to the resistance of the membrane.

Presented is a diagram illustrating the resistance distribution within the PEM cell operating at 1.52V.

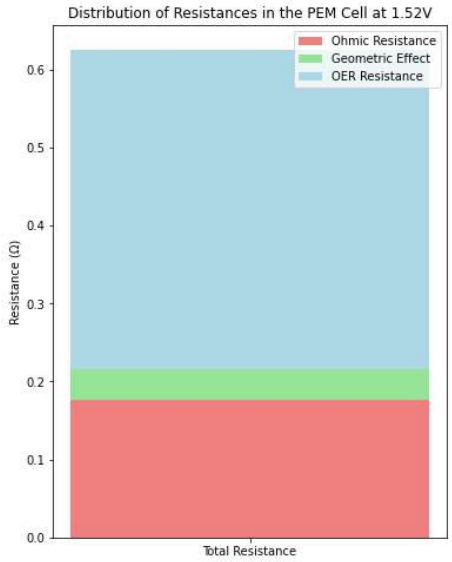

Figure 4.7.: *Equivalent electrical circuit used for fitting the Nyquist diagram in the spectroscopic impedance analysis of the PEM.*

In Figure 4.8, the U-I curve is plotted to observe the behavior of the cell as a function of the applied DC voltage. From 1.52 V onward, it can be inferred that the cell operates in a linear regime, where the overpotential loss due to the ohmic effect increases with current.

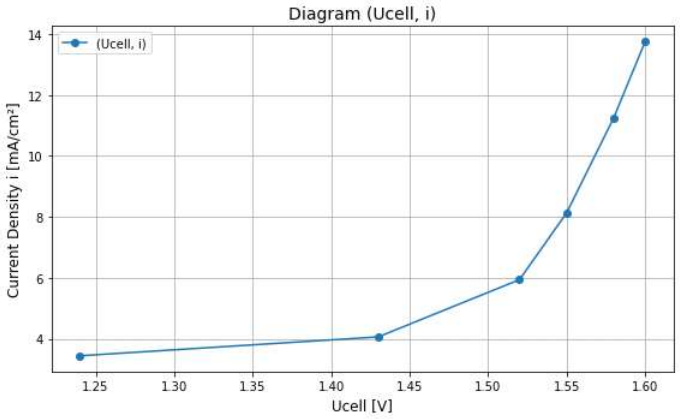

Figure 4.8.: *Distribution Diagram of Resistances in the PEM at 1.52V*

4.3. AEM Design 3.0 Cell Impedance Spectroscopy Analysis with Different Parameters

Various parameters of the AEM cell were modified to assess their influence on the cell's impedance. The primary source of variation comes from the type of reactive liquid used for CO_2 absorption. Four different reactive liquids were used: KOH, AMP, MEA, and K_2CO_3. The analysis results are therefore divided into four sections, one for each reactive liquid. The different parameters studied are summarized in Table 4.2.

Absorber	**Varied Parameters**
KOH	Voltage Temperature (30°C and 40°C) Measurement time (after 30min of operation) N_2 injection
AMP	Voltage Temperature (30°C, 40°C and 50°C)
MEA	Voltage Temperature (30°C, 40°C and 50°C) Concentration (30%wt, 20%wt, 10%wt, 5%wt) Pumping
K_2CO_3	Voltage Temperature (40°C and 60°C) Concentration (0.5%wt and 0.25%wt)

Table 4.2.: *Summary of varied parameters for each absorption solution*

For all analyses, the circuit in Figure 4.9 is used for fitting the Nyquist diagram. It consists of an ohmic resistance in series with three resistances (R1, R2, R3), each in

parallel with a corresponding CPE (CPE1, CPE2, and CPE3). While the PEM could be modeled using two R circuits in parallel with CPEs, the equivalent circuit of the AEM cell design 3.0 requires a third R circuit in parallel with a CPE. This is because modeling with only two parallel circuits failed to fully represent the Nyquist plot, particularly in the low-frequency region.

Since the inductance is an effect of the PSM3750's limitation as mentioned in section 3.2.3, the equivalent inductance value in the Nyquist diagram will not be considered during the fitting process.

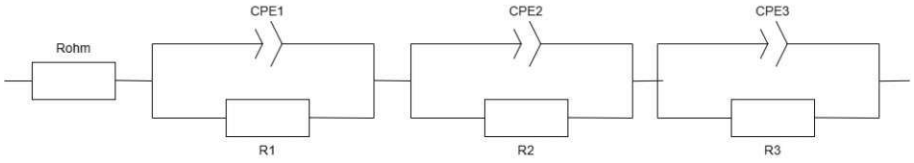

Figure 4.9.: *Equivalent electrical circuit used for fitting the Nyquist diagram in the spectroscopic impedance analysis of the AEM 3.0 Design for different parameters*

4.3.1. CO_2 absorption with KOH

The following configurations were selected for the analysis of the cell with KOH :

- FAA-3-130 as membrane
- Titanium Flow Fields
- Carbon gas diffusion layer coated with silver nanoparticules as cathode electrocatalyst
- Nickel foam as anode electrocatalyst

Voltage Variation

With the temperature set to ambient temperature $T = 21°C$. The frequency window ranges from 10^5 Hz to 10^{-1} Hz, and the amplitude of the AC signal is set to 30 mV.

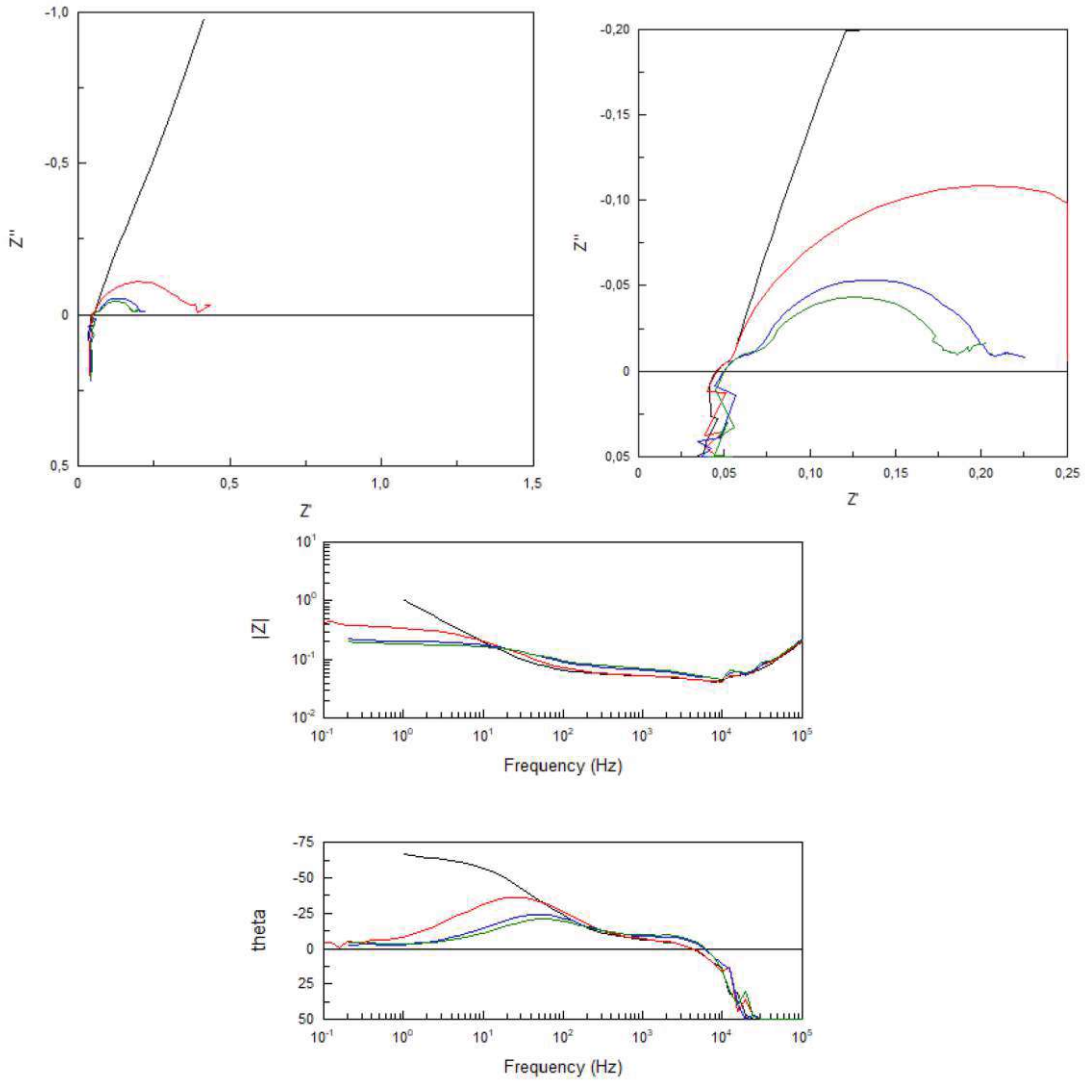

Figure 4.10.: *Nyquist (top) Bode diagram (botton) of voltage variation using KOH*

In the Nyquist diagram, the characteristic line of the Warburg impedance model, depicted in black for a specific DC voltage of 1.5V, represents the resistance associated with semi-infinite species diffusion.

The second system, (R2//CPE2), corresponds to the oxygen oxidation reaction at the anode. The resistance is observed to decrease inversely with the current, consistent with the theoretical resistance associated with the overpotential of the surface half-reaction.

Additionally, the resistance corresponding to a third semicircle is measurable. This resistance may originate from the cathodic reaction, though its precise value is challeng-

Ucell DC [V]	Icell [A]	Rohm [Ω]	R 1cc [Ω]	C 1cc [F]	P 1cc [1]
2	0,41	0,046	0,007	0,06	0,75
2,25	1,15	0,05	0,02	0,03	0,75
2,4	1,73	0,05	0,023	0,03	0,74
R 2cc [Ω]	**C 2cc [F]**	**P 2cc [1]**	**R 3cc [Ω]**	**C 3cc [F]**	**P 3cc [1]**
0,29	0,15	0,8	0,06	20	0,8
0,133	0,1	0,8	0,027	60	0,8
0,11	0,1	0,8	0,045	40	0,8

Table 4.3.: *Table of different impedance characteristic values for voltage variation using KOH*

ing to determine due to the limitation of the studied frequency range.

Time Variation

At an ambient temperature of $T = 21°C$, the frequency range spans from 10^5Hz to 10^{-1} Hz, with an AC signal amplitude of 30 mV. Both analyses were conducted 30 minutes apart. The two presented curves can be compared since the current flowing through the cell during the analysis is similar in both cases (1.73A and 1.62A).

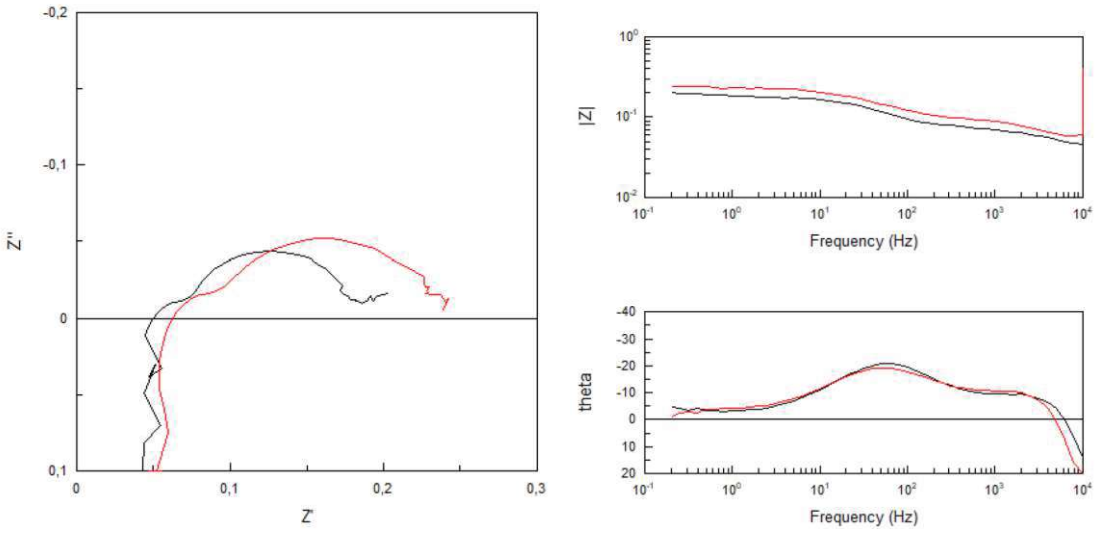

Figure 4.11.: *Nyquist (left) Bode diagram (right) of time variation using KOH*

After 30 minutes, an increase in ohmic resistance is observed, which can be attributed to several potential factors. One hypothesis is the stagnation of the alkaline KOH solu-

Ucell DC [V]	Icell [A]	Rohm [Ohm]	R 1cc [Ohm]	C 1cc [F]	P 1cc [1]
2,4	1,73	0,05	0,023	0,03	0,74
2,75	1,62	0,063	0,03	0,025	0,74
R 2cc [Ohm]	**C 2cc [F]**	**P 2cc [1]**	**R 3cc [Ohm]**	**C 3cc [F]**	**P 3cc [1]**
0,11	0,1	0,84	0,045	40	0,8
0,145	0,13	0,76	x	x	x

Table 4.4.: *Table of different impedance characteristic values for time variation using KOH. Black is associated to the first measurement, whereas red to the one after 30min*

tion within the cell, which may lead to membrane degradation. This degradation could result in a decrease in conductivity, thereby contributing to the observed increase in resistance.

The charge transfer resistance R2cc associated with the overpotential of the OER reaction also increases after 30 minutes.

Temperature Variation

The frequency window ranges from 10^5 Hz to 10^{-1} Hz, and the amplitude of the AC signal is set to 30 mV. Spectroscopic analyses are conducted at temperatures of 30°C and 40°C degrees, and the impact of the temperature increase on the cell impedance value is studied. One possible explanatory hypothesis could be the degradation of the catayst.

Ucell DC [V]	Icell [A]	Rohm [Ohm]	R 1cc [Ohm]	C 1cc [F]	P 1cc [1]
2 (30°C)	0,5	0,048	0,0142	0,06	0,71
2 (40°C)	0,57	0,044	0,022	0,04	0,71
2,25 (30°C)	1,32	0,049	0,017	0,05	0,71
2,25 (40°C)	1,27	0,046	0,024	0,05	0,71
R 2cc [Ohm]	**C 2cc [F]**	**P 2cc [1]**	**R 3cc [Ohm]**	**C 3cc [F]**	**P 3cc [1]**
0,24	0,2	0,82	0,03	25	0,8
0,22	0,22	0,82	0,045	20	0,8
0,123	0,18	0,85	0,05	50	0,8
0,118	0,19	0,85	0,05	40	0,8

Table 4.5.: *Table of different impedance characteristic values for temperature variation using KOH*

The temperature appears to influence the ohmic resistance, as it decreases with increasing temperature. However, the resistance R1cc, associated with geometric resistance, seems to increase with temperature. The sum of these two types of resistance appears to remain constant.

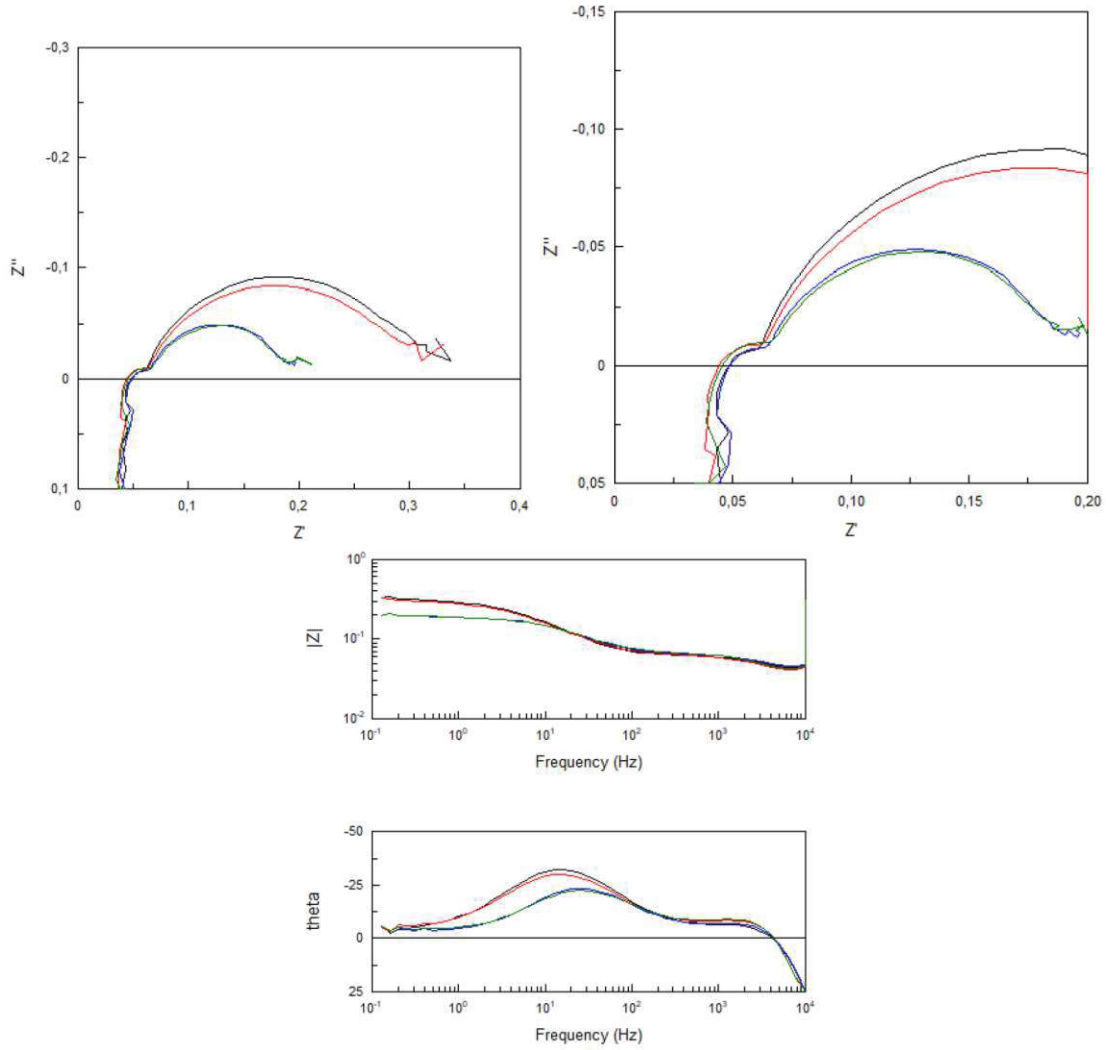

Figure 4.12.: *Nyquist (top) Bode diagram (botton) of temperature variation using KOH*

Temperature seems to have a slight effect on the resistance associated with the overpotential of the OER reaction, but this effect is not significant enough to draw a definitive conclusion about its impact.

Removal of physically absorbed CO_2 by N_2 injection

At an ambient temperature of $T = 21°C$ and the frequency window ranges from 10^5 Hz to 10^{-1} Hz, the amplitude of the AC signal for measurement is set to 30 mV. To determine if physically absorbed CO_2 impacts the cell impedance during its reduction, a measurement with CO_2 injection will be compared to another with N_2 injection to

remove the physically absorbed CO_2.

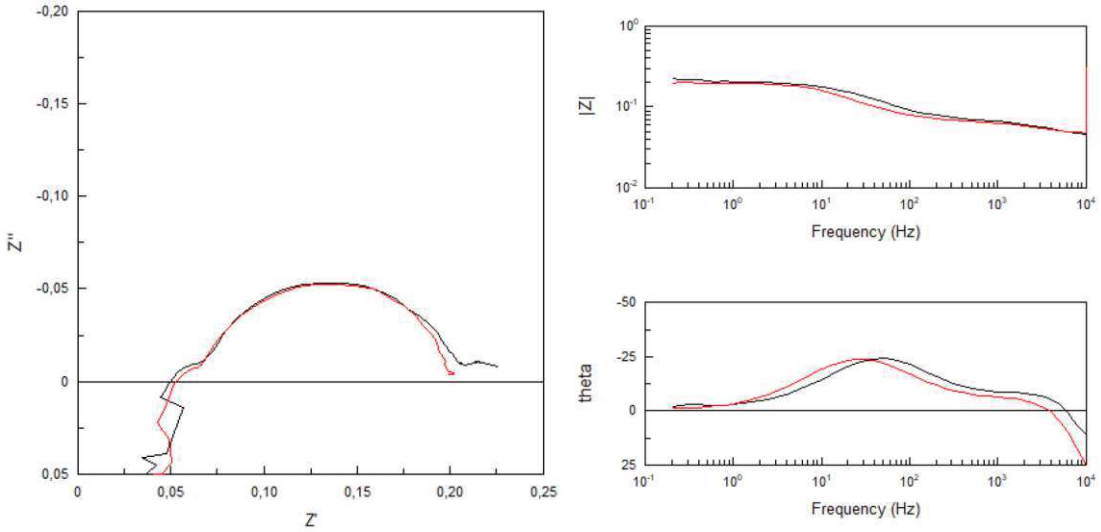

Figure 4.13.: *Nyquist (left) and Bode diagram (right) with N_2 injection using KOH for current in close proximity*

Ucell DC [V]	**Icell [A]**	**Rohm [Ohm]**	**R 1cc [Ohm]**	**C 1cc [F]**	**P 1cc [1]**
2,25	1,15	0,05	0,02	0,03	0,75
2,2	1,02	0,053	0,014	0,1	0,71
R 2cc [Ohm]	**C 2cc [F]**	**P 2cc [1]**	**R 3cc [Ohm]**	**C 3cc [F]**	**P 3cc [1]**
0,133	0,22	0,87	0,027	60	0,8
0,133	0,17	0,86	x	x	x

Table 4.6.: *Table of different impedance characteristic values with CO_2 injection (black) and N_2 injection (red) using KOH for current in close proximity*

It is therefore expected that the injection of N_2 would impact the CO_2 reduction reaction at the cathode, provided it is possible to distinguish it without a reference electrode. A remarkable result is that for two different test currents, one around 1.1 A and the other around 1.7 A, a semi-circular arc at low frequencies disappears each time during the injection of N_2. This would suggest, assuming the detected semicircle is associated with the charge transfer resistance of the CO_2 reduction reaction, that the reduction reaction at the cathode is indeed affected. However, this does not allow for the conclusion that the reaction is entirely absent but rather suggests a modification in the reaction occurring at the cathode.

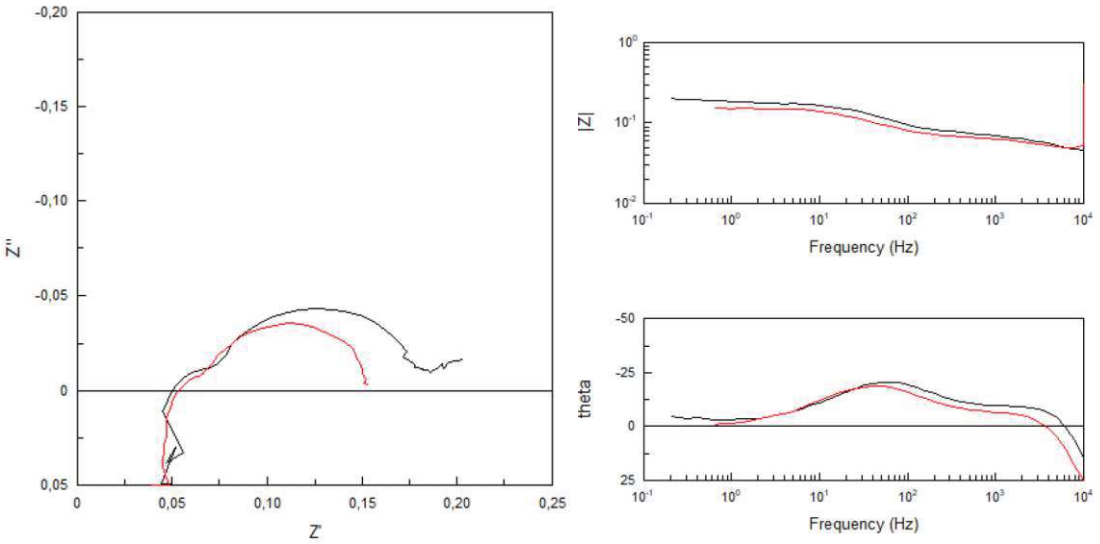

Figure 4.14.: *Nyquist (left) and Bode diagram (right) with N_2 injection using KOH for current in close proximity (1.7A)*

Ucell DC [V]	Icell [A]	Rohm [Ohm]	R 1cc [Ohm]	C 1cc [F]	P 1cc [1]
2,4	1,73	0,05	0,023	0,03	0,74
2,3	1,65	0,053	0,014	0,1	0,71
R 2cc [Ohm]	**C 2cc [F]**	**P 2cc [1]**	**R 3cc [Ohm]**	**C 3cc [F]**	**P 3cc [1]**
0,11	0,1	0,84	0,045	40	0,8
0,09	0,17	0,85	x	x	x

Table 4.7.: *Table of different impedance characteristic values with CO_2 injection (black) and N_2 injection (red) using KOH for current in close proximity (1.7A)*

The injection of N_2 also appears to influence the resistance associated with the geometric artifact of the cell. One possible explanation could be the variation in the type of physically dissolved species affecting the distribution of the electric field within the catholyte.

4.3.2. CO_2 absorption with AMP

The following configurations were selected for the analysis of the cell with AMP :

- FAA-3-130 as membrane
- Titanium Flow Fields
- Carbon gas diffusion layer coated with silver nanoparticules as cathode electrocatalyst
- Nickel foam as anode electrocatalyst

Voltage Variation

At an ambient temperature of $T = 21°C$, the frequency range spans from 10^5 Hz to 10^{-1} Hz, with an AC signal amplitude of 30 mV.

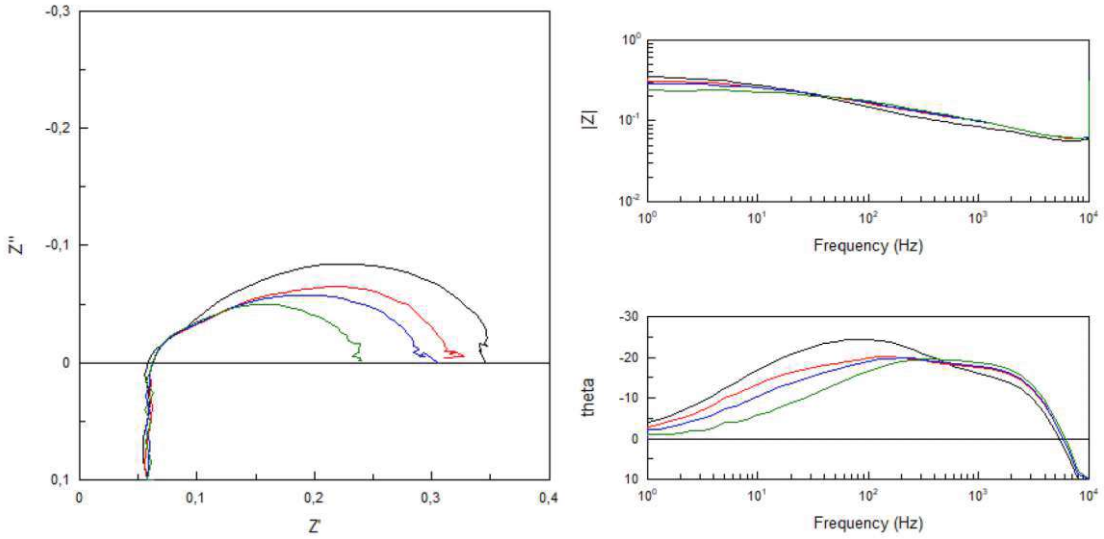

Figure 4.15.: *Nyquist (left) and Bode diagram (right) of voltage variation using AMP*

Ucell DC [V]	Icell [A]	Rohm [Ohm]	R 1cc [Ohm]	C 1cc [F]	P 1cc [1]
2	0,42	0,058	0,036	0,05	0,71
2,1	0,83	0,062	0,046	0,04	0,71
2,2	1,09	0,062	0,046	0,04	0,71
2,35	1,77	0,062	0,046	0,03	0,75
R 2cc [Ohm]	**C 2cc [F]**	**P 2cc [1]**	**R 3cc [Ohm]**	**C 3cc [F]**	**P 3cc [1]**
0,22	0,09	0,74	0,055	0,9	0,84
0,12	0,12	0,71	0,1	0,3	0,84
0,12	0,1	0,71	0,07	0,3	0,84
0,11	0,09	0,75	0,02	0,3	0,84

Table 4.8.: *Table of different impedance characteristic values for voltage variation using KOH*

Using AMP as the reactive absorber fluid, the presence of two distinct semicircles corresponding to two different overpotential reaction resistances is less evident. The charge transfer resistances associated with these two reactions, R2cc and R3cc, decrease with an increase in current density. R2cc is likely still associated with the OER, while R3cc corresponds to the reduction occurring at the cathode.

Temperature Variation

The frequency window ranges from 10^5 Hz to 10^{-1} Hz, and the amplitude of the AC signal is set to 30 mV. Spectroscopic analyses are conducted at temperatures of 30°C, 40°C and 50°C degrees, and the impact of the temperature increase on the cell impedance value is studied. For a more accurate comparison of the temperature influence on the Nyquist plot, the curves are compared at a current value as close as possible (around 1.77A). In this case, the cell is subjected to the same charge flux.

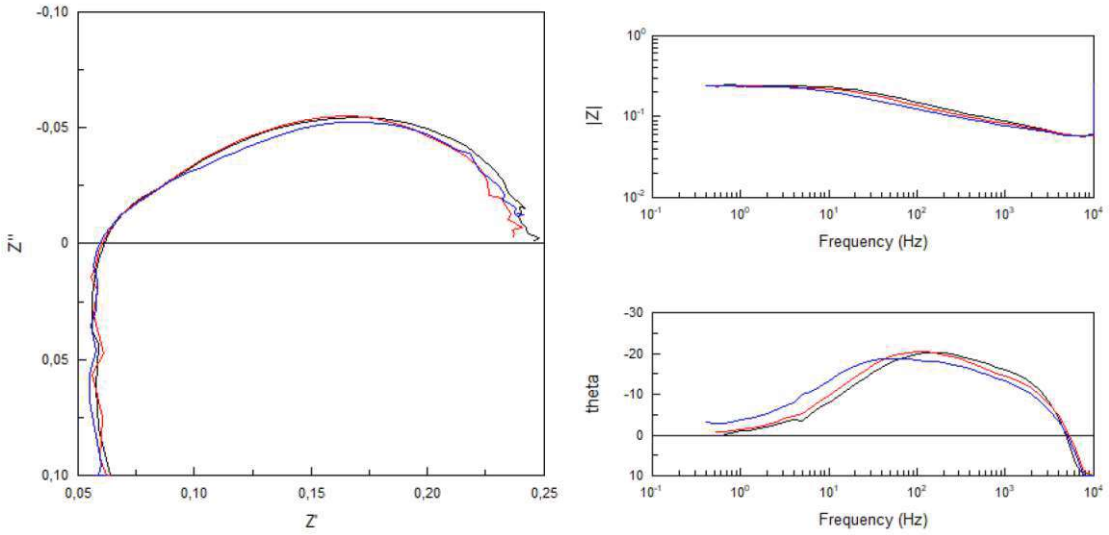

Figure 4.16.: *Nyquist (left) and Bode diagram (right) of temperature variation using AMP*

Ucell DC [V]	Icell [A]	Rohm [Ohm]	R 1cc [Ohm]	C 1cc [F]	P 1cc [1]
2,85 (30°C)	1,83	0,061	0,03	0,06	0,71
2,75 (40°C)	1,77	0,061	0,03	0,065	0,71
2,6 (50°C)	1,74	0,061	0,05	0,07	0,71
R 2cc [Ohm]	**C 2cc [F]**	**P 2cc [1]**	**R 3cc [Ohm]**	**C 3cc [F]**	**P 3cc [1]**
0,156	0,08	0,75	x	x	x
0,148	0,079	0,79	x	x	x
0,135	0,15	0,79	x	x	x

Table 4.9.: *Table of different impedance characteristic values for temperature variation using AMP*

In this case, a more distinct dependence of the impedance on the reaction overpotential is observed. The charge transfer resistance R2cc decreases with increasing temperature. No charge transfer resistance R3cc is detected, likely because the characteristic time of the cathodic reaction closely overlaps with that of the oxygen evolution reaction (OER).

4.3.3. CO_2 absorption with MEA

The following configurations were selected for the analysis of the cell with AMP :

- FAA-3-130 as membrane
- Titanium Flow Fields
- Carbon gas diffusion layer coated with silver nanoparticules as cathode electrocatalyst
- Nickel foam as anode electrocatalyst

Voltage Variation

At an ambient temperature of $T = 21°C$, the frequency range extends from 10^5 Hz to 10^{-1} Hz with an AC signal amplitude of 30 mV. The concentration of the MEA solution chosen as the absorber fluid for the voltage measurement is 5% wt.

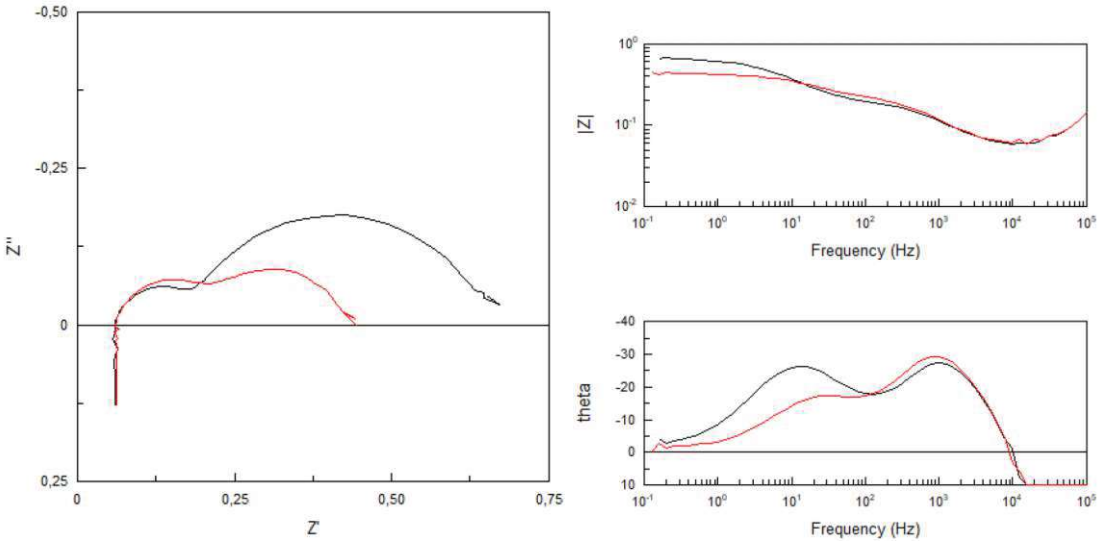

Figure 4.17.: *Nyquist (left) and Bode diagram (right) of voltage variation using MEA*

Similarly, a decrease in the charge transfer resistance R2cc is observed with an increase in current density. However, no distinct third semicircle associated with the reaction overpotential resistance of the cathodic reduction is clearly observed.

Ucell DC [V]	Icell [A]	Rohm [Ohm]	R 1cc [Ohm]	C 1cc [F]	P 1cc [1]
2,25	0,45	0,061	0,11	0,005	0,91
2,5	0,93	0,061	0,12	0,006	0,91
R 2cc [Ohm]	**C 2cc [F]**	**P 2cc [1]**	**R 3cc [Ohm]**	**C 3cc [F]**	**P 3cc [1]**
0,49	0,13	0,78	x	x	x
0,25	0,15	0,76	x	x	x

Table 4.10.: *Table of different impedance characteristic values for voltage variation using MEA 5%wt*

Concentration Variation

With the temperature set to ambient temperature $T = 21°C$. The frequency window ranges from 10^5 Hz to 10^{-1} Hz, and the amplitude of the AC signal is set to 30 mV. Four variations of MEA solution concentration were tested for the analysis: 30%wt, 20%wt, 10%wt, and 5%wt. To enable comparison at the same current density, the results of a comparison between a 30%wt and 20%wt solution are compared at the same current density of 1.3, as well as between a 20%wt and 5%wt solution.

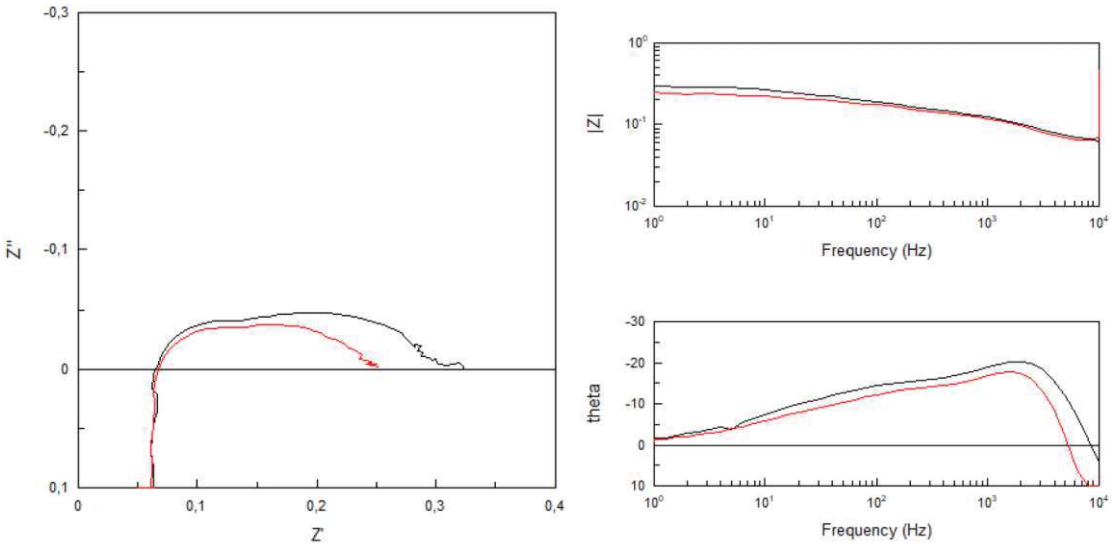

Figure 4.18.: *Nyquist (left) and Bode diagram (right) of concentration variation using MEA*

At first glance, the trend appears to suggest a reduction in the reaction overpotential impedance as the MEA concentration increases. However, the result appears surprising if the MEA concentration influences the OER reaction impedance, which could be possible in the case of leakage.

Ucell DC [V]	Icell [A]	Rohm [Ohm]	R 1cc [Ohm]	C 1cc [F]	P 1cc [1]
2,5 (20%wt)	1,65	0,066	0,07	0,0055	0,85
2,25 (30%wt)	1,65	0,066	0,06	0,006	0,85
R 2cc [Ohm]	**C 2cc [F]**	**P 2cc [1]**	**R 3cc [Ohm]**	**C 3cc [F]**	**P 3cc [1]**
0,12	0,1	0,71	0,04	1	0,84
0,09	0,1	0,71	0,03	1	0,84

Table 4.11.: *Table of different impedance characteristic values for concentration variation using MEA* 20%*wt and* 30%*wt*

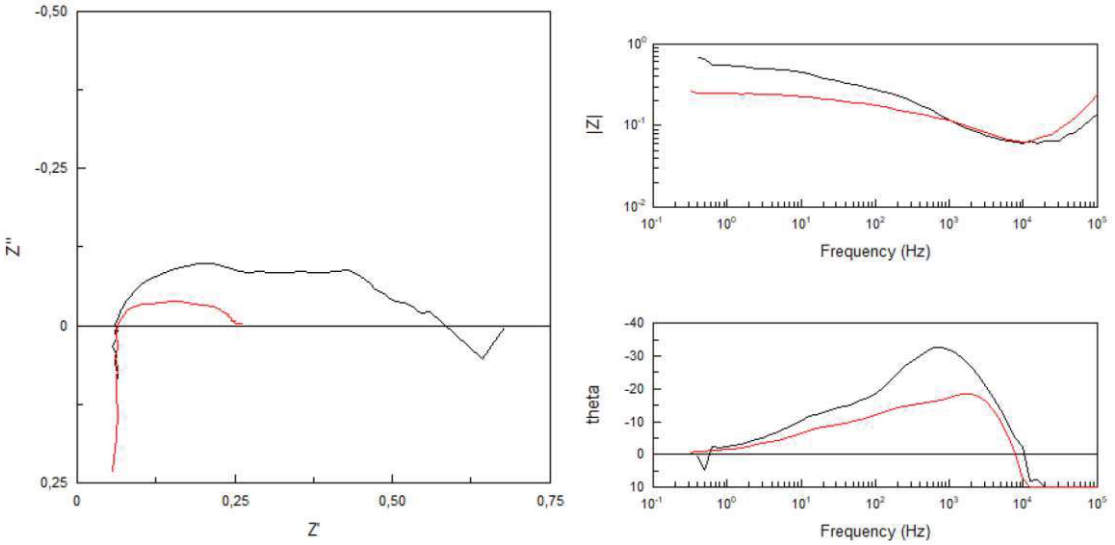

Figure 4.19.: *Nyquist (left) and Bode diagram (right) of concentration variation using MEA*

Ucell DC [V]	Icell [A]	Rohm [Ohm]	R 1cc [Ohm]	C 1cc [F]	P 1cc [1]
2,75 (5%wt)	1,4	0,066	0,2	0,0075	0,85
2,25 (20%wt)	1,48	0,066	0,055	0,006	0,85
R 2cc [Ohm]	**C 2cc [F]**	**P 2cc [1]**	**R 3cc [Ohm]**	**C 3cc [F]**	**P 3cc [1]**
0,17	0,25	0,71	0,06	0,5	0,84
0,095	0,09	0,71	0,035	1	0,84

Table 4.12.: *Table of different impedance characteristic values for concentration variation using MEA* 5%*wt and* 20%*wt*

A more likely hypothesis would be that the third semicircle is instead associated here with a diffusion impedance. Indeed, the increase in MEA concentration enhances the formation of dissolved ionic species from CO_2, such as carbonate CO_3^{2-} or bicarbonate HCO_3^- ions, which conduct the current in the cell.

However, there is also a reduction in the charge transfer resistance R2cc, typically associated with the OER reaction. This suggests that the concentration of the catholyte globally affects both overpotential-related impedances.

Temperature Variation

The frequency window ranges from 10^5 Hz to 10^{-1} Hz, and the amplitude of the AC signal is set to 30 mV. Spectroscopic analyses are conducted at room temperatures 21°C and 50°C degrees, and the impact of the temperature increase on the cell impedance value is studied.

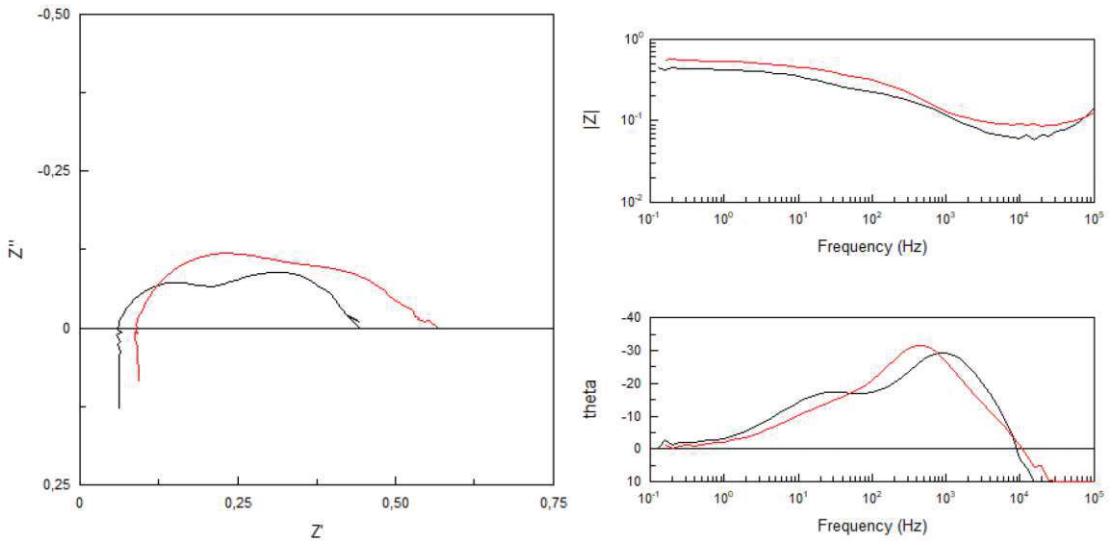

Figure 4.20.: *Nyquist (left) and Bode diagram (right) of temperature variation between 21° and 50° using MEA*

Ucell DC [V]	Icell [A]	Rohm [Ohm]	R 1cc [Ohm]	C 1cc [F]	P 1cc [1]
2,5 (21°C)	0,93	0,061	0,12	0,006	0,91
2,5 (50°C)	0,92	0,09	0,2	0,006	0,91
R 2cc [Ohm]	**C 2cc [F]**	**P 2cc [1]**	**R 3cc [Ohm]**	**C 3cc [F]**	**P 3cc [1]**
0,25	0,15	0,76	x	x	x
0,25	0,15	0,7	x	x	x

Table 4.13.: *Table of different impedance characteristic values for temperature variation between 21° and 50° using MEA 5%wt*

Overall, it appears that the increase in temperature has a negative impact on the cell

impedance, as the values of ohmic resistance and geometric resistance increase with rising temperature. This phenomenon is also observed when comparing the cell impedance between 30°C and 40°C .

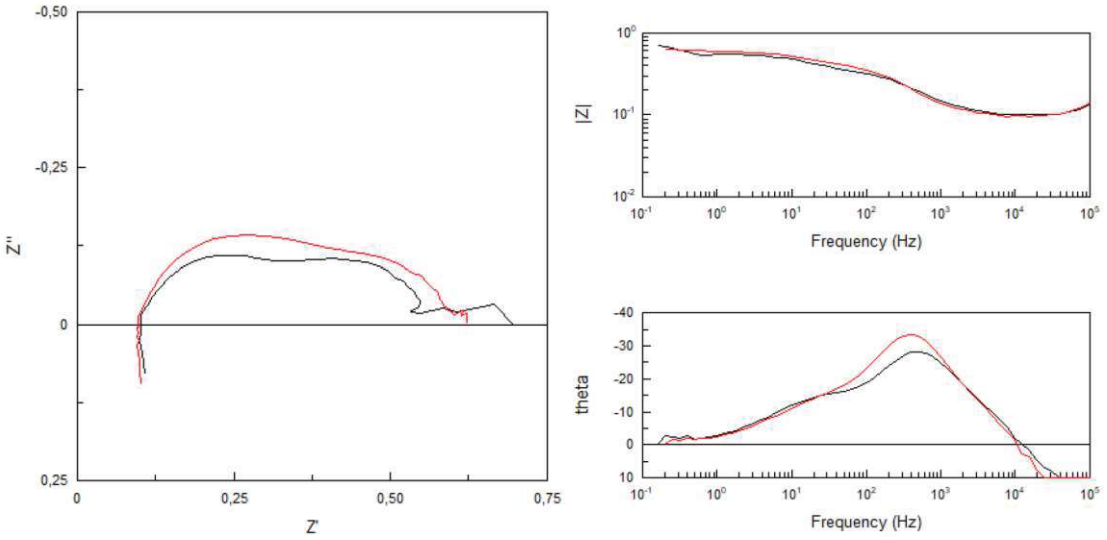

Figure 4.21.: *Nyquist (left) and Bode diagram (right) of temperature variation between* 30° *and* 40° *using MEA*

Ucell DC [V]	Icell [A]	Rohm [Ohm]	R 1cc [Ohm]	C 1cc [F]	P 1cc [1]
2,5 (30°C)	0,71	0,098	0,18	0,006	0,91
2,5 (40°C)	0,78	0,098	0,22	0,006	0,91
R 2cc [Ohm]	**C 2cc [F]**	**P 2cc [1]**	**R 3cc [Ohm]**	**C 3cc [F]**	**P 3cc [1]**
0,91	0,3	0,7	x	x	x
0,91	0,3	0,7	x	x	x

Table 4.14.: *Table of different impedance characteristic values for temperature variation between* 30° *and* 40° *using MEA* 5%*wt*

Therefore, increasing the temperature does not appear to improve the cell impedance; on the contrary, it seems to have a negative effect.

With or Without the Use of Pumping

At an ambient temperature of $T = 21°C$ impedance measurements were conducted over a frequency range of 10^5 Hz to 10^{-1} Hz, with an AC signal amplitude of 30 mV. The absorber fluid used was a 20% wt MEA solution. To assess the presence of species transport resistance, measurements were performed both with and without the operation of

the pumps supplying reactants to the cathode and anode.

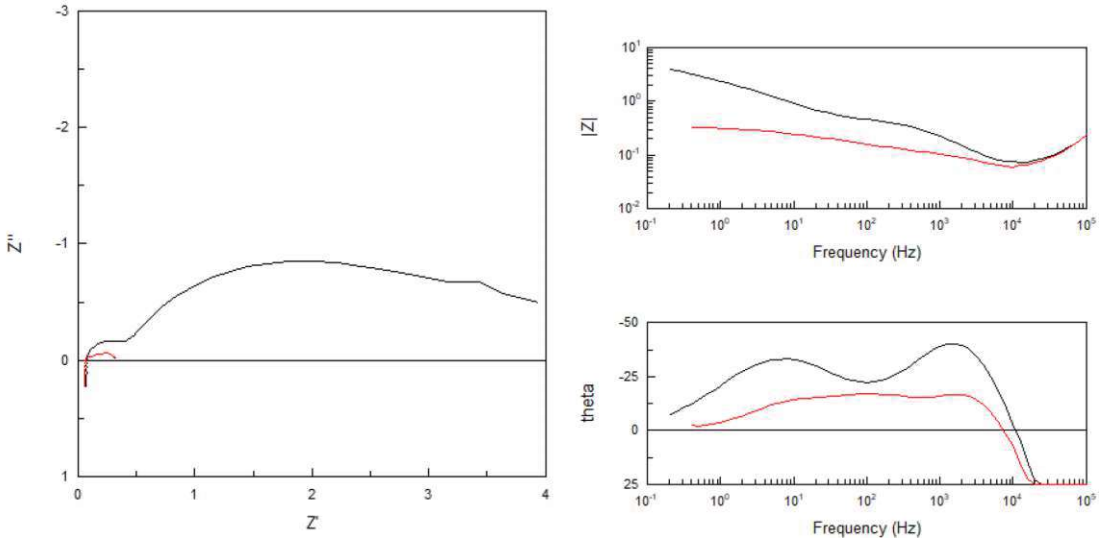

Figure 4.22.: *Nyquist (left) and Bode diagram (right) with and without pumping using MEA 20%wt*

Ucell DC [V]	Icell [A]	Rohm [Ohm]	R 1cc [Ohm]	C 1cc [F]	P 1cc [1]
2 (No Supply)	0,08	0,076	0,35	0,002	0,88
2	0,64	0,064	0,04	0,0075	0,88
R 2cc [Ohm]	**C 2cc [F]**	**P 2cc [1]**	**R 3cc [Ohm]**	**C 3cc [F]**	**P 3cc [1]**
2,6	0,08	0,69	1,2	2,4	0,8
0,06	0,3	0,65	0,16	0,4	0,7

Table 4.15.: *Nyquist (left) and Bode diagram (right) with and without pumping using MEA 20%wt*

A significant increase in the total impedance of the cell is observed. The observed change in impedance is likely attributable to the accumulation of gas bubbles within the flow field. These trapped bubbles impede the ionic charge transfer between the electrodes by obstructing the conductive pathways in the electrolyte.

4.3.4. CO_2 absorption with K_2CO_3

The following configurations were selected for the analysis of the cell with AMP :

- Sustainion X37-50 as membrane
- Titanium Flow Fields
- Carbon gas diffusion layer coated with silver nanoparticules as cathode electrocatalyst
- Carbon gas diffusion layer coated with iridium oxide particules as cathode electrocatalyst

Voltage Variation

With the temperature set to ambient temperature $T = 21°C$. The frequency window ranges from 10^5 Hz to 10^{-1} Hz, and the amplitude of the AC signal is set to 30 mV. The concentration of the K_2CO_3 solution chosen as the absorber fluid for the voltage measurement is 0.25% wt.

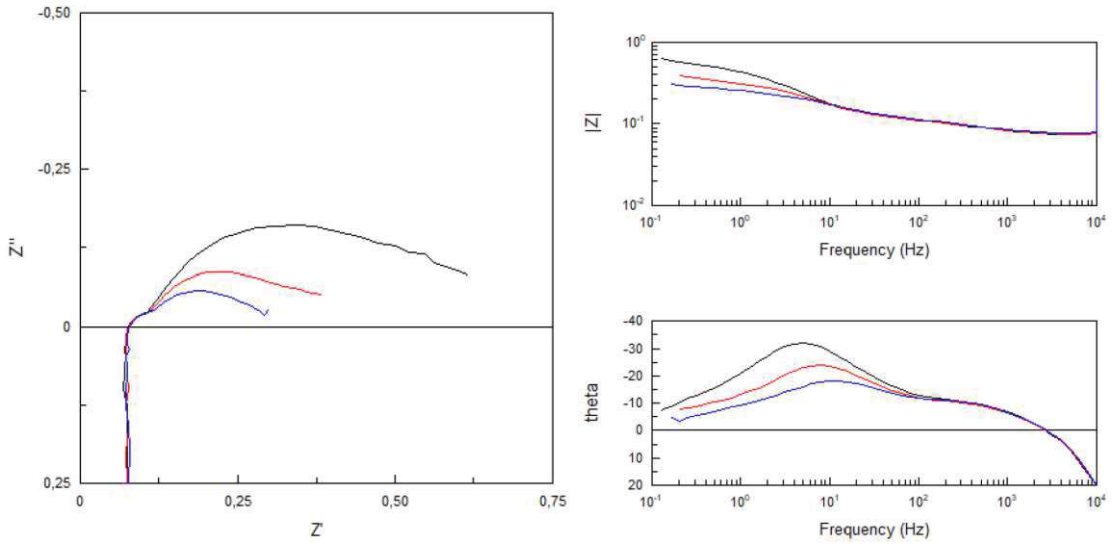

Figure 4.23.: *Nyquist (left) and Bode diagram (right) of voltage variation using* K_2CO_3 0.25%*wt*

As with the previous solutions, a typical decrease in reaction overpotential impedance is observed with increasing current density.

Ucell DC [V]	Icell [A]	Rohm [Ohm]	R 1cc [Ohm]	C 1cc [F]	P 1cc [1]
2	0,8	0,076	0,03	0,08	0,79
2,2	1,1	0,076	0,03	0,08	0,79
2,35	1,42	0,078	0,03	0,065	0,79
R 2cc [Ohm]	**C 2cc [F]**	**P 2cc [1]**	**R 3cc [Ohm]**	**C 3cc [F]**	**P 3cc [1]**
0,42	0,38	0,78	0,14	10	0,8
0,22	0,38	0,78	0,1	10	0,8
0,16	0,4	0,79	0,035	15	0,8

Table 4.16.: *Table of different impedance characteristic values for voltage variation using* K_2CO_3 0.25%*wt*

Concentration Variation

With the temperature set to ambient temperature $T = 21°C$. The frequency window ranges from 10^5 Hz to 10^{-1} Hz, and the amplitude of the AC signal is set to 30 mV. Two variations of K_2CO_3 solution concentration were tested for the analysis: 0.5%wt and 0.25%wt.

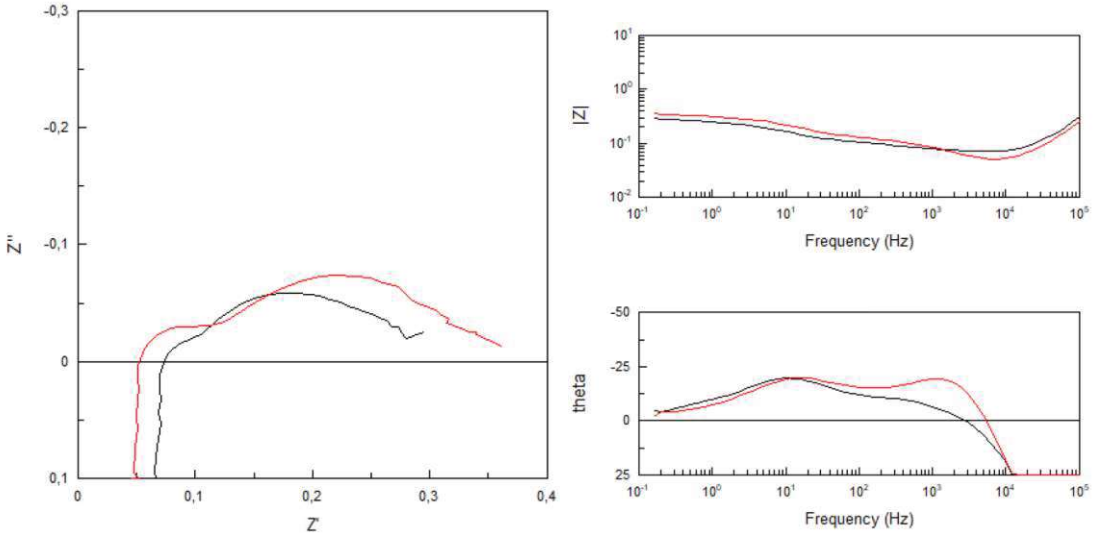

Figure 4.24.: *Nyquist (left) and Bode diagram (right) of concentration variation using* K_2CO_3

What is interesting here, unlike with MEA, is that the cell impedance is smaller when the K_2CO_3 concentration decreases. In fact, the ohmic resistance decreases with the increase in concentration, but the reaction overpotential impedance increases.

Ucell DC [V]	Icell [A]	Rohm [Ohm]	R 1cc [Ohm]	C 1cc [F]	P 1cc [1]
2,25 (0.25%wt)	1,39	0,074	0,03	0,07	0,8
2,4 (0.5%wt)	1,4	0,052	0,07	0,016	0,8
R 2cc [Ohm]	**C 2cc [F]**	**P 2cc [1]**	**R 3cc [Ohm]**	**C 3cc [F]**	**P 3cc [1]**
0,16	0,38	0,78	0,03	20	0,8
0,2	0,23	0,78	0,04	20	0,8

Table 4.17.: *Table of different impedance characteristic values for concentration variation using K_2CO_3 0.25%wt*

Temperature Variation

The frequency window ranges from 10^5 Hz to 10^{-1} Hz, and the amplitude of the AC signal is set to 30 mV. Spectroscopic analyses are conducted at room temperatures 21°C, 40°C and 60°C, and the impact of the temperature increase on the cell impedance value is studied. The concentration of K_2CO_3 is set to 0.25%wt.To accurately assess the influence of temperature on the Nyquist plot, the curves are compared at a current value as close as possible (approximately 1.4A), ensuring that the cell experiences the same charge flux.

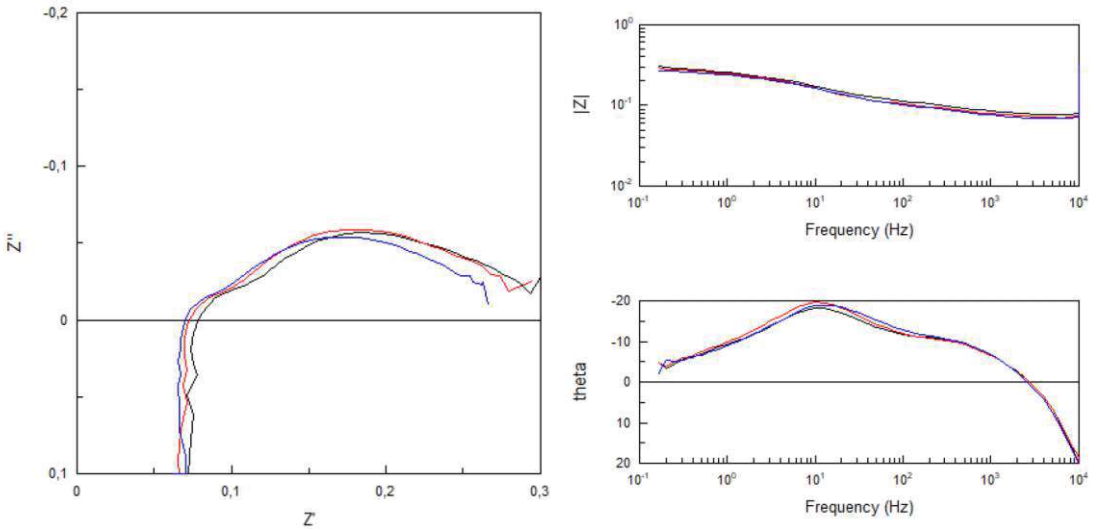

Figure 4.25.: *Nyquist (left) and Bode diagram (right) of temperature variation between 21°, 40° C and 60° using K_2CO_3*

The ohmic resistance and the charge transfer resistance for OER (R2cc) decrease as the temperature increases.

Ucell DC [V]	Icell [A]	Rohm [Ohm]	R 1cc [Ohm]	C 1cc [F]	P 1cc [1]
2,35 (21°C)	1,42	0,078	0,03	0,065	0,79
2,25 (40°C)	1,39	0,074	0,03	0,07	0,8
2,17 (60°C)	1,39	0,07	0,03	0,08	0,79
R 2cc [Ohm]	**C 2cc [F]**	**P 2cc [1]**	**R 3cc [Ohm]**	**C 3cc [F]**	**P 3cc [1]**
0,16	0,4	0,75	0,035	15	0,8
0,16	0,38	0,8	0,03	20	0,8
0,14	0,38	0,79	0,035	15	0,8

Table 4.18.: *Table of different impedance characteristic values for temperature variation using* K_2CO_3 0.25%*wt*

4.3.5. Summary

A summary of the obtained results is presented below:

- For KOH, the increase in temperature improves the cell's resistance for each different source. A low-frequency semicircular arc is observed, which vanishes upon the introduction of N_2. This behavior may indicate the occurrence of the CO_2 reduction reaction. Further confirmation is required using a newly designed cell optimized for spectroscopic impedance measurements.
- For AMP, charge transfer appears to be more efficient compared to KOH. Temperature variations does seem to have a slight effect on the cell's resistance with a decrease in OER impedance, and the detection of CO reduction remains inconclusive.
- For MEA, increasing the concentration at room temperature has a significant impact on the cell's resistance. However, raising the temperature appears to have a negative effect on resistance, affecting both the charge transfer resistance of the reaction and the ohmic resistance.
- For K_2CO_3, the cell resistance decreases with a reduction in concentration, while the equivalent double-layer capacitance is also impacted by this variation. Furthermore, an increase in temperature leads to a reduction in resistance.

A detailed summary table of the results is provided in the conclusion in table 5.1. To visually compare the different absorbers, the distribution of resistance sources for each absorber is presented under the same temperature conditions and at a similar current value (1.4A) in a bar chart in Figure 4.26.

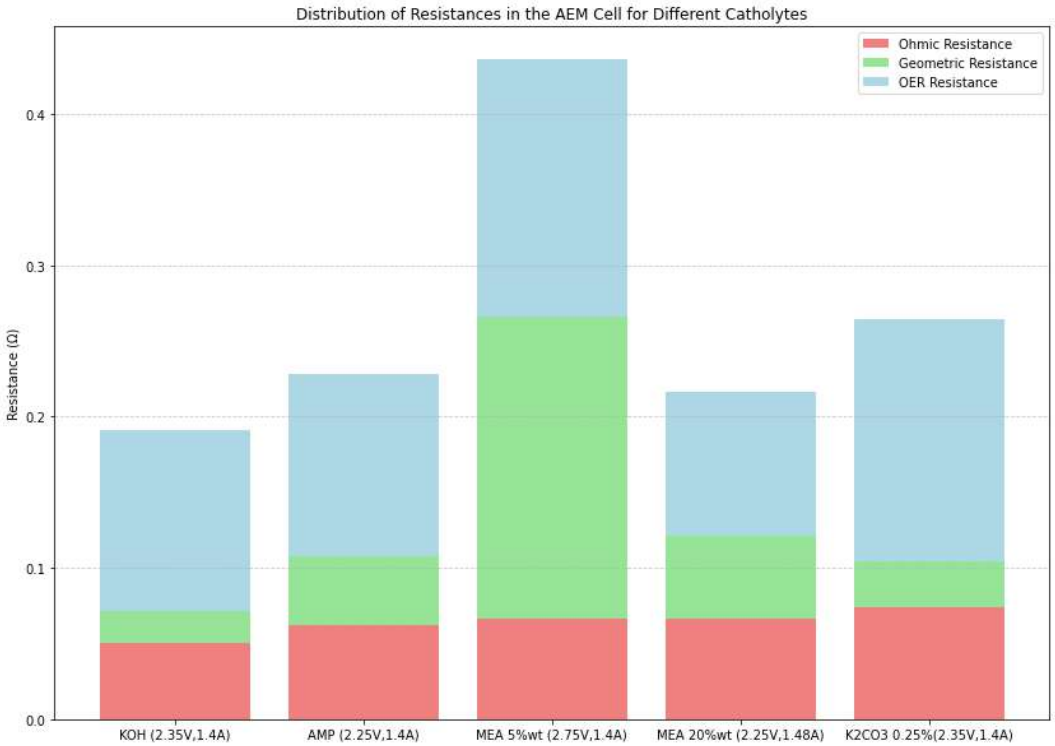

Figure 4.26.: *Comparison of the distribution of resistive effects for the AEM Design 3.0 cell with 4 different catholytes, under the same temperature conditions and at 1.4A*

- The ohmic resistance remains generally around the same value. Therefore, varying the catholyte at the same temperature does not significantly impact the ohmic resistance.
- The resistance attributed to geometric artifact varies significantly between measurements. Since the catalysts at the anode and cathode were not replaced during the experiments, this variation could potentially be explained by irreversible damage caused by the alkaline CO_2 absorption solution on both catalysts. The results are presented in the order of measurement, and a clear increase in this geometric artifact resistance is observed, which aligns with this hypothesis. Notably, the anode catalyst was replaced for the final measurement with K_2CO_3.
- The resistance associated with the electrochemical reaction, particularly the OER, varies slightly depending on the absorbent solution. If the OER resistance domi-

nates the portion of resistance related to the electrochemical reaction, this slight variation could be influenced by the CO_2 reduction reaction, which depends on the absorbent solution. To investigate further, it would be beneficial to study the reaction at each electrode. This can be achieved by introducing a reference electrode, as implemented in the new cell design with an active surface area of 16 cm^2.

It is important to note that the plausibility of certain results is influenced by the irreversible damage caused by the different alkaline solutions to various cell components. Despite the great care taken, it is important to emphasize that impedance measurements are highly sensitive. Errors may also arise from varying external conditions or from the application of the signal to the cell through contact with its terminals.

Finally, a visualization of the best measured configuration for each parameter setting is presented in the bar chart in Figure 4.27.

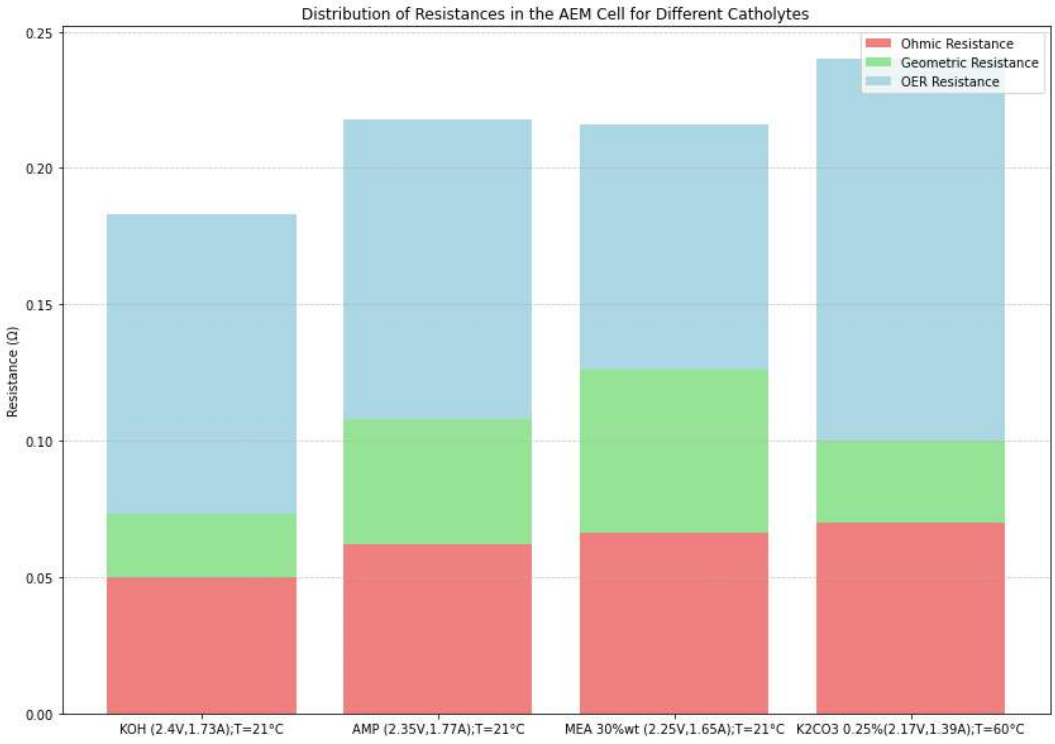

Figure 4.27.: *Comparison of the distribution of resistive effects for the AEM Design 3.0 cell with the best measured configuration for every catholyte*

- For KOH, a measured voltage of 2.4V at T = 21°C. This corresponds to a current of 1.73A.
- For AMP, a voltage of 2.35 V at T = 21°C was measured. This corresponds to a current of 1.77A.

- For MEA 30% wt, a measured voltage of 2.25V at T = 21°C corresponds to a current of 1.65A.
- For 0.25% wt K_2CO_3, a measured voltage of 2.17V at T = 60°C. This corresponds to a current of 1.39A.

It is observed that the cell with KOH has the lowest overall impedance in its optimal configuration. However, as previously mentioned, this result must be considered in light of the damage caused by the alkaline solution to the various cell components.

5. Conclusion and Outlook

In this thesis, a method was first developed to perform impedance spectroscopy analysis on low-resistance CO-electrolysis cells. Key points include reducing parasitic noise using shielded cables and utilizing an external device, such as the Solartron connected to the PSM3750 spectroscope, capable of delivering higher currents by lowering the shunt resistance used for current measurement.

The testing of different configurations of the Design 3.0 cell was conducted primarily by varying the chemical solution used for CO_2 capture at the cathode. The influence of temperature and concentration on the cell impedance varies depending on the nature of the absorption solution. A summary of the results obtained during the experiments is presented in Table 5.1 below. The values of the various resistances contributing to potential loss during cell operation were precisely evaluated. For each catholyte, efforts were made to detect the charge transfer resistance associated with CO_2 reduction to highlight the process through spectroscopic impedance measurements. However, this detection proves challenging without the use of a reference electrode.

A smaller cell with an active surface area of 16 cm^2, better suited for impedance spectroscopy measurements, was designed.It includes a system that enables the placement of a small reference electrode at the anode or cathode, allowing for more detailed spectroscopic impedance analysis at the electrodes. This cell design makes it possible to study potential losses at each electrode, thereby facilitating the efficient detection of potential CO_2 reduction and the measurement of the reaction's charge transfer resistance. Additionally, a new parallel-grid flow field design was created to allow comparisons with the serpentine flow field design of the Design 3.0 cell. The cell has been sent to production for the preparation of components and will soon be available for assembly and upcoming tests.

Absorber	Varied Parameter	Observed Effect	Possible Cause
KOH	Voltage	General Decrease in Impedance with Significant Reduction in OER Impedance	Increase in Current reduces OER Impedance
	Temperature	Slight Decrease in OER and Ohmic Impedance	Increase in the OER Reaction Rate and Ionic Conductivity
	Measurement time after 30min	Increase in Ohmic and OER Impedance	Membrane and Catalyst Degradation
	N_2 injection	Disappearance of the third semicircle	Change in CO_2 Reduction Reaction
AMP	Voltage	General Decrease in Impedance with Significant Reduction in OER Impedance	Increase in Current reduces OER Impedance
	Temperature	Decrease in OER Impedance	Increase in the OER Reaction Rate
MEA	Voltage	General Decrease in Impedance with Significant Reduction in OER Impedance	Increase in Current reduces OER Impedance
	Temperature	Increase in General Impedance	Decrease in conductivity due to MEA properties
	Concentration	General decrease in Impedance	Increase in Ionic Conductivity
	Pumping	Increase in Impedance	Diffusion Effect
K_2CO_3	Voltage	General Decrease in Impedance with Significant Reduction in OER Impedance	Increase in Current reduces OER Impedance
	Temperature	Slight Decrease in OER and Ohmic Impedance	Increase in the OER Reaction Rate and Ionic Conductivity
	Concentration	Increase in Ohmic Impedance and slight Decrease in Reaction Impedance	Increase in Membrane Conductivity but change in Double Layer Structure

Table 5.1.: *Summary of the Influence of Parameters on AEM Design 3.0 Cell Impedance*

Bibliography

[1] Shahbaz Ahmad. "An overview of proton exchange membranes for fuel cells : Materials and manufacturing". In: *International Journal of Hydrogen Energy* (2022), pp. 19086–19131. ISSN: 0360-3199. DOI: 10.1016/j.ijhydene.2022.04.099.

[2] Tanvir E. Alam et al. "Basics of Electrochemical Impedance Spectroscopy". In: *Applied Energy* 154 (2015), pp. 92–101. ISSN: 03062619. DOI: 10.1016/j.apenergy.2015.04.086.

[3] Tanvir E. Alam et al. "Electrochemical Impedance Spectroscopy - A Tutorial". In: *Applied Energy* 154 (2015), pp. 92–101. ISSN: 03062619. DOI: 10.1016/j.apenergy.2015.04.086.

[4] Tanvir E. Alam et al. "Impedance Basics". In: *Applied Energy* 154 (2015), pp. 92–101. ISSN: 03062619. DOI: 10.1016/j.apenergy.2015.04.086.

[5] COMMSCOPE. "Design fundamentals for high-bandwidth BNC connectors". In: *commscope.com* (2017).

[6] DWK Life Sciences, ed. *DURAN Original Laboratory Bottles*. Germany, 2024.

[7] Felix Ettlinger. "Process Control, Instrumentation, Commissioning and Start-Up of a Co-Electroysis Pilot Plant". In: *Diplomarbeit, Institute for Energy Systems and Thermodynamics* (2024).

[8] Fuelcell Store, ed. *GDL 34 35 Series Gas Diffusion Layer - Datasheet*. USA, 2024.

[9] Fuelcell Store, ed. *Nickel Foam (80-120 PPI) - Datasheet*. USA, 2024.

[10] G.Fafilek. "Elektrochemimsche Messtechniken und Untersuchungsmethoden". In: *Vorlesung Skriptum* (2024).

[11] G.Fafilek. "The use of voltage probes in impedance spectroscopy". In: *Solid State Ionic* (2004). ISSN: 0167-2738. DOI: 10.1016/j.ssi.2004.06.024.

[12] Sahil Garg. "How membrane characteristics infuence the performance of CO2 and CO electrolysis". In: *The Royal Society of Chemistry* 15 (2022), pp. 4440–4469. DOI: 10.1039/d2ee01818g.

[13] Guillot. "Reduction des emissions de CO2 : objectifs et actions de l'UE". In: *Parlement européen* (2024), pp. 1–7. ISSN: 20180305STO99003.

[14] H-TEC EDUCATION, ed. *Operating Instructions - E208 - Cell Rebuildable PEM Elektrolyzer Kit*. USA, 2019.

[15] Ismatec, ed. *Ismatec ecoline pump datasheet*. Germany, 2024.

[16] Jerry Janesh. "Two-wire vs. four-wire resistance measurements". In: *EDN* (2013).

[17] Dino Klotz. "Hands-on Electrochemical Impedance Spectroscopy (EIS)". In: *Zurich Instrument Webinar* (2022). DOI: 10.1021/acs.iecr.6b01080.

[18] Geonhui Lee. "Electrochemical upgrade of CO2 from amine capture solution". In: *Nature Energy* 6 (2021), pp. 46–53. DOI: 10.1038/s41560-020-00735-z.

[19] M.Haider. "Thermodynamik in der Energietechnik". In: *Vorlesung Skriptum* (2023).

[20] MAdelaine. "Captage de carbone : Londres accelere". In: *LesEchos* (2024). DOI: https://www.lesechos.fr/industrie-services/energie-environnement/captage-de-carbone-londres-accelere-2123512#:~:text=Le%20gouvernement%20britannique%20a%20annonc%C3%A9,est%20encore%20infime%20et%20on%C3%A9reuse.

[21] Ministere du travail et de l'emploi, GOUV.FR, ed. *Les risques professionels lies au monoxyde de carbone*. France, 2023.

[22] Newton4th Ltd., ed. *Application Note - PSM Series Impedance analysis with an external DC bias*. United Kingdom, 2024.

[23] Newtons4th Ltd., ed. *Frequency Response Analyze User Manual*. United Kingdom, 2024.

[24] Rauline. "Captage et stockage de carbone : les quatres chiffes inquietants pour l'Europe". In: *LesEchos* (2024). DOI: https://www.lesechos.fr/industrie-services/energie-environnement/captage-et-stockage-de-carbone-les-quatre-chiffres-inquietants-pour-leurope-2124488.

[25] Martin Schulz. "Engineering, Construction and Commissioning of a Co-Electrolysis Plant". In: *Diplomarbeit, Institute for Energy Systems and Thermodynamics* (2024).

[26] Smooth-On, ed. *Durometer Shore Hardness Scale*. https://www.smooth-on.com/page/durometer-shore-hardness-scale/, 2024.

[27] Solartron Group Ltd., ed. *SI1287 Electrochemical Interface - User Guide*. United Kingdom, 1999.

[28] John Wiley Sons, ed. *Electrochemical Engineering*. Hoboken, USA: Academic Press is an imprint of Elsevier, 2018. ISBN: 9781119446583.

[29] John Wiley Sons, ed. *Electrochemical methods : fundamentals and applications*. Hoboken, USA: Academic Press is an imprint of Elsevier, 2001. ISBN: 0471043729.

[30] Texas Instruments, ed. *OPA541 High Power Monolithic Operational Amplifier - Datasheet*. USA, 2000.

[31] Xiao-Dong Wange. "Determination of the optimal active area for proton exchange membrane fuel cells with parallel, interdigitated or serpentine designs". In: *International Journal of Hydrogen Energy* (2009), pp. 3823–3832. DOI: 10.1016/j.ijhydene.2008.12.049.

[32] Hugh Warkentin. "Early Warning for the Electrolyzer : Monitoring CO2 Reduction via In-Line Electrochemical Impedance Spectroscopy". In: *ChemSusChem, Chemistry Europe* (2023). DOI: 10.1002/cssc.202300657.

[33] Wikipedia. "Standard electrode potential (data page)". In: *Industrial & Engineering Chemistry Research* (2024). DOI: 10.1021/acs.iecr.6b01080.

[34] Quicheng Xu. "Integrated Reference Electrodes in Anion Exchange-Membrane Electrolyzers: Impact of Stainless-Steel Gas-Diffusion Layers and Internal Mechanical Pressure". In: *ACS Energy Letters* (2024), pp. 305–312. ISSN: 0888-5885. DOI: 10.1021/acsenergylett.0c02338.

[35] Shi Mo Xuebin Ye Dandan Zhang. "Influence of Grounded Shield on Cable Broadband Imepdance Spectroscopy Measurement". In: *International Conference on Electrical Engineering, Control and Robotics* (2023), pp. 80–84. ISSN: 0888-5885. DOI: 10.1109/eecr56827.2023.10150179.

[36] Lu Yuhe. "Investigation of oxygen evolution reaction kinetic process and kinetic parameters on iridium electrode by electrochemistry impedance spectroscopy analysis". In: *Journal of Electroanalytical Chemistry* (2020). ISSN: 1572-6657. DOI: 10.1016/j.jelechem.2020.114281.

[37] Zihan Zhou. "Channel/rib patterns optimization of a proton exchange membrane fuel cell by combining down-the-channel performance model and genetic algorithm". In: *International Journal of Heat and Mass Transfer* (2022). ISSN: 0888-5885. DOI: 10.1016/j.ijheatmasstransfer.2021.122235.

List of Figures

List of Tables

A. Additional Material

A.1. Calculations of exchange current density

An estimation of the exchange current density is attempted using the developed Ag/AgCl reference electrode. To achieve this, a membrane bridge is constructed by extending the AEM with a thin strip of charged membrane [34].

Figure A.1.: *Membrane strip wth Reference Electrode*

The electrode is placed directly in contact with the membrane. A tube filled with KOH facilitates charge conductivity at the contact point. This setup allows both the measurement of the current passing through the cell and the potential difference between the membrane and the electrode of interest. For the measurement of the exchange current density, the anode was chosen for two main reasons.

1. The potential drop at the anode is predominant in the surface reaction-related potential loss effects compared to the cathode, as demonstrated in Section 2. Therefore, from an impedance measurement perspective, it is more relevant to determine i_0 for OER.

2. The potential of the OER is easier to measure since only the OER reaction predominantly occurs at the anode.

The obtained data are presented in the table A.1. i_0 is determined using the Tafel approximation by plotting the anodic overpotential as a function of the logarithm of i [28].

$V_{\text{n\_anode\_measured}}\,[V]$	$i\,[A/m^2]$
1.43	20
1.55	40
1.65	60
1.78	90
1.89	120
2.00	150
2.11	180
2.22	210
2.33	240
2.43	270
2.54	310

Table A.1.: *Measured anodic potential and current density*

Only a small current flows between the reference electrode and the working electrode, making it similar to a Luggin capillary. Therefore, the potential difference must be corrected by considering the reference electrode's potential value and the ohmic drop potential[34].

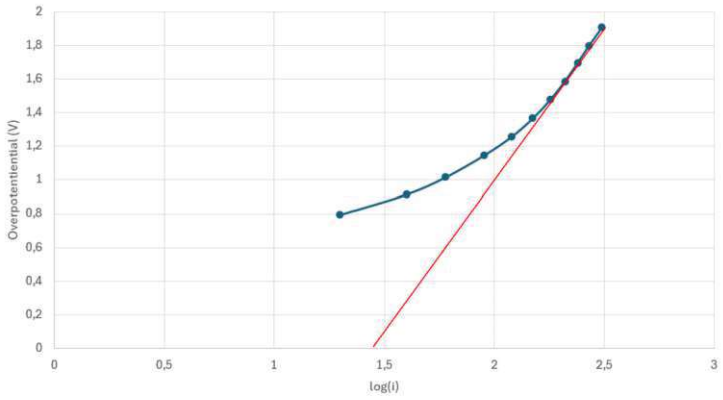

Figure A.2.: *Plot of overpotential as a function of logarithm of i in Excel*

The curve plotted in Figure A.2 exhibits the linear region characteristic of the Tafel approximation at high overpotential values. By the intersection of the linear approximation (at high overpotential values) with the x-axis, the exchange current density value

is determined graphically. The graphical reading of the exchange current density gives a value of 5 mA/cm^2, which is high for an OER reaction at the anode .

A.2. Drawings

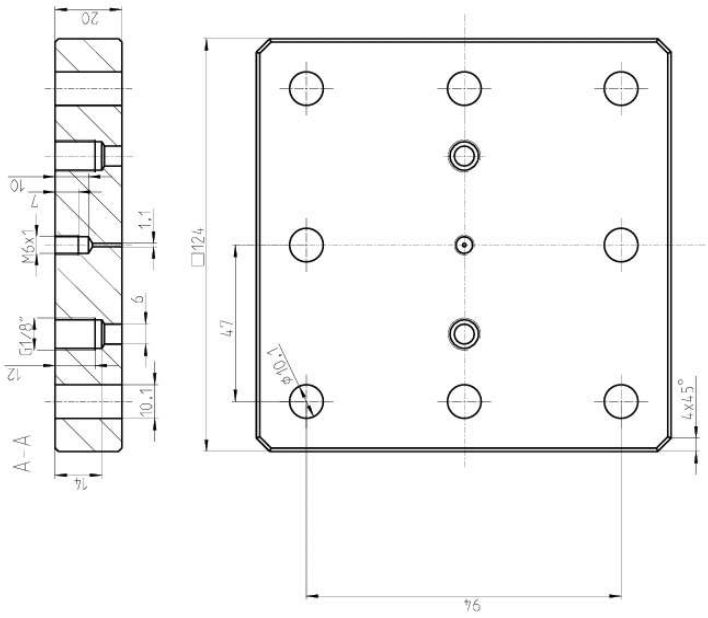

Figure A.3.: *Technical drawing of the endplate*

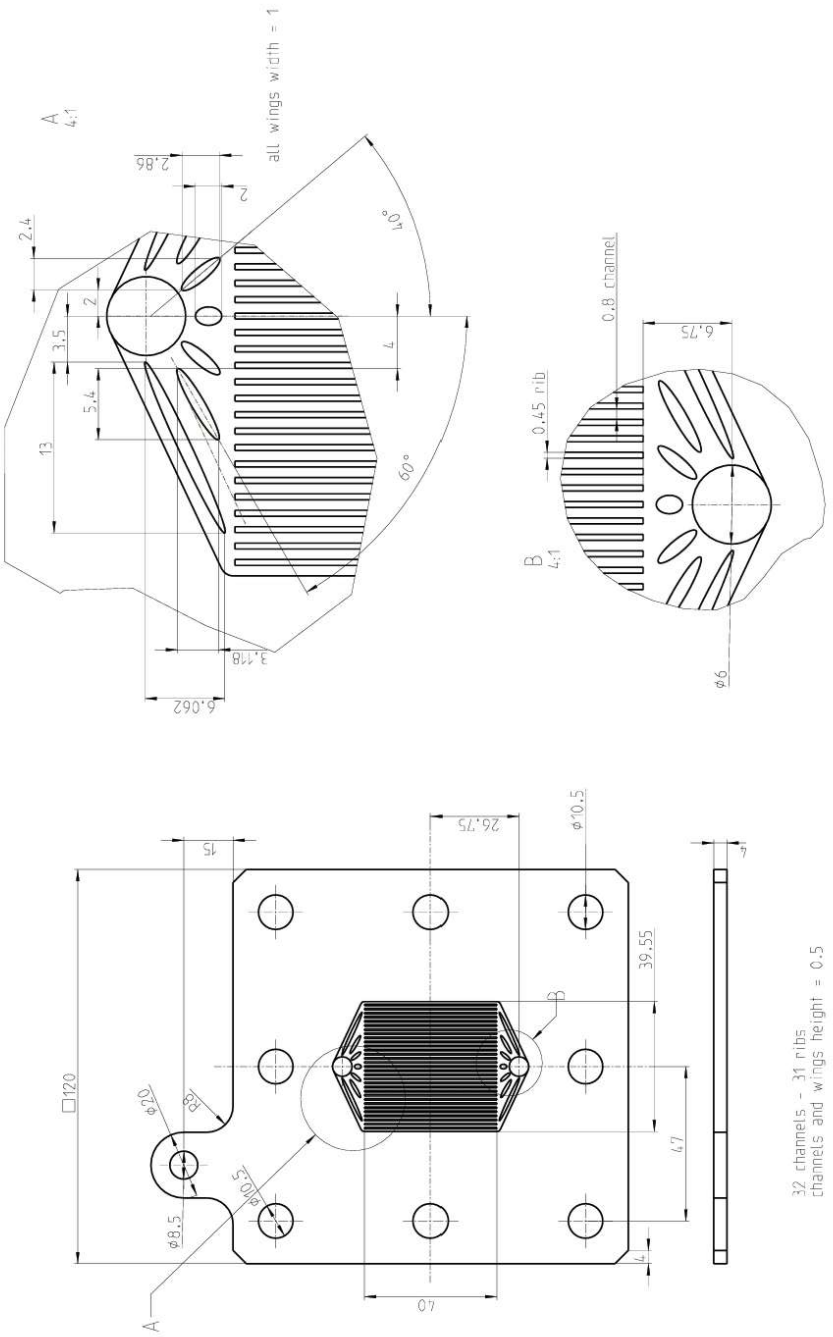

Figure A.4.: *Technical drawing of the flowfield plate*